# Physical aspects of bacterial cell division

Dissertation
zur
Erlangung des Doktorgrades
der Naturwissenschaften
(Dr. rer. nat.)

dem

Fachbereich Physik
der Philipps-Universität Marburg

vorgelegt von

Mischa Schmidt

aus

Darmstadt

Marburg/Lahn, 2010

Vom Fachbereich Physik der Philipps-Universität

als Dissertation angenommen am: 8.2.2011

Erstgutachter: Prof. Dr. Peter Lenz

Zweitgutachter: Prof. Dr. Frank Bremmer

Tag der mündlichen Prüfung: 25.2.2011

# Deutsche Zusammenfassung

Das Wachstum einer Bakterienpopulation wird bestimmt durch das Wachstum und die Zellteilung der einzelnen Zellen innerhalb einer Population. Da bei jeder Zellteilung zwei neue Zellen entstehen, ist das Wachstum einer Population exponentiell. Die Eigenschaften von Populationen können als Mittelwerte über die Eigenschaften aller einzelnen Zellen verstanden werden. Da eine Population aus sehr vielen einzelnen Zellen besteht, sind unter gleichen Bedingungen auch die Mittelwerte und damit die Populationseigenschaften immer gleich. Auf Einzelzellebene allerdings existieren Variationen zwischen den einzelnen Zellen. Zahlreiche aktuelle Untersuchungen zeigen, wie stark gewisse Eigenschaften innerhalb einer Population variieren können.

Manche Bakterien haben Mechanismen entwickelt, um zu starke Fluktuationen zwischen den Zellen zu vermeiden. So wurde beobachtet, dass einige Zelleigenschaften stärker schwanken als andere. Zum Bespiel ist der Ort der Zellteilung sehr präzise reguliert, andere Wachstumseigenschaften hingegen verhalten sich sehr divers. Daraus ergibt sich die Frage, welchen Einfluss Fluktuationen auf Einzelzellebene unter verschiedenen Bedingungen auf die gesamte Population haben.

In dieser Arbeit werden Eigenschaften und Strategien im Zusammenhang mit Zellteilungsprozessen an Bakterien untersucht. In den untersuchten biologischen Systemen wird das makroskopische Verhalten einer Population von den Eigenschaften der Zellen auf mikroskopischer Ebene bestimmt. Zunächst in Kapiteln 2 und 3 untersuchen wir Mechanismen mit denen eine einzelne Zelle den Ort ihrer eigenen Teilung festlegen kann. Die Position, an der die Teilung erfolgt, wird von speziellen Proteinen kontrolliert. Wir simulieren die Diffusion und die Reaktionen einzelner Proteine in der Zelle und schliessen daraus auf das Verhalten auf zellulärer Ebene. Im Anschluß in Kapitel 4 widmen wir uns der Population als ganzes. Hier wird das Wachstumsverhalten der Population aus dem Wachstum und der Teilung ihrer Zellen abgeleitet.

Um eine unkontrollierte Zellteilung zu hemmen, verwendet das Bakterium *Caulobacter crescentus* (*C. crescentus*) das kürzlich entdeckte Protein MipZ. Experimentell konnte gezeigt werden, dass die Konzentration von MipZ an den Zellpolen am höchsten ist, und in der Zellmitte ein Minimum aufweist. Der molekulare Mechanismus, der zu diesem Verhalten führt, ist unbekannt. In Kapitel 2 verwenden wir numerische und analytische Methoden, um einen Reak-

tionsmechanismus zu finden, der den MipZ Konzentrationsgradienten erklärt. Hierbei fliessen aktuelle experimentelle Befunde über die chemischen Eigenschaften von MipZ und seinen Reaktionspartnern in die Modellierung ein. Schlussendlich sind wir in der Lage, einen plausiblen Reaktionsmechanismus vorschlagen zu können. Dafür wurde eine weitere, bisher nicht untersuchte, Wechselwirkung eingeführt, die durch ein einfaches Experiment quantifiziert werden kann. Damit kann die genaue Form des Gradienten numerisch bestimmt werden.

Im Genesatz zu *C. crescentus* wird in dem Bakterium *Escherichia coli* (*E. coli*) der Ort der Zellteilung durch das Protein MinC festgelegt (siehe Kapitel 3). Genau wie MipZ aus *C. crescentus* ist MinC ein Inhibitor der Zellteilung. Aber im Gegensatz zu MipZ zeigt MinC keinen statischen Konzentrationsgradienten, sondern, wie experimentell gezeigt werden konnte, beschreibt MinC eine periodische Bewegung von einem Zellpol zum anderen. Für dieses Verhalten sind die Proteine MinD und MinE verantwortlich. Diese periodische Bewegung führt dazu, dass die Aufenthaltswahrscheinlichkeit von MinC in der Zellmitte am geringsten ist. In Kapitel 3 untersuchen wir den Einfluss der Zelllänge und der Anzahl an Proteinen in der Zelle auf die Aufenthaltswahrscheinlichkeit der Min Proteine. Die Wechselwirkungen zwischen MinD und MinE sind qualitativ bekannt, allerdings wurden die Geschwindigkeitskonstanten noch nicht gemessen. Aus diesem Grund verwenden wir die Geschwindigkeitskonstanten als freie Parameter, was einen größeren numrischen Aufwand bedeutet. Nachdem wir das Verhalten des Min Systems untersucht haben, wird das Modell um das Molekül FtsZ erweitert. FtsZ polymerisiert an der Zellmembran bis sich ein geschlossener Ring, der Z-Ring, gebildet hat. Dieser Ring legt den Ort der Zellteilung fest. MinC hemmt die Zellteilung, indem es die FtsZ Polymerisation unterbindet. Mit diesem neuen Modell sind wir in der Lage, die Lokalisation von FtsZ in der Zelle zu beobachten. Wir können zeigen, dass das Min System in unserem Modell tatsächlich eine Anlagerung von FtsZ in der Zellmitte bewirken kann. Dies ist aber nur in bestimmten Parameterbereichen möglich, für die wir die biologische Relevanz diskutieren.

In Kapitel 4 untersuchen wir den Effekt der ungleichen Zellteilung auf die Wachstumsrate einer bakteriellen Population. Das Wachstum der gesamten Population wird von dem Wachstum und der Teilungsrate der einzelnen Zellen in der Population bestimmt. Wie bereits eingangs erwähnt können sich die einzelnen Zellen in einer Population voneinander unterscheiden. Bei einer ungleichen Zellteilung entstehen zwei Zellen mit geringfügig unterschiedlicher Masse. Die kleinere der beiden Tochterzellen mit der kleineren Geburtsmasse braucht länger, um sich selbst teilen zu können, als ihre größere Schwesterzelle mit der grösseren Geburtsmasse. Der Einfluss dieser ungleichen Teilung auf die Wachstumsrate der Population hängt von der Stärke der Fluktuationen und vom Wachstumsverhalten der einzelnen Zellen ab. Außerdem gibt er an, ob die Population einen Wachtumsvorteil aus einer Unterdrückung der Fluktuationen ziehen kann.

Zum Abschluss von Kapitel 4 wird ein Modell diskutiert, das eine Population unter zwei periodisch wechselnden Umweltbedingungen beschreibt. Um unter den unterschiedlichen Bedingungen zu wachsen, brauchen die Zellen unterschiedliche Moleküle, die sie vorher produzieren

müssen. In unserem Modell können die Zellen zwischen zwei Strategien, wie sie auf die permanenten Wechsel reagieren, wählen. Entweder sie passen sich immer an die aktuelle Umwelt an, oder sie sind ständig auf beide Bedingungen eingestellt. Im ersten Fall haben sie den Nachteil, dass sie sich nach einer Umweltveränderung zunächst anpassen müssen, ohne wachsen zu können. Im zweiten Fall brauchen sie sich nach einer Umweltveränderung nicht anzupassen, wachsen aber langsamer da sie die Moleküle für beide Umweltbedingungen gleichzeitig produzieren. Je nachdem wie oft die Umwelt wechselt und wie lange die Zellen zur Anpassung brauchen ist eine dieser beiden Strategien von Vorteil. In unserer Simulation wird dieser Bereich quantifiziert. Danach untersuchen wir, ob es von Vorteil ist, wenn die Zellen in der Population alle mit der gleichen Strategie wachsen, oder ob eine Mischung von beiden Strategien das schnellste Wachstum liefert.

# Contents

# Chapter 1

# General Introduction

Cell division is one of the most fundamental processes in all living cells; In plant cells and animal cells as well as in bacterial cells. The life cycle of every single cell regardless of animal, plant or bacterial cell, starts with this event. Subsequently, a newborn cell begins to grow until it itself divides into two daughter cells. In eukaryotic cells, cell division is part of a highly regulated life cycle in which fundamental processes are carried out in temporally well-separated phases. These processes include cell enlargement, DNA replication, separation of the chromosomes, and after all cell division. In eukaryotic cells the DNA is organized in several chromosomes that are located in the cell nucleus. During the process of separation, the chromosomes of the two daughters are actively pulled apart by protein filaments called microtubules (Atlas, 1997).

Bacteria are lacking the sub-cellular compartmentalization of eukaryotes. In particular, they do not have a nucleus and possess only one circular chromosome. In some bacteria the separation of the two daughter chromosomes prior to cell division takes place while the replication is still in progress (Thanbichler and Shapiro, 2006a). In bacteria, the processes of cell elongation, chromosome duplication and separation are carried out simultaneously. This makes the life cycle of bacteria much simpler and better suited for theoretical modeling (Atlas, 1997).

Bacterial cells have amazing growth properties that allow them to reproduce very fast. For instance, *Escherichia coli* (*E. coli*) can grow at doubling times down to 20 minutes. The doubling time of the cells depends on their environment including temperature, pH, salinity, availability of nutrients and oxygen and other physical or chemical properties of the surrounding medium. Bacteria exhibit ranges of tolerances for these factors that are remarkably large (Atlas, 1997). In order to adapt to the growth conditions, bacteria have control devices that adjust cellular properties to react to the environment. In this way, the chemical composition of the cells depends on the growth environment. Also other cellular properties such as mass or volume are adjusted to adapt to the environment (Bremer et al., 1996; Neidhardt et al., 1990).

In addition to the physiological adjustments made by bacteria in order to grow in a certain medium, they have also developed mechanisms to withstand very hostile environments. Even though under these conditions the cells do not grow and reproduce, they have elaborate

mechanisms to enable their survival. If the environment switches to better growth conditions again, the population continues growing.

For example parts of an *E. coli* population are able survive exposure to antibiotics. Their survival is enabled by entering a dormant state (Balaban et al., 2004; Levin, 2004; Shah et al., 2006). In this state, the cells do not grow at all. However, when the population is exposed to antibiotics, these cells do not die. When the antibiotic is diluted from the growth medium and the cells leave their dormant state, they start growing and dividing normally. In this way, part of the population survives the antibiotic exposure. Other bacteria make use of a similar process called sporulation (Maughan and Nicholson, 2004; Veening et al., 2006). When these cells detect that the environmental conditions become unfavorable they can reduce themselves into a metabolically inactive spore. The spores are completely inactive, but stay viable under very extreme conditions. When a spore detects more viable environmental conditions, it germinates again and starts growing. Amazingly, Cano and Borucki (1995) were able to revive bacterial spores that were enclosed in amber for 25-40 million years.

The growth of a population of living cells can be regarded as a sequence of single cell division events. A newborn cell grows until it has doubled its size and then divides into two daughter cells. In this way, the population exhibits exponential growth. Thus, the division process of the single cells, a population consists of, is the essential step for the overall growth of the population. In particular, the population growth rate is determined by the time that the single cells in the population need to double.

When the bacterial cell is about to divide, it has to partition DNA and all other cellular components between the two daughter cells. Most of the rod-shaped bacteria divide by mid-cell constriction of their cell envelope. The bacteria considered in this work belong to this category. The constriction is accomplished by formation of a so-called septum (Atlas, 1997). It is initiated as a ring at the inner surface of the cell membrane usually at mid-cell position. By adding newly synthesized cell wall material, the septum grows inwards. In this way, the septal ring is getting smaller and smaller until it closes completely and two separate daughter cells have formed. In order to form two viable daughter cells, the bacterium has to regulate both, the timing and the placement of septum formation (Harry, 2001). In particular, the dividing cell has to guarantee that both daughter cells are equipped with one complete genome.

In the bacterial systems considered in this work, the protein FtsZ is responsible for initiation of septum formation (Bi and Lutkenhaus, 1991). In this way, FtsZ positions the septum and thus the future division site. FtsZ is a cytoplasmic protein that forms polymers at the inner surface of the membrane. These polymers form a closed ring, and recruit other proteins required for contraction of the septal ring (Weiss, 2004). Thus, to investigate the precision of cell division, one has to observe those mechanisms that are responsible for the sub-cellular positioning of FtsZ.

Astonishingly, different bacteria have developed different mechanisms to regulate the sub-cellular positioning of FtsZ. In this work, we investigate the properties of two of these mecha-

nisms, namely in the bacteria *E. coli* and *Caulobacter crescentus*.

*E. coli* is one of the best studied bacteria and a large amount of information about its properties is available (see i.e. ecocyc.org). It lives in the digestive system of warm-blooded animals. In this environment, it is supplied with a large number and variety of nutrients. As a consequence, it is able to metabolize and catabolize many different nutrients such as sugars and amino acids. *E. coli* needs 40 minutes to replicate its chromosome and after replication is finished, there is a lag phase of 20 minutes before the cell divides. For cells growing at doubling times of 60 minutes, the replication of the chromosome is thus finished right before cell division. However, *E. coli* can grow at doubling times lower than 60 minutes, down to only 20 minutes. These fast-growing cells initiate DNA replication more often than every 60 minutes (Cooper and Helmstetter, 1968). Thus, in fast-growing cells, more than one round of DNA replication takes place at the same time. At the moment of cell division, the mother cell then passes more than one chromosome to the daughter cells. Thus, the grandmother cell might have initiated the replication that is completed in a cell prior to its cell division. As a consequence, cells that grow at high growth rates contain more DNA than slow-growing cells. This is one of the reasons, that fast-growing *E. coli* cells are larger than the slow-growing cells (Pierucci, 1978; Bremer et al., 1996).

Because of its unique life cycle, *C. crescentus* is a model organism for bacterial development. *C. crescentus* is distributed in fresh water lakes and streams. At cell division, two different cells are produced, one motile swarmer cell and one stationary stalked cell. The swarmer cell possesses a flagellum at one cell pole that is used for active movement. It does not grow in size, replicate DNA, or divide, but swims in the medium to disperse the population. At one point, the swarmer cell differentiates into a stalked cell. Therefore, the cell ejects its flagellum and develops a stalk. This stalk is used to attach to a surface. After surface-attachment, the cell starts DNA-replication, grows in size and finally divides into a stalked cell and a swarmer cell. Because of this interesting live style, there are numerous studies on the temporal and spatial regulation of the *C. crescentus* life cycle (Jenal and Stephens, 2002; Jensen et al., 2002; Quardokus and Brun, 2003; McGrath et al., 2004).

The cell division of *E. coli* functions at an astonishing precision. The two daughter cells differ in less than 10% of their mass (Koppes et al., 1978; Trueba, 1982; Guberman et al., 2008). Other cellular processes are not that precisely implemented and show a large variation from cell to cell. Some of these noisy processes fundamentally influence the growth behavior of single cells (Smits et al., 2006; Davidson and Surette, 2008). Thus, it seems that for some processes, the population draws advantages from a precise regulation, whereas for other processes advantages can be drawn from diversity.

Due to novel experimental methods quantitative data that characterizes bacterial behavior on the single cell level is available. In this context, the visualization of molecules in living cells with fluorescent labels plays an important role (Xie et al., 2008). The results of these single cell experiments provide important information for theoretical investigations. With the

help of computer simulations, chemical reactions can be modeled on the single-molecule level. Then, conclusions for the cell as a whole can be drawn, and the behavior can be compared to experimental findings on the cellular level. In order to perform a simulation, certain parameters such as the reaction rate constants or diffusion constants of the molecules are chosen. Some of these parameters were determined experimentally, others are unknown. We can vary the unknown parameters and then make predictions on their magnitude. We can also cancel single reactions in the system to see their significance for system behavior. The range of parameters for which a system shows the expected behavior gives information of the robustness towards parameter fluctuations.

When a simulation fails to reproduce the experimentally observed behavior, additional interactions can be assumed and simulated. Thus, it can be tested, in which way the model has to be modified to obtain the experimentally known properties. In this way, modeling can propose further experiments which help elucidating underlying mechanisms. The results of these experiments can then again lead to modifications of the models. Hence, theory and experiment can go hand in hand to finally explain the mechanism behind an observed behavior.

Similar to studying the properties of a cell by considering the molecules it contains, it is possible to deduce the properties of a bacterial population by considering the behavior of single cells. By following the growth and division of single cells, the growth behavior of the whole population can be studied. The situation becomes more interesting, when the population does not consist of cells that all grow in the same way, but differ in their growth properties. By simulating both, a homogeneous and a heterogeneous population, the influence of the single cell behavior can by explained.

The outline of this thesis is as follows. Chapter 2 considers the mechanism for the correct placement of cell division in *C. crescentus*. This bacterium is known to make use of a static bipolar concentration gradient of the cell division inhibitor MipZ. This macroscopic behavior has been seen experimentally (Thanbichler and Shapiro, 2006b). The underlying mechanism of how the molecular properties of the proteins in the cell lead to gradient formation is unknown. Recently, some of the interactions between these molecules have been quantified experimentally. We introduce different models of how the concentration gradients could be established. We discuss how the recent experimental findings influence the different models and propose a new experiment that will help to find the mechanism behind the formation of the MipZ concentration gradient.

In chapter 3, the mechanism of correct placement of the cell division site in *E. coli* is observed. In contrast to *C. crescentus*, *E. coli* does not use a static concentration gradient of its cell division inhibitor. Instead, the molecules responsible for correct placement of the division site show periodic movements within the cell (de Boer et al., 1989; Rothfield et al., 2001; Hu et al., 2003; Shih et al., 2003; Touhami et al., 2006). This collective motion causes cell division to take part exclusively in the cell center. The system has been studied theoretically before and we choose a model for our own simulations (Huang et al., 2003; Kerr et al., 2006).

With a huge computational effort, we perform simulations at different sets of parameters. In this way, the system robustness towards parameter changes is studied. We particularly focus on parameter values known from experiments to test the applicability of the model to the biological system. Finally, we extend the model in a way that FtsZ polymerization can be studied and thus further visualize the position of septum formation.

Chapter 4 focuses on the bacterial population as a whole. As mentioned above, the cells in a population show individual behavior on the single cell level. With the mechanisms discussed in chapters 2 and 3, the cells achieve the division into two daughter cells of similar size. The variation in birth size depends on the precision of cell division. Here, we ask how an imprecise cell division affects the properties of the population. The most interesting question in this context is if the population can draw growth advantages from the precision of cell division. We consider different scenarios concerning the growth and division properties of the single cells and test the impact on the growth rate of the population. As a next step, we allow the single cells of the population to choose individual growth strategies in fluctuating environments. Depending on the nature of the growth environment, the population growth rate is affected by these choices and we observe advantages and disadvantages in strategy choice.

In chapter 5, the findings are summarized and general conclusions are drawn.

# Chapter 2

# Concentration gradient of the protein MipZ in *C. crescentus*

## 2.1 Introduction

Concentration gradients of proteins in cells play an important role in many different biological processes like cell differentiation (De Robertis, 2006), embryonic development (Driever and Nuesslein-Volhard, 1988; Ephrussi and Johnston, 2004) and cell division (Fuller et al., 2008; Martin and Berthelot-Grosjean, 2009; Moseley et al., 2009). Theoretically well-described is the gradient formation mostly in eukaryotic cells, as reviewed by Wartlick et al. (2009). However, also procaryotic cells make use of concentration gradients. Here, we consider the recently discovered MipZ concentration gradient in *Caulobacter crescentus* (*C. crescentus*) (Thanbichler and Shapiro, 2006b).

Bacteria are lacking the sub cellular compartmentalization of eukaryotes. As a consequence, molecules can freely diffuse through the whole cell. Since a *C. crescentus* cell is in the order of $2\,\mu$m long, a protein with a typical diffusion coefficient of $10\,\mu\mathrm{m}^2\mathrm{s}^{-1}$ (Deich et al., 2004) can move through the entire cell within a few seconds. Thus, if diffusion is rate determining for the intracellular distribution of the molecules, the concentration of proteins is constant over the cell.

However, in some cases bacterial cells need a spatially inhomogeneous behavior. The most prominent example is the cell division. It has to take place exclusively at the mid-cell position. In *C. crescentus* as well as other bacteria the localization of the future division site is carried out by a highly conserved protein called FtsZ (Bi and Lutkenhaus, 1991). This homologue of eukaryotic tubulin is able to form polymers. These polymers form a ring, the so-called Z-ring, on the membrane. The position of this ring sets the position of the cell division. Thus, the cell has to prevent Z-ring formation at the poles of the cell in order to accomplish mid-cellular division. In *C. crescentus*, the inhibition of Z-ring formation is achieved by the ATPase MipZ (Thanbichler and Shapiro, 2006b). MipZ forms a static bipolar concentration gradient, with

its minimum at the cell center. This causes the Z-ring to form exclusively in the middle of the cell. It is the aim of this work to elucidate the mechanism behind the formation of the MipZ concentration gradient.

In order to understand the behavior of MipZ we have to study those chemical reactions in the cell which influence the MipZ concentration. For these reactions one important reactant is ParB, which is also associated to the chromosome duplication that takes place just before cell division. *C. crescentus* possesses one single circular chromosome. Before chromosome duplication starts, the origin of replication is immobilized at one cell pole (Jensen and Shapiro, 1999; Viollier et al., 2004). The localization of the origin is mediated by ParB, a DNA binding protein (Mohl and Gober, 1997). ParB selectively binds to DNA close to the replication origin at a sequence called *parS* (Lin and Grossman, 1998). MipZ was shown to interact with ParB and the MipZ concentration maximum is located at the ParB position (Thanbichler and Shapiro, 2006b). After the initiation of the chromosome replication, the newly synthesized replication origin immediately moves to the opposite call pole (Toro et al., 2008). This is accomplished by active separation of the ParB complexes with the help of the ATPase ParA (Figge et al., 2003). As a consequence, right before cell division, the moment of division site placement, two ParB clusters exist each at one of the two cell poles. This correlates with two maxima of the MipZ concentration and a minimum of the MipZ concentration at the cell center.

These findings suggest that the interactions of MipZ with ParB and DNA have to be studied in order to explore the nature of the MipZ concentration gradient in this work. Recently, new experimental findings elucidated many of the interactions of the players in the system, namely MipZ, ParB and DNA (Kiekebusch et al., unpublished results). Three different models are presented here that differ in the set of reactions under consideration. The corresponding reaction-diffusion system is modeled numerically. The details of the computational method are described in section 2.7.

The first model is reported in section 2.2. It was inspired by the fact that ParB alters the ratio of the ATP to ADP bound form of ParA (Easter and Gober, 2002). The assumption that ParB functions in a similar way for MipZ as for ParA leads to a simple set of reactions. This model results indeed in a gradient of the MipZ concentration. However, recent findings prove that ParB has no influence on MipZ ATPase activity (Kiekebusch et al., unpublished results). Therefore this model had to be modified.

In model 2, given in section 2.3, we take into account all reactions of MipZ known from the literature and the set of rate equations becomes more complex. Disappointingly, solving these equations does not lead to a concentration gradient of MipZ. Comparing model 1 and 2 we deduced the essential effect of this failure. This effect is demonstrated by a general analogous model, which we call toy model. It is presented in section 2.4.

The comparison of model 1 and 2 also gives us an idea in which direction model 2 has to be modified to explain the concentration gradient of MipZ. This leads to model 3 explained in section 2.5. We assume additionally a catalytic activity of ParB. We could show that this

assumption does not contradict any experimental finding. The numerical implementation of model 3 yields stable MipZ concentration gradients. An analytical treatment of the rate equations of the system gives us the reason for this surprising result.

Having understood the origin of the gradient in model 3, we present in section 2.6 the effect of parameter scans of the system to learn more about the respective influences of the different reactions. Knowing these dependencies, we can make predictions of the answer of the system when using MipZ mutant proteins instead of the wild-type. These effects can be tested experimentally.

In model 3 there is one unknown rate constant and in section 2.6.4 we propose an experiment that is able to determine this parameter. We analytically analyzed the impact of model 3 on *in vitro* experiments and found a cooperative behavior of DNA and ParB on the average turnover number for ATP hydrolysis of MipZ. This fact is experimentally testable, and can determine the unknown rate constant of our model.

## 2.2 Model 1: Nucleotide exchange at ParB

Our first model to analyze the concentration profile of MipZ is based on the experimental results of Thanbichler and Shapiro (2006b). As mentioned above the authors found that MipZ is responsible for the cell division inhibition and that its concentration profile shows a gradient. With the help of a computer simulation we want to study the MipZ concentration $c_{\mathrm{MipZ}}(x)$ as a function of position $x$ in the cell in oder to understand the formation of the gradient of $c_{\mathrm{MipZ}}(x)$. The experimental findings about the role of MipZ (Thanbichler and Shapiro, 2006b) are as follows: First, MipZ functions as an ATPase. It can exist in an ATP bound state and an ADP bound state, thus an equilibrium between these two MipZ species is formed in the cell,

$$\mathrm{MipZ}\cdot\mathrm{ADP} \quad \leftrightharpoons \quad \mathrm{MipZ}\cdot\mathrm{ATP}. \tag{2.1}$$

The ATP bound state is assumed to be the active one, that can destroy FtsZ-filaments and hence prevent cell-division. Thus, the concentration of MipZ·ATP should have a minimum in the cell center, where cell division takes place. Second, cells that expresses MipZ mutant proteins with impaired ATP hydrolysis do not show a MipZ concentration gradient. For this reason it seems that the balance between the ATP and ADP bound form of MipZ is important for the gradient formation. Third, it is also known that MipZ·ATP can bind to DNA:

$$\mathrm{MipZ}\cdot\mathrm{ATP}+\mathrm{DNA} \quad \xrightarrow{\tilde{k}_2} \quad \mathrm{MipZ}\cdot\mathrm{ATP}\cdot\mathrm{DNA} \tag{2.2}$$

which obviously hinders the diffusion of MipZ·ATP. After MipZ is bound to DNA according to reaction (2.2), MipZ is released from DNA by ATP hydrolysis:

$$\mathrm{MipZ}\cdot\mathrm{ATP}\cdot\mathrm{DNA} \quad \xrightarrow{k_3} \quad \mathrm{MipZ}\cdot\mathrm{ADP}+\mathrm{DNA}. \tag{2.3}$$

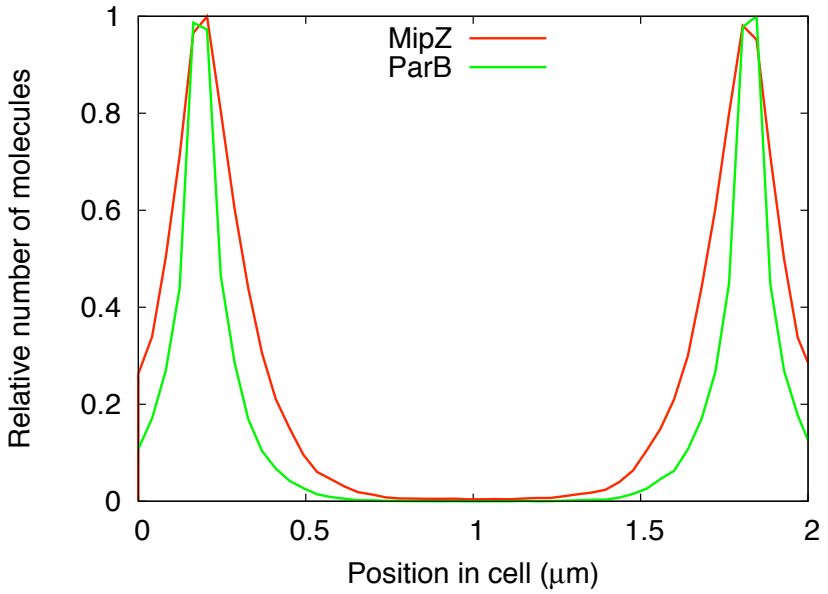


Figure 2.1: Concentration profile of MipZ and ParB. The concentration of MipZ, $c_{\mathrm{MipZ}}(x)$ (red) and ParB (green) is shown as function of sub-cellular position. Simulations were carried out according to model 1 as given by reactions (2.2) - (2.4). The MipZ molecules co-localize with the ParB molecules, that are positioned at the cell poles. Almost all MipZ is DNA bound. Parameters are: $k_1 = 0.6\,\mu\mathrm{M}^{-1}\mathrm{s}^{-1}$, $k_2 = 65\,\mathrm{s}^{-1}$ and $k_3 = 0.011\,\mathrm{s}^{-1}$.

In our simulations, we assume that DNA is equally distributed in the cell and present in excess. As a consequence, we can use an effective rate constant $k_2 = \tilde{k}_2\,[\mathrm{DNA}]$ to describe reaction (2.2), which includes the almost constant concentration of DNA. In addition we do not have to define explicit DNA binding sites. Recently, the rate constants $k_2$ and $k_3$ were determined experimentally, $k_2 = 65\,\mathrm{s}^{-1}$ and $k_3 = 0.011\,\mathrm{s}^{-1}$ (Kiekebusch et al., unpublished results).

Forth and finally we have to take into account processes which take place explicitly near the region of the cell poles where the replication origins are attached. Close to the replication origin the protein ParB selectively binds to a specific DNA sequence. ParB is interacting with MipZ, but also with ParA which is another ATPase that is implicated in chromosome segregation. It was shown that ParB stimulates ATPase activity of ParA (Easter and Gober, 2002). In this way, ParB can regulate the ratio of the ATP and ADP bound form of ParA. This regulation has an important physiological meaning for the cell, because the ATP and ADP bound form of ParA perform different tasks. The former dissociates ParB from the DNA, the latter binds

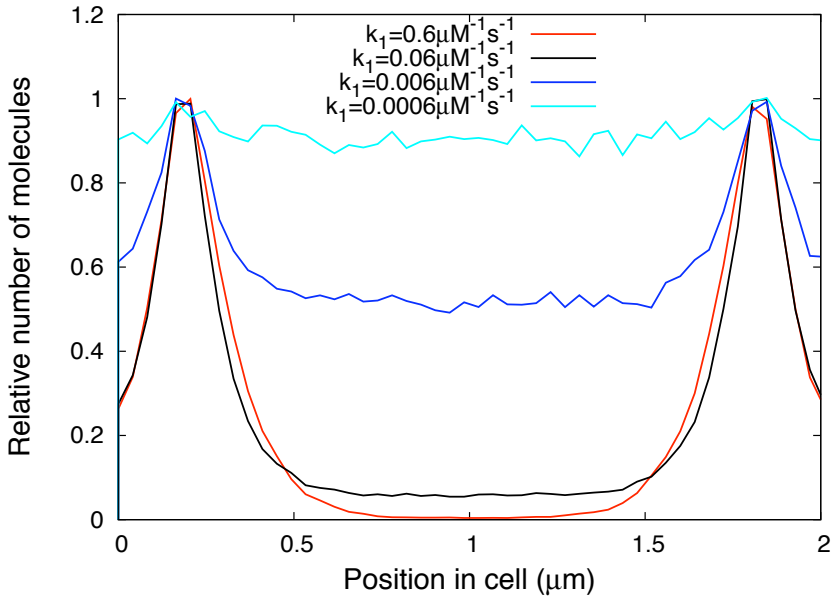


Figure 2.2: MipZ profiles in *C. crescentus* for different charging rate constants $k_1$ are plotted. In the case of $k_1 = 6 \cdot 10^{-4}\,\mu\mathrm{M}^{-1}\mathrm{s}^{-1}$ (cyan line) almost all MipZ molecules are ADP bound, whereas for $k_1 = 0.6\,\mu\mathrm{M}^{-1}\mathrm{s}^{-1}$ (red line), nearly all MipZ is bound to DNA.

single stranded DNA.

Now to get a specific behavior of MipZ in the region around the cell poles in comparison to the bulk behavior we assume in our model 1 that ParB acts on MipZ similar to ParA, namely by altering the nucleotide bound state:

$$\mathrm{MipZ} \cdot \mathrm{ADP} + \mathrm{ParB} \quad \xrightarrow{k_1} \quad \mathrm{MipZ} \cdot \mathrm{ATP} + \mathrm{ParB}. \tag{2.4}$$

This reaction is the conversion of ADP bound MipZ to ATP bound MipZ. In other words, ParB charges MipZ with ATP. Since this reaction takes place in the presence of ParB, it is only carried out at the cell poles.

To summarize, our model 1 is expressed in the three reactions (2.2), (2.3) and (2.4), where the rate constant $k_1$ is unknown and has to be used as a variable parameter. We know that the number of MipZ molecules per cell is approximately 1000 and that there are several hundred ParB Proteins. In our simulation we use 200 at each pole. The reaction-diffusion processes have been studied on a grid. Each reaction volume (bin) has a size of $6.4 \cdot 10^{-5}\,\mu\mathrm{m}^3$ and the whole cell is assumed to have the size $2\,\mu\mathrm{m} \times 0.5\,\mu\mathrm{m} \times 0.5\,\mu\mathrm{m}$. Details about the simulation

technique are given below in section 2.7. Here we only report the results of the simulations.

Figure 2.1 shows the MipZ concentration profile $c_{\mathrm{MipZ}}(x)$ for $k_1 = 0.6\,\mu\mathrm{M}^{-1}\mathrm{s}^{-1}$. It strongly resembles the profiles found experimentally by Thanbichler and Shapiro (2006b). The exact shape of $c_{\mathrm{MipZ}}(x)$ depends on the value of $k_1$.

In Figure 2.2 we see the MipZ concentration profile $c_{\mathrm{MipZ}}(x)$ for different values of $k_1$. For very small values of $k_1$, $k_1 < 0.0006\,\mu\mathrm{M}^{-1}\mathrm{s}^{-1}$ the influence of the reaction at the cell pole is too week and there is a pure bulk diffusion. With increasing $k_1$ the effect of equation (2.4) becomes more and more important and finally for $k_1 = 0.6\,\mu\mathrm{M}^{-1}\mathrm{s}^{-1}$ we get a distinct static gradient for $c_{\mathrm{MipZ}}(x)$. MipZ exists predominantly in the ATP form, that binds DNA. As a consequence, it the MipZ concentration maximum co-localizes with ParB which is shown in Figure 2.1. For $k_1 = 0.0006\,\mu\mathrm{M}^{-1}\mathrm{s}^{-1}$, almost only the ADP form of MipZ exists. Since this molecule cannot bind to DNA, it diffuses freely in the cell resulting in an equal distribution.

To characterize the gradients quantitatively, we introduce the center of mass in the left cell half $C$, defined by:

$$C := \frac{1}{N} \int_0^{l/2} x c_{\mathrm{MipZ}}(x)\, dx \tag{2.5}$$

where $l = 2\,\mu\mathrm{m}$ is the length of the cell. $N$ is the total number of MipZ molecules in the left cell half:

$$N := \int_0^{l/2} c_{\mathrm{MipZ}}(x)\, dx. \tag{2.6}$$

We calculated $C$ for the $c_{\mathrm{MipZ}}(x)$ profiles shown in Figure 2.2. For $k_1 = 0.6\,\mu\mathrm{M}^{-1}\mathrm{s}^{-1}$ (red line) we get $C = 0.22\,\mu\mathrm{m}$. This can be considered as a strong gradient. When $k_1$ is reduced, the gradient becomes less strong, and the center of mass in the left cell half increases. We get $C\left(k_1 = 0.06\mu M^{-1}s^{-1}\right) = 0.26\,\mu\mathrm{m}$, $C\left(k_1 = 0.006\,\mu\mathrm{M}^{-1}\mathrm{s}^{-1}\right) = 0.43\,\mu\mathrm{m}$, and $C\left(k_1 = 0.0006\,\mu\mathrm{M}^{-1}\mathrm{s}^{-1}\right) = 0.48\,\mu\mathrm{m}$. In the case of equally distributed molecules, the center of mass in the left cell half is $C = 0.5\,\mu\mathrm{m}$. In conclusion, the center of mass in the left cell half is a good measure to judge how pronounced a gradient is.

We saw in this section that we get indeed a static gradient profile of $c_{\mathrm{MipZ}}(x)$ using model 1. We can also detect the reason for this behavior. With the help of ParB (reaction (2.4)) we have a permanent source for MipZ·ATP at the cell poles and MipZ·ATP diffuses in the bulk but the migration is hindered by the docking at the DNA.

However, during this work it is found experimentally, that ParB does not shift the ratio of the ATP to ADP bound MipZ species by effectively charging MipZ with ATP (Kiekebusch et al., unpublished results). And therefore the key summation of our model 1 is not fulfilled and this brings us to model 2.

## 2.3 Model 2: Dynamic localization cycle

Recent experimental findings further resolved the interactions of the molecules (Kiekebusch et al., unpublished results). Here we present the outcome of these findings which lead to model 2. A new aspect came into consideration. It was shown that the ATP bound form of MipZ forms dimers,

$$2\ \mathrm{MipZ}\cdot\mathrm{ATP} \quad \underset{k_6}{\overset{k_5}{\rightleftharpoons}} \quad (\mathrm{MipZ}\cdot\mathrm{ATP})_2 \tag{2.7}$$

that these dimers bind to DNA

$$\mathrm{DNA} + (\mathrm{MipZ}\cdot\mathrm{ATP})_2 \quad \underset{k_8}{\overset{\tilde{k}_7}{\rightleftharpoons}} \quad \mathrm{DNA}\cdot(\mathrm{MipZ}\cdot\mathrm{ATP})_2 \tag{2.8}$$

and that DNA·(MipZ·ATP)$_2$ performs the reactions needed for the inhibition of Z-ring formation. As explained in section 2.2, we do not explicitly simulate DNA binding sites and use an effective rate constant $k_7 = \tilde{k}_7[\mathrm{DNA}]$ to describe equation (2.8).

The ADP bound form of MipZ cannot dimerize but the MipZ dimer can decay to two ADP bound monomers by hydrolysis:

$$(\mathrm{MipZ}\cdot\mathrm{ATP})_2 \quad \xrightarrow{k_9} \quad 2\ \mathrm{MipZ}\cdot\mathrm{ADP}. \tag{2.9}$$

This reaction is performed by a dimer independent weather it is bound to DNA or not. However, since MipZ·ADP cannot bind to DNA, the dimer hydrolysis causes MipZ to be detached from DNA:

$$\mathrm{DNA}\cdot(\mathrm{MipZ}\cdot\mathrm{ATP})_2 \quad \xrightarrow{k_9} \quad 2\ \mathrm{MipZ}\cdot\mathrm{ADP} + \mathrm{DNA}. \tag{2.10}$$

It follows that MipZ can exist in three forms: as monomers with either ATP or ADP bound, and as ATP bound dimers. The reaction

$$\mathrm{MipZ}\cdot\mathrm{ADP} \quad \underset{k_2}{\overset{k_1}{\rightleftharpoons}} \quad \mathrm{MipZ}\cdot\mathrm{ATP} \tag{2.11}$$

describes the nucleotide exchange reaction of the monomers.

All the reactions considered until now can take place everywhere in the cell. As in model 1 position dependent reactions are reactions with ParB. ParB binds all MipZ species irrespective of its nucleotide and dimerization state,

$$\mathrm{ParB} + \mathrm{MipZ}\cdot\mathrm{ANP} \quad \underset{k_4}{\overset{k_3}{\rightleftharpoons}} \quad \mathrm{ParB}\cdot\mathrm{MipZ}\cdot\mathrm{ANP} \tag{2.12}$$

$$\mathrm{ParB} + (\mathrm{MipZ}\cdot\mathrm{ATP})_2 \quad \underset{k_4}{\overset{k_3}{\rightleftharpoons}} \quad \mathrm{ParB}\cdot(\mathrm{MipZ}\cdot\mathrm{ATP})_2\,. \tag{2.13}$$

The reactions (2.7)-(2.13) are the basis of our model 2. The rate constants are known from the literature as given in Table 2.1. Since the hydrolysis was shown to be the dominant decay

Table 2.1: Parameters of model 2

| Parameter | Determined by |
|---|---|
| $k_1 = 100\,\mathrm{s}^{-1}$ | MipZ - ATP binding rate constant is $10^5\,\mathrm{s}^{-1}\mathrm{M}^{-1}$ and [ATP] = 1 mM |
| $k_2 = 2\,\mathrm{s}^{-1}$ | directly measured |
| $k_3 = 5\,\mu\mathrm{M}^{-1}\mathrm{s}^{-1}$ | $K_\mathrm{D} = 1.55\,\mu$M (Thanbichler and Shapiro, 2006b) |
| $k_4 \approx 10\,\mathrm{s}^{-1}$ | Mutant G14V is diffusion limited |
| $k_5 = 1.5\,\mathrm{mM}^{-1}\mathrm{s}^{-1}$ | $K_\mathrm{D} = 8\,\mu$M |
| $k_6 = 0$ | |
| $k_7 = 65\,\mathrm{s}^{-1}$ | $K_\mathrm{D} \simeq 130\,$nM, $k_9 = 0.67\,\mathrm{min}^{-1}$, [DNA] = 16 mM and 20 nucleotides per MipZ |
| $k_8 = 0$ | |
| $k_9 = 0.67\,\mathrm{min}^{-1}$ | directly measured |

path for the dimers, $k_6$ equals zero. In addition, the MipZ dimers do not dissociate from DNA without hydrolysis, therefore $k_8 = 0$.

We implemented these reactions in our computer simulations and calculated the profile of $c_\mathrm{MipZ}(x)$. The results are shown in Figure 2.3 (A). The $c_\mathrm{MipZ}(x)$ profiles from this Figure do show two localized maxima at the cell poles but also a wide plateau in the bulk of the cell. This is in contrast to the continuously decreasing $c_\mathrm{MipZ}(x)$ of model 1 (see Figure 2.1) and more importantly, in contrast to the experimental findings (Thanbichler and Shapiro, 2006b). To understand the formation of the plateau we show in Figure 2.3 (B) the concentration profiles of the different MipZ species that contribute to $c_\mathrm{MipZ}(x)$. Only those MipZ species are plotted that exist at considerable amount, namely the free ATP bound monomers, the ParB bound monomers and the DNA bound dimers. The number of these molecules in the simulations are 650, 180 and 80, respectively. Thus, there is only a comparably small number DNA bound dimers, which is the functionally active form of MipZ.

The concentrations of DNA·$(\mathrm{MipZ{\cdot}ATP})_2$ and MipZ·ATP are almost constant over the whole cell where the concentration of ParB·MipZ·ATP shows a sharp peak near the cell poles. This can be interpreted by considering two different mechanisms. First the MipZ molecules are bound and are released by ParB at high rates ($k_4 = 10\,\mathrm{s}^{-1}$). The forward and backward reaction runs into an equilibrium like an adsorption equilibrium at any interface where the desorption and adsorption rates are the same. That is the number of bound and released molecules per time are the same and the reactions at the interface (in this case the ParB cluster) can be neglected for the rest of the reactions. These reactions are position independent and therefore we get the constant concentration profile for DNA·$(\mathrm{MipZ{\cdot}ATP})_2$ and MipZ·ATP seen in Figure 2.3 (B). We want to support this finding by a toy model, that describes binding and unbinding of MipZ to and from ParB given in the next section.

Finally in this section we want to point out that the MipZ mutant G14V, which is unable

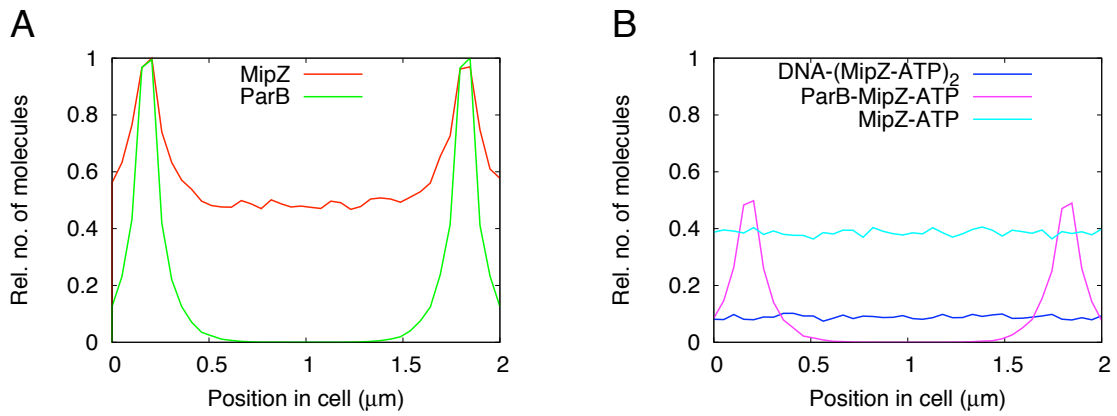


Figure 2.3: Profiles of molecules resulting from model 2. (A): The profile of MipZ, $c_{\mathrm{MipZ}}(x)$ in the cell is shown in green, ParB concentration profile in red. The contributions of the respective MipZ species are shown in (B). The cyan and magenta lines show free and ParB bound MipZ·ATP monomers, respectively. DNA bound MipZ dimers are shown in blue. The ADP bound form of MipZ, ParB bound Dimers and the free dimers are present at less than 10 copies in the cell and not included in the figure.

to form dimers shows a $c_{\mathrm{MipZ}}(x)$ gradient similar to the one shown in Figure 2.3 (A). This seems to be a hint that in our model 2 something is missing in the reactions in which the dimers are involved.

## 2.4 Toy Model: capture and release at poles

In the previous section, we have seen that model 2 fails to show a gradient-like behavior of the concentration of MipZ although there are peaks of ParB bound MipZ at the cell poles. As mentioned above, these peaks follow from a kind of adsorption equilibrium which does not influence the processes in the bulk phase of the cell. The desorption and the adsorption rates are the same independent on the forward and back reaction rate constants $k_3$ and $k_4$ in reactions (2.12) and (2.13). Therefore the reactions (2.12) and (2.13) have not to be considered for the processes in the bulk phase.

To illustrate the reactions at the cell poles, we use the toy model sketched in Figure 2.4. We consider one molecule species, MipZ, that freely diffuses within the cell. At the poles, it can bind to the membrane with a rate constant $k_+$, and subsequently be released with rate constant $k_-$. We simulated the toy model on a 2D grid of size $50 \times 100$ mesh points with initially 50000 equally distributed molecules. Figure 2.5 shows the stationary behavior using $k_+ = 0.1s^{-1}$ and $k_- = 0.01s^{-1}$. As illustrated in Figure 2.5, there is no concentration gradient

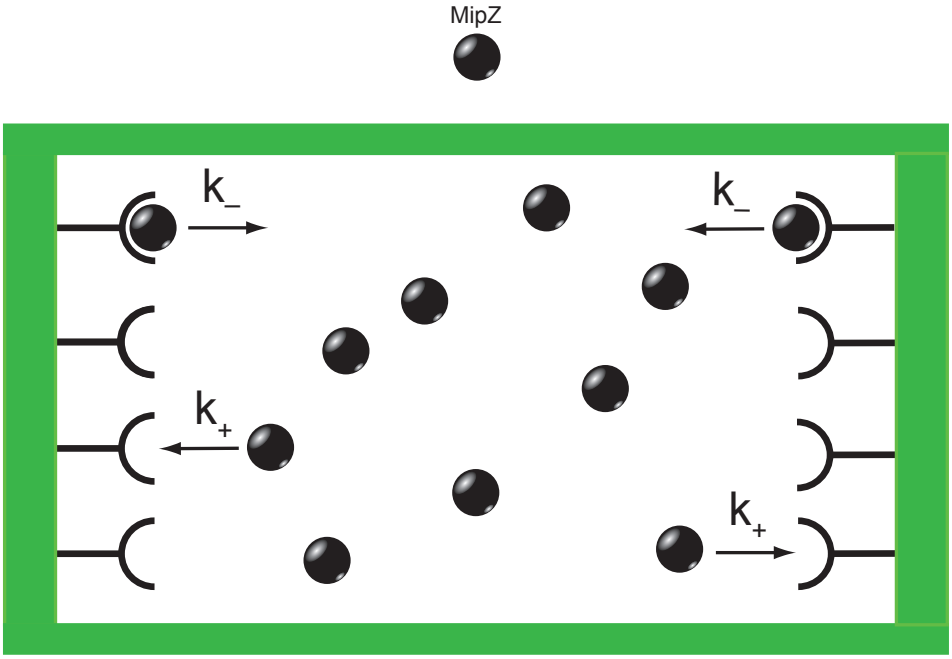


Figure 2.4: Toy Model: MipZ diffuses freely in the cell. At the poles, it can attach to the membrane with a rate constant $k_+$, and detach from the membrane with a rate constant $k_-$

in the system.

At the poles, the concentration of MipZ shows a sharp peak and in the bulk the concentration is constant. This sharp peak can be considered a jump rather than a continuous gradient. This is due to the fact that the molecules in the bulk diffuse freely and hence distribute equally within the cell. At the poles, we have the following rate equation:

$$\frac{d}{dt}c_\mathrm{b} = k_+ c_\mathrm{f} - k_- c_\mathrm{b}. \tag{2.14}$$

$c_\mathrm{f}$ and $c_\mathrm{b}$ are concentrations of free and bound MipZ molecules, respectively. By setting the time derivative to zero, equation 2.14 easily tells us the ratio of free to bound molecules in the steady state:

$$c_\mathrm{b} = \frac{k_+}{k_-} c_\mathrm{f}. \tag{2.15}$$

For $k_+ = 0.1\,\mathrm{s}^{-1}$ and $k_- = 0.01\,\mathrm{s}^{-1}$, there are ten times as many bound molecules as free ones. The same holds for the numerical simulation shown in Figure 2.5.

In conclusion, the toy model showed that if a molecule is bound and released in the polar regions of the cell, its concentration does not show a gradient-like behavior but only a peak of

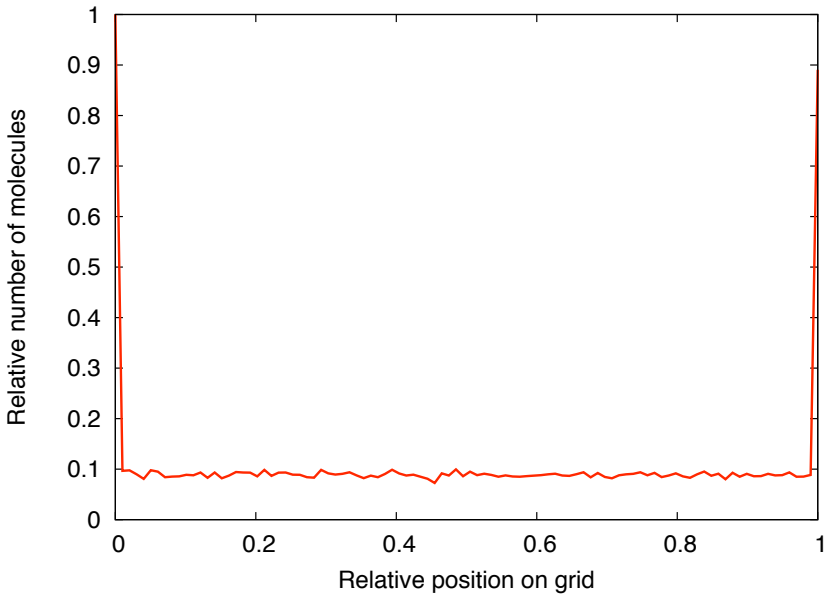


Figure 2.5: Simulation Results of the Toy Model. In this case $c_\mathrm{b} = 10c_\mathrm{f}$, thus the concentration of the bound molecules is ten times as high as the concentration of free molecules. The free molecules distribute equally in the cell.

the adsorbed molecules. The flux of molecules detaching from the pole $j_\mathrm{out}$ is given by:

$$j_\mathrm{out} = k_- c_\mathrm{b}. \tag{2.16}$$

In the steady state, we can use equation (2.15) to see:

$$k_- c_\mathrm{b} = k_+ c_\mathrm{f} = j_\mathrm{in} \tag{2.17}$$

thus, the fluxes of the source and the sink in the steady state are equally high and there is no resulting flux left that could give rise to a gradient. In other words, the source and the sink for MipZ are equally strong, only the height of the peak at the interface is set by the rate constants $k_+$ and $k_-$.

## 2.5 Model 3: ParB as an enzyme

In the previous sections we have seen that the chemical reactions in the cell for which the rate constants are known can not explain the formation of a gradient of the concentration of MipZ, $c_\mathrm{MipZ}(x)$. Possibly, one or more reactions are missing which influences the composition of the

different MipZ species in the bulk. Furthermore, it seems that the behavior of the dimers at the cell poles play a decisive role for $c_{\mathrm{MipZ}}(x)$. One possibility could be that ParB changes the equilibrium of the dimerization reaction of MipZ. However, it was found experimentally that this is not true. But it might be that ParB acts catalytically and accelerates the dimerization reaction without changing the position of the equilibrium. This assumption that ParB acts like an enzyme for MipZ dimerization is the key feature of our model 3. Before introducing model 3 quantitatively, we will make some reasonable simplifications concerning the reactions in model 2 to keep the analysis as simple as possible.

### 2.5.1 Simplification steps

The complete model 2 with all its reactions (2.7)-(2.13) is rather complicated and the parameter space is huge. However, we can ignore some interactions because they only cause minor changes in the concentration of the molecules in the system.

First, we will consider the ADP bound form of MipZ. This molecule is involved in the nucleotide exchange reaction of MipZ, reaction (2.11)

$$\mathrm{MipZ}\cdot\mathrm{ADP} \underset{k_2}{\overset{k_1}{\rightleftharpoons}} \mathrm{MipZ}\cdot\mathrm{ATP}$$

as well as in the hydrolysis reactions (2.9), and (2.10):

$$\begin{aligned} (\mathrm{MipZ}\cdot\mathrm{ATP})_2 &\xrightarrow{k_9} 2\ \mathrm{MipZ}\cdot\mathrm{ADP} \\ \mathrm{DNA}\cdot(\mathrm{MipZ}\cdot\mathrm{ATP})_2 &\xrightarrow{k_9} 2\ \mathrm{MipZ}\cdot\mathrm{ADP} + \mathrm{DNA}. \end{aligned}$$

The ADP bound monomer is produced in reactions with rate constants $k_2$ and $k_9$ and consumed with rate constant $k_1$. Since $k_1 \gg k_2 \gg k_9$, the ADP bound MipZ monomer is immediately converted into the ATP form, whenever it is formed. The large magnitude of $k_1$ results from the high ATP concentration in the cell. As a consequence, the ADP form of MipZ hardly exists in the cell and therefore we neglect this form of MipZ and consider only one monomeric form of MipZ, MipZ·ATP.

Second, model 2 includes the binding of MipZ to ParB and the rate constants for this reaction $k_3$ and $k_4$ are measured. Now we want to add an enzyme-catalyzed reaction, based on the following consideration. It is known that ParB homologs in other organisms form dimers (Funnell, 1991; Bartosik et al., 2004; Leonard et al., 2004). If this is also the case in *C. crescentus*, these ParB dimers could thus bind one MipZ molecule,

$$\mathrm{MipZ} + \mathrm{ParB} \underset{k_4}{\overset{k_3}{\rightleftharpoons}} \mathrm{ParB}\cdot\mathrm{MipZ} \tag{2.18}$$

and subsequently another MipZ molecule with the same rate constant,

$$\mathrm{ParB} \cdot \mathrm{MipZ} + \mathrm{MipZ} \quad \underset{k_4}{\overset{k_3}{\rightleftharpoons}} \quad \mathrm{ParB} \cdot \mathrm{MipZ} \cdot \mathrm{MipZ}. \tag{2.19}$$

When two MipZ molecules are bound to ParB, the probability of dimerization may be higher than when two MipZ molecules collide in the bulk because of steric and bonding effects,

$$\mathrm{ParB} \cdot \mathrm{MipZ} \cdot \mathrm{MipZ} \quad \underset{\tilde{k}_{12}}{\overset{\tilde{k}_{11}}{\rightleftharpoons}} \quad \mathrm{ParB} + (\mathrm{MipZ})_2\,. \tag{2.20}$$

The reactions (2.18) - (2.20) can be implemented in the simulations by only one effective catalytic reaction,

$$\mathrm{ParB} + 2\ \mathrm{MipZ} \quad \underset{k_{12}}{\overset{k_{11}}{\rightleftharpoons}} \quad \mathrm{ParB} + (\mathrm{MipZ})_2\,, \tag{2.21}$$

which describes the MipZ dimerization with ParB acting as a catalyst. Since a catalyst is not changing the equilibrium of the reaction, the following condition is fulfilled:

$$\frac{k_{12}}{k_{11}} = K_\mathrm{D} = \frac{k_9}{k_5}, \tag{2.22}$$

where $K_\mathrm{D}$ is the dissociation constant of the MipZ dimer. As a consequence, the new enzyme reaction only introduces one unknown rate constant, because the ratio of $k_{12}$ to $k_{11}$ is fixed.

### 2.5.2 Introduction of model 3

The experimental findings listed in section 2.3, the assumed catalytic property of ParB and the simplifications discussed in the previous paragraph are the basis of our model 3. The key features of the model are two properties. First, MipZ dimers are not only formed directly from two monomers (reaction (2.7)) like in model 2, but dimerization is also catalyzed by ParB (reaction (2.21)).

$$2\ \mathrm{MipZ} \quad \underset{k_9}{\overset{k_5}{\rightleftharpoons}} \quad (\mathrm{MipZ})_2 \tag{2.23}$$

$$\mathrm{ParB} + 2\ \mathrm{MipZ} \quad \underset{k_{12}}{\overset{k_{11}}{\rightleftharpoons}} \quad \mathrm{ParB} + (\mathrm{MipZ})_2$$

Second, considering the dimerization of MipZ only the dimers can bind to DNA

$$(\mathrm{MipZ})_2 \quad \xrightarrow{k_7} \quad \mathrm{DNA} \cdot (\mathrm{MipZ})_2 \tag{2.24}$$

$$\mathrm{DNA} \cdot (\mathrm{MipZ})_2 \quad \xrightarrow{k_9} \quad 2\ \mathrm{MipZ} \tag{2.25}$$

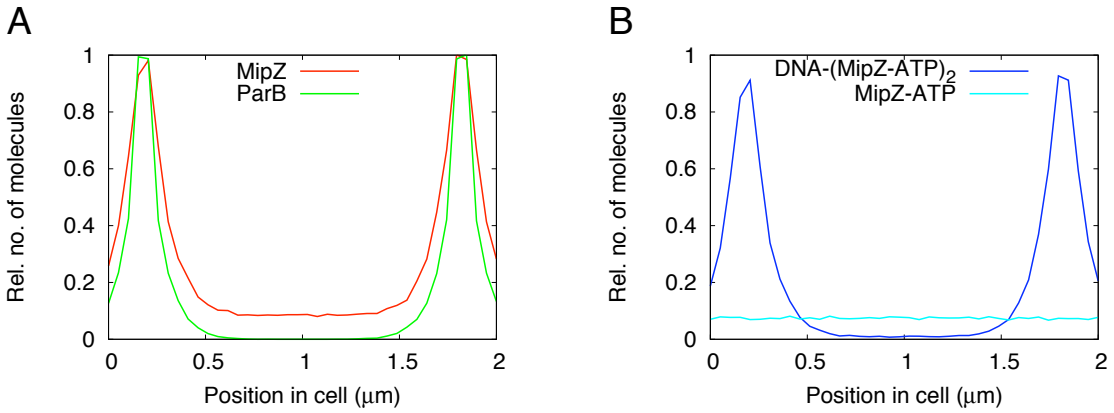


Figure 2.6: Simulation results of model 3. (A) Concentration profile of MipZ, $c_{\mathrm{MipZ}}(x)$, is shown in red and ParB concentration profile is shown in green. (B) Concentration profiles of different MipZ species: In the cell there are in total 400 dimers (blue), all bound to DNA and 200 monomers (cyan). The monomers distribute equally. See text for parameters.

The rate constants $k_5$, $k_7$, and $k_9$ are known experimentally, and because of the condition

$$K_{\mathrm{D}} = \frac{k_9}{k_5} = \frac{k_{12}}{k_{11}}, \tag{2.26}$$

only rate constant of the catalysis reaction is unknown. We chose this last free parameter to be $k_{12} = 0.29\,\mu\mathrm{M}^{-1}\mathrm{s}^{-1}$ to perform a simulation. The effect of different values of $k_{12}$ is discussed below in section 2.6.3. For our simulation, we used the same initial distribution of molecules as in model 2. After equilibration of the system, there are 400 dimers all bound to DNA, and 200 MipZ monomers. For comparison: simulations of model 2 (see section 2.3) yield only 80 dimers. This distinct difference is caused by the interplay of a) the faster reaction of the dimerization at the cell poles and b) the fact that only the dimers bind to DNA. These combined effects create a sink for the monomers near the cell poles. Quantitatively, the profile of the concentration of MipZ, $c_{\mathrm{MipZ}}(x)$, is shown in Figure 2.6 (A) (red curve). The ParB position is shown in green. The dimers are predominantly formed near the cell poles and diffuse into the bulk. Their free diffusion is hindered by the interaction with the DNA. The free monomers on the other hand are distributed equally in the cell. This leads to a background of MipZ monomers in the cell center, as seen in Figure 2.6 (B).

The data given in Figure 2.6 (A) agree quite well with the experimental data and therefore, model 3 can verify a gradient-like behavior of $c_{\mathrm{MipZ}}(x)$. In the following section 2.5.3, we discuss the mechanism behind this behavior in more detail.

Subsequently in sections 2.6.1 - 2.6.3, we will investigate the influence of the magnitude of the rate constants on the behavior of the system. Finally in section 2.6.4, we propose how the

unknown rate constants $k_{11}$ and $k_{12}$ of the system can be determined by experiment.

### 2.5.3 Mechanism of gradient formation

According to the catalytic effect of ParB, the dimerization equilibrium of MipZ is set faster at the cell poles than in the bulk. In the previous section we have pointed out that this assumption results in a smaller number of monomers although ParB does not change the position of the equilibrium

$$2\ \mathrm{MipZ} \leftrightharpoons (\mathrm{MipZ})_2\,.$$

But as DNA only reacts with $(\mathrm{MipZ})_2$, the respective dissociation constants $K_{\mathrm{pole}}$ and $K_{\mathrm{bulk}}$ differ as will be outlined next.

In the bulk, there is no ParB, so we have to consider the following reactions:

$$2\ \mathrm{MipZ} \underset{k_9}{\overset{k_5}{\rightleftharpoons}} (\mathrm{MipZ})_2 \xrightarrow{k_7} \mathrm{DNA}\cdot(\mathrm{MipZ})_2 \xrightarrow{k_9} \mathrm{MipZ}. \tag{2.27}$$

As there are two different species of dimers, the DNA bound and the free ones, the local dissociation constant is given by:

$$K_{\mathrm{bulk}} := \left(\frac{m^2}{m_2+b}\right)_{\mathrm{bulk}} \tag{2.28}$$

$m$, $m_2$ and $b$ denote the concentrations of MipZ, $(\mathrm{MipZ})_2$ and DNA·$(\mathrm{MipZ})_2$, respectively. From the reaction scheme (2.27), we get the following steady state equation for the MipZ dimer concentration:

$$\frac{dm_2}{dt} = 0 = k_5 m^2 - m_2\,(k_7+k_9)\,. \tag{2.29}$$

For the concentration of DNA bound dimers it is true that:

$$\frac{db}{dt} = 0 = k_7 m_2 - k_9 b. \tag{2.30}$$

It follows:

$$b = m_2 \frac{k_7}{k_9} \tag{2.31}$$

and thus,

$$m_2 + b = m_2\left(1+\frac{k_7}{k_9}\right) \tag{2.32}$$

$$\Rightarrow m_2 = (m_2+b)\,\frac{k_9}{k_9+k_7}. \tag{2.33}$$

Insertion of (2.33) into (2.29) yields:

$$K_{\text{bulk}} = \left(\frac{m^2}{m_2 + b}\right)_{\text{bulk}} = \frac{k_9}{k_5} = K_{\text{D}}. \tag{2.34}$$

Hence, we can see that the equilibrium between monomers and dimers is not changed in the presence of DNA. This is due to the fact, that DNA bound dimers decay with rate constant $k_9$, just like free dimers.

At the poles on the other hand, we have to consider additionally the reactions with ParB,

$$\text{ParB} + 2\ \text{MipZ} \quad \underset{k_{12}}{\overset{k_{11}}{\rightleftharpoons}} \quad \text{ParB} + (\text{MipZ})_2 \tag{2.35}$$

$$2\ \text{MipZ} \quad \underset{k_9}{\overset{k_5}{\rightleftharpoons}} \quad (\text{MipZ})_2 \tag{2.36}$$

$$(\text{MipZ})_2 \quad \xrightarrow{k_7} \quad \text{DNA} \cdot (\text{MipZ})_2 \tag{2.37}$$

$$\text{DNA} \cdot (\text{MipZ})_2 \quad \xrightarrow{k_9} \quad 2\ \text{MipZ}. \tag{2.38}$$

Since ParB is assumed to act like an enzyme, it is true that: $k_{11}p \gg k_5$ and $k_{12}p \gg k_9$, where $p$ is the ParB concentration. As a consequence, we can neglect reaction (2.36).

For these reactions, the steady state equation for free dimers is:

$$\frac{dm_2}{dt} = 0 = k_{11}pm^2 - m_2\left(k_7 + k_{12}p\right). \tag{2.39}$$

For DNA bound dimers, the equation (2.33) for the bulk holds, and we can insert it into (2.39) to get:

$$K_{\text{pole}} = \left(\frac{m^2}{m_2 + b}\right)_{\text{pole}} = \frac{k_9\left(k_7 + k_{12}p\right)}{k_{11}p\left(k_7 + k_9\right)}. \tag{2.40}$$

Together with:

$$\frac{k_{12}}{k_{11}} = K_{\text{D}} \tag{2.41}$$

it follows that:

$$K_{\text{pole}} = K_{\text{D}}\frac{\frac{k_7}{k_{12}p} + 1}{\frac{k_7}{k_9} + 1}. \tag{2.42}$$

Now we can compare the dissociation constants in the bulk and at the poles using (2.34):

$$\frac{K_{\text{pole}}}{K_{\text{bulk}}} = \left(\frac{k_7}{k_{12}p} + 1\right)\left(\frac{k_7}{k_9} + 1\right)^{-1} \tag{2.43}$$

and since $k_{12}p \gg k_9$:

$$K_{\text{pole}} < K_{\text{bulk}}. \tag{2.44}$$

As a consequence, there are more dimers at the poles than in the bulk. We can also see that

DNA binding is responsible for this fact: If $k_7 = 0$, equation (2.43) shows that $K_{\text{pole}} = K_{\text{bulk}}$. The DNA alters the dissociation constant by removing dimers from the solution. This can be understood by comparing the situations $k_7 = 0$, and $k_7 = \infty$.

If $k_7 = 0$, no dimers bind to DNA. The probability that a dimer forms is higher at the poles than in the bulk, because ParB promotes dimerization. However, the probability that a dimer decays to two monomers is also higher at the poles, because ParB acts like an enzyme and does not shift the equilibrium of the dimerization reaction. As a consequence, the local dissociation constants at the poles and in the bulk are equal.

If $k_7 = \infty$, every dimer that is formed immediately binds to DNA. As a consequence, it is not transformed into two monomers by ParB, but binds to DNA instead. Subsequently, it decays with rate constant $k_9$. This rate constant is smaller than that of the catalysis reaction $k_{12}p$. Thus, by binding of MipZ, the DNA removes dimers, that can not be transformed back to monomers by ParB.

Note that large $k_7$ can be accomplished by high DNA concentrations, because it is the effective rate constant for the dimer-DNA binding. In *C. crescentus* this is the case, the DNA concentration is 16 mM and exceeds the concentration of the other participating molecules by far.

## 2.6 Applications of model 3

In this section we want to show how the system is affected by changing various parameters. Especially two aspects are interesting: The prediction of the behavior of mutant proteins and the system robustness. Point mutations at the binding site of a protein can alter the binding rate constants. Thus, a prediction made by scanning the magnitude of these rate constants could be experimentally testable. In addition, observation of the system behavior with changing parameters gives us a measure for the stability of the system. Robustness against parameter changes is an extremely important issue for a biological system that is constantly exposed to noise.

### 2.6.1 Influence of DNA binding rate constant

The DNA binding rate constant $k_7$ in reaction 2.37 has an influence on the height of the maxima of the gradient as well as the size of the monomer concentration, seen as background intensity on fluorescence pictures.

This influence can be understood as follows: when a dimer is formed, the rate constant $k_7$ determines the mean distance $\langle x \rangle$ a dimer diffuses before it binds to DNA. For $k_7 = 65\,\text{s}^{-1}$ and a typical diffusion constant of a protein in *C. crescentus* of $D \approx 10\,\mu\text{m}^2\text{s}^{-1}$ (Deich et al.,

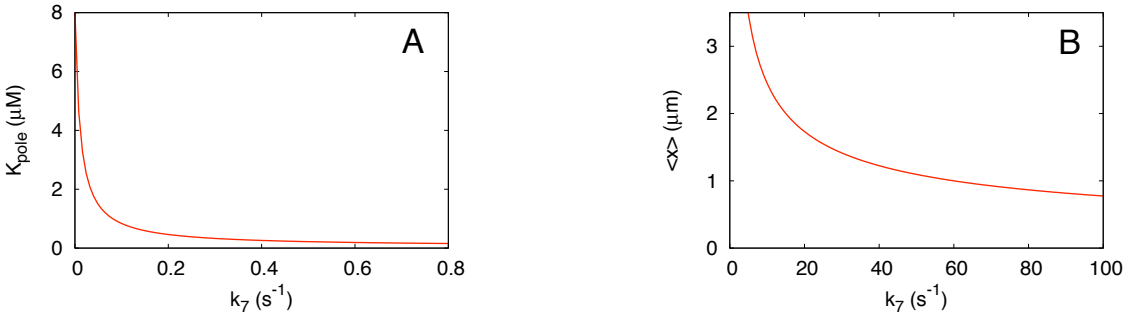


Figure 2.7: (A) Influence of DNA binding rate constant $k_7$ the local dissociation constant $K_{\text{pole}}$ as given in equation (2.42). Measurements showed that $k_7 = 65\,\text{s}^{-1}$, thus $K_{\text{pole}}$ is clearly saturated. (B) Influence of $k_7$ on the mean length that a dimer diffuses before binding to DNA $\langle x \rangle$, eq. (2.45). Parameters are $p = 6.6\,\mu\text{M}$ and $k_{12} = 0.28\,\mu\text{M}^{-1}\text{s}^{-1}$

2004), a dimer diffuses an average length $\langle x \rangle$ of:

$$\langle x \rangle = \sqrt{\frac{6D}{k_7}} \approx 1\,\mu\text{m}. \tag{2.45}$$

As diffusion and binding is a poison process, equation (2.45) implies that 63% of the dimers that are formed at the pole bind to DNA in the same cell half. On the other hand, since a dimer decays with rate constant $k_9 = 0.011\,\text{s}^{-1}$, it diffuses an average length of $\langle x \rangle \approx 70\,\mu\text{m}$ before it decays. Thus, the diffusion of dimers is slowed down by DNA, and a gradient becomes sharp. The dependence of mean dimer diffusion length $\langle x \rangle$ on $k_7$ is shown in Figure 2.7 (B). For $k_7 = 65\,\text{s}^{-1}$, we get a sharp gradient as seen in Figure 2.6 (A).

In addition to the sharpness of the gradient, the ratio of DNA bound to free dimers is set by $k_7$. As explained in section 2.5.3, binding to DNA prevents dimers from being converted to monomers by ParB. Thus, the ratio of bound to free dimers in turn influences the ratio of monomers to dimers: The lower $k_7$, the more monomers there are. This fact is illustrated in figure 2.7 (A). The dissociation constant at the pole decreases with increasing DNA binding rate constant. For $k_7 = 0$, $K_{\text{pole}}$ is the same as in bulk: $K_{\text{pole}} = K_{\text{D}} = 8\,\mu\text{M}$. With growing $k_7$, the local dissociation constant converges to

$$\lim_{k_7 \to \infty} K_{\text{pole}} = K_{\text{D}} \frac{k_9}{k_{12} p}. \tag{2.46}$$

As we can see in Figure 2.7 (A), the measured value of $k_7 = 65\,\text{s}^{-1}$ is far in the saturated regime. The dissociation constant at the poles $K_{\text{pole}}$ in fact is set by $k_{12}$.

The influence of $k_7$ on the mean diffusion length of dimers seems to be more critical as

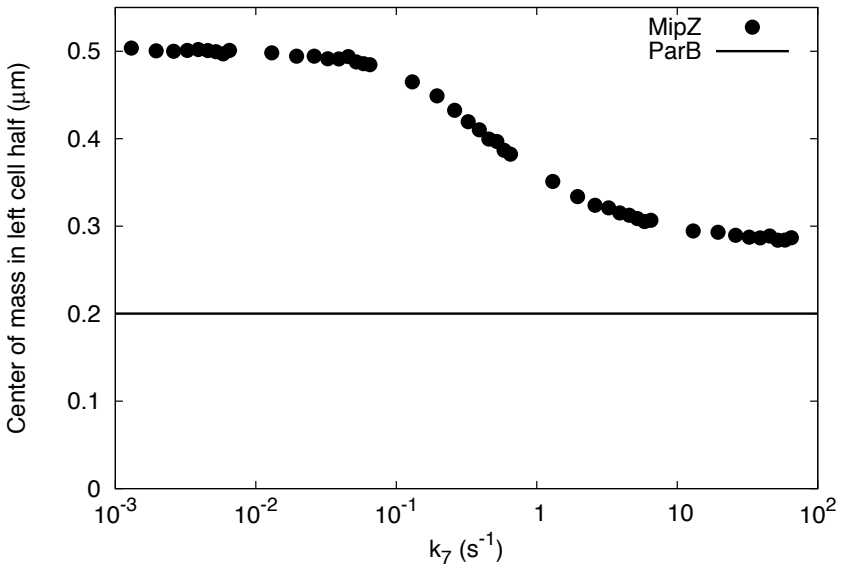


Figure 2.8: The center of mass in the left cell half of MipZ (dots) as a function of DNA binding rate constant $k_7$. The mean position of ParB is $0.2\,\mu$m (solid line). For selected parameter values, the respective gradients are shown in Figure 2.9. The effective DNA binding rate constant of the wild-type is $k_7 = 65\,\mathrm{s}^{-1}$.

outlined in Figure 2.7 (B). If $k_7$ is too small, say $15\,\mathrm{s}^{-1}$, the mean distance of a dimer that formed at the pole would be $2\,\mu$m, the cell length.

As introduced in section 2.2, the center of mass in the left cell half $C$, defined in eq. (2.5) gives a measure of the shape of the gradient. To quantify the influence of the DNA binding rate constant, we performed simulations of the system with varying $k_7$ and measured the center of mass in the left cell half. The result of this parameter study is given in Figure 2.8. For selected binding strengths, the respective MipZ concentration profiles are shown in Figure 2.9. As expected, the gradient vanishes if $k_7$ is too small. As explained above, the vanishing of the MipZ concentration gradient for small $k_7$ is due to a combination of a shift in dimer-monomer equilibrium and free diffusion of dimers through the whole cell.

Taken the results of our parameter study, the gradient seems to be robust towards alterations in DNA binding rate constant.

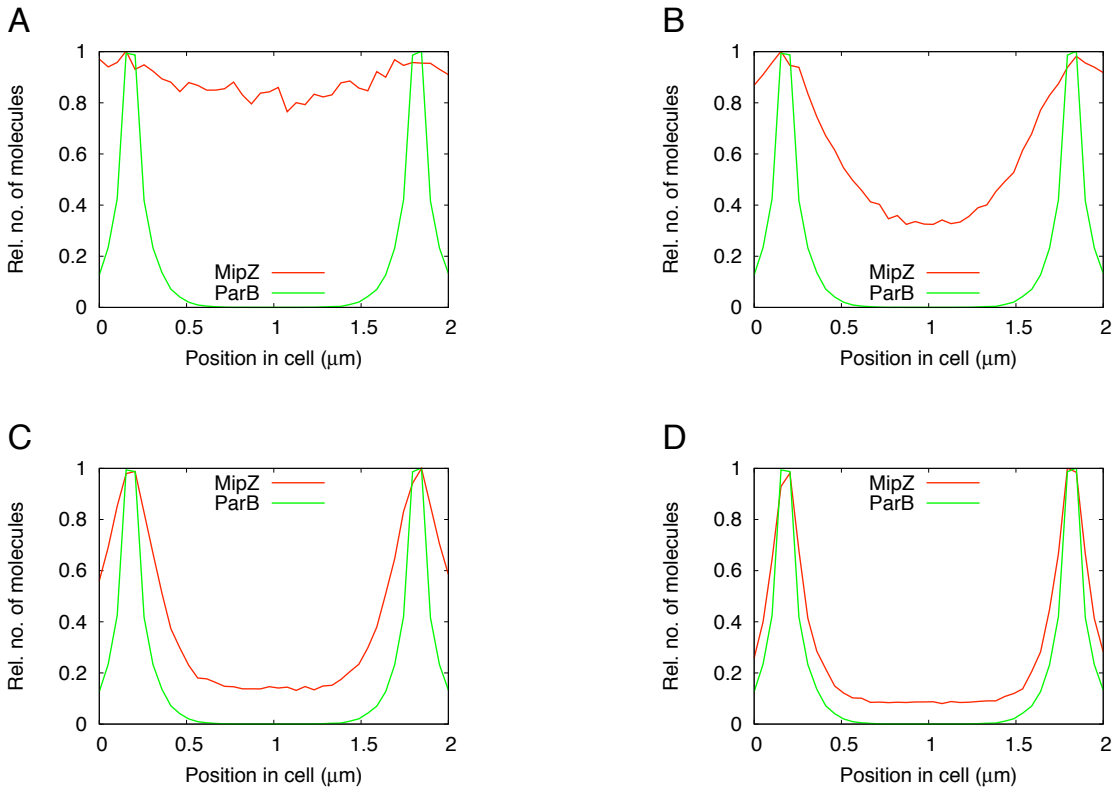


Figure 2.9: The relative number of molecules as function of intracellular position. MipZ is shown in red and ParB is shown in green. The effective DNA binding rate constant $k_7$ is varied and the center of mass in the left cell half $C$ is determined as given by eq. (2.5). A: $k_7 = 0.065\,\mathrm{s}^{-1}$, $C = 0.48\,\mu$m. B: $k_7 = 0.65\,\mathrm{s}^{-1}$, $C = 0.38\,\mu$m. C: $k_7 = 0.65\,\mathrm{s}^{-1}$, $C = 0.30\,\mu$m. D: $k_7 = 65\,\mathrm{s}^{-1}$, $C = 0.28\,\mu$m.

### 2.6.2 Influence of dimerization rate constant

In addition to a MipZ point mutation that alters the binding strength to DNA, it is also possible, that a mutation in the MipZ-MipZ binding site changes the dimerization reaction. In this case, the dissociation constant $K_\mathrm{D} = k_9/k_5$, and thus the monomer-dimer equilibrium changes.

Since ParB in our model is considered to act like an enzyme, the condition (2.26) has to hold also for a MipZ mutant. To make the analysis as simple as possible, we fixed the two parameters $k_9 = 0.011\,\mathrm{s}^{-1}$ and $k_{11} = 0.036\,\mu\mathrm{M}^{-2}\mathrm{s}^{-1}$, the values at which we found the stable MipZ gradients shown in section 2.5.2. Then we performed simulations of the system with varying $k_5$, and adjusted $k_{12}$ according to eq. (2.26).

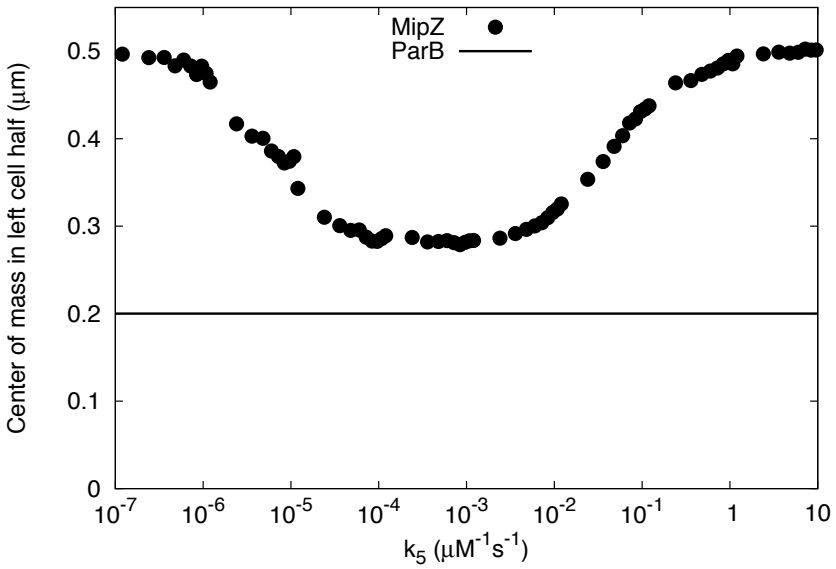


Figure 2.10: The center of mass in left cell half of MipZ (dots) is shown for varying dimerization rate constants $k_5$. The mean ParB position is $0.2\,\mu$m (solid line). Catalysis rate constant is $k_{11} = 0.036\mu M^{-2}s^{-1}$ and $k_9 = 0.011s^{-1}$. $k_{12}$ is adjusted according to eq. (2.26). The measured WT value is at $k_5 = 1.5 \cdot 10^{-3}\mu M^{-1}s^{-1}$.

The results of this parameter scan are shown in Figure 2.10. Obviously, the gradient gets lost at low as well as high dimerization rate constants $k_5$, because a center of mass in the left cell half of $0.5\,\mu$m corresponds to an equal distribution of $c_{\mathrm{MipZ}}(x)$.

For small dimerization rate constants, the ratio of monomers to dimers is too high. In a cell with $k_5 = 10^{-7}\,\mu\mathrm{M}^{-1}\mathrm{s}^{-1}$, 940 out of the 1000 MipZ molecules are monomers. Since the monomers distribute equally in the cell, The gradient is lost.

High dimerization rates on the other hand destroy the gradient, because $K_{\mathrm{bulk}}$ is too high. This can be understood as follows: If

$$k_5 > k_{11}p, \tag{2.47}$$

the monomers are not preferentially formed at the poles anymore. In this case, dimers form everywhere in the cell at the same probability, resulting in an equal distribution of dimers. In a cell with $k_5 = 10\,\mu\mathrm{M}^{-1}\mathrm{s}^{-1}$, 990 out of the 1000 MipZ molecules are dimeric.

In our simulations, there are 200 ParB molecules at each pole, normally distributed with a standard deviation of $0.2\,\mu$m. Hence, the concentration of ParB can be estimated to:

$$p = 4000\,\mu\mathrm{m}^{-3} = 6.6\,\mu\mathrm{M}. \tag{2.48}$$

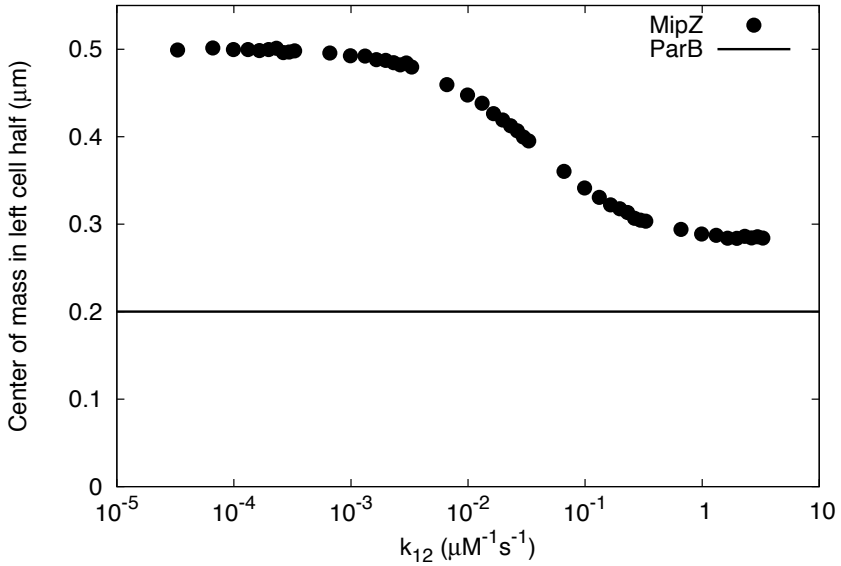


Figure 2.11: Center of mass in left cell half of MipZ (dots) for varying ParB catalysis rate constants. The mean position of ParB is $0.2\,\mu$m (solid line). All other parameters were measured by experiment and are given in Table 2.1.

As a consequence, condition (2.47) is fulfilled at $k_5 \approx 0.2\,\mu\mathrm{M}^{-1}\mathrm{s}^{-1}$. This is supported by Figure 2.10, because $k_5 = 0.2\,\mu\mathrm{M}^{-1}\mathrm{s}^{-1}$ is the lower side of the right plateau, where the gradient is lost.

The measured wild-type value of $k_5 = 1.5 \cdot 10^{-3}\,\mu\mathrm{M}^{-1}\mathrm{s}^{-1}$ lies in the regime of minimal center of mass. Thus, at the wild-type value, the gradient is comparably strong.

### 2.6.3 Influence of ParB catalysis

Most of the parameters of our model 3 are known experimentally. The only free parameter is the catalysis rate constant of ParB. Since ParB functions as an enzyme in model 3, the ratio of $k_{11}$ to $k_{12}$ is fixed. However, the value of $k_{12}$ is not known. In section 2.6.4 we will see that it could be determined by experiment to test our model. Here we wish to show the influence of this parameter on the gradient.

Figure 2.11 shows the influence of the parameter $k_{12}$ on the gradient of $c_{\mathrm{MipZ}}(x)$. If the catalysis by ParB is too week, the gradient vanishes, and the center of mass in the left cell half is $C = 0.5\,\mu$m. This can be understood by the ratio of the local dissociation constants, eq. (2.43). If it was true that $k_{12}p = k_9$, then the catalytic function of ParB would be lost.

Since the concentration of ParB in our simulations is approximately $p = 6.6\,\mu$M, the catalytic function of ParB is lost at

$$k_{12} = \frac{k_9}{p} = 0.0016\,\mu\mathrm{M}^{-1}\mathrm{s}^{-1}. \tag{2.49}$$

This is supported by Figure 2.11, because at a $k_{12}$ below this value, the gradient is vanishing and the center of mass in the left cell half saturates a value of $C = 0.5\,\mu$m.

### 2.6.4 Prediction of *in vitro* behavior

Our model 3 makes use of the assumption that ParB acts like an enzyme. In this section we will emphasize that this assumption does not contradict experimental results. In addition, we will introduce an experiment that can test the validity of this assumption, and as a consequence, either verify or discount our theory.

*In vitro*, the ATP-hydrolysis of the MipZ dimer can be detected via radioactive labeling. In particular, Kiekebusch et al. (unpublished results) measure the average turnover number for ATP hydrolysis $k_{\mathrm{app}}$ as a function of total MipZ concentration $m_{\mathrm{t}}$. As the dimers decay with the rate constant $k_9$, the average turnover number is given by:

$$k_{\mathrm{app}} = 2k_9\frac{m_2}{m_{\mathrm{t}}}. \tag{2.50}$$

The equilibrium of the reaction:

$$2\ \mathrm{MipZ} \quad \underset{k_9}{\overset{k_5}{\rightleftharpoons}} \quad (\mathrm{MipZ})_2 \tag{2.51}$$

yields a dissociation constant of:

$$K_{\mathrm{D}} = \frac{m^2}{m_2} = \frac{k_9}{k_5}. \tag{2.52}$$

Together with $m_{\mathrm{t}} = m + 2m_2$, we see that:

$$K_{\mathrm{D}}m_2 = (m_{\mathrm{t}} - 2m_2)^2\,. \tag{2.53}$$

Equation (2.53) is solved by:

$$m_2 = \frac{m_{\mathrm{t}}}{2} + \frac{K_{\mathrm{D}} - \sqrt{(K_{\mathrm{D}})^2 + 8m_{\mathrm{t}}K_{\mathrm{D}}}}{8}, \tag{2.54}$$

inserting this into (2.50) yields:

$$k_{\mathrm{app}} = 2k_9\left(\frac{1}{2} + \frac{K_{\mathrm{D}} - \sqrt{8m_{\mathrm{t}}K_{\mathrm{D}} + (K_{\mathrm{D}})^2}}{8m_{\mathrm{t}}}\right). \tag{2.55}$$

With the help of these ATPase activity curves, $K_{\mathrm{D}} = 8\,\mu$M and $k_9 = 0.011\,\mathrm{s}^{-1}$ were determined experimentally. In addition, it was shown that neither presence of DNA nor ParB changed $K_{\mathrm{D}}$

or $k_9$.

Now we wish to test the influence of ParB and DNA on $k_{\text{app}}$ if ParB acts like an enzyme, which was necessary to our model 3, to see if the above observation contradicts our model. The reactions we have to take into account are the MipZ dimerization that is catalyzed by ParB,

$$\text{ParB} + 2\ \text{MipZ} \quad \underset{k_{12}}{\overset{k_{11}}{\rightleftharpoons}} \quad \text{ParB} + (\text{MipZ})_2\,. \tag{2.56}$$

And the reactions carried out between MipZ and DNA,

$$(\text{MipZ})_2 \quad \xrightarrow{k_7} \quad \text{DNA} \cdot (\text{MipZ})_2 \tag{2.57}$$

and

$$\text{DNA} \cdot (\text{MipZ})_2 \quad \xrightarrow{k_9} \quad 2\ \text{MipZ} \tag{2.58}$$

again taken into account that the enzyme reaction of ParB considerably accelerates dimerization. Now, since both the free and DNA-bound MipZ dimers perform hydrolysis, both species contribute to the ATPase activity. If $b$ is the concentration of DNA bound monomers, then

$$k_{\text{app}} = 2\ k_9 \frac{m_2 + b}{m_{\text{t}}}. \tag{2.59}$$

The steady-state equations for reactions (2.56) - (2.58) yield:

$$0 \;=\; \frac{db}{dt} \;=\; k_7 m_2 - k_9 b \tag{2.60}$$

$$\Rightarrow b \;=\; \frac{k_7}{k_9} m_2 \tag{2.61}$$

and:

$$0 \;=\; \frac{dm_2}{dt} \;=\; k_{11} p m^2 - (k_7 + k_{12} p)\, m_2 \tag{2.62}$$

$$\Rightarrow m_2 \;=\; \frac{k_{11} p}{k_7 + k_{12} p} m^2. \tag{2.63}$$

Thus, from (2.61), (2.63) and the condition $k_{12}/k_{11} = K_{\text{D}}$ we get:

$$m_2 + b \;=\; m_2 \left(1 + \frac{k_7}{k_9}\right) \tag{2.64}$$

$$\;=\; \left(1 + \frac{k_7}{k_9}\right) \frac{k_{11} p}{k_7 + k_{12} p} m^2 \tag{2.65}$$

$$\;=\; K_{\text{D}}^{-1} \left(1 + \frac{k_7}{k_9}\right) \frac{1}{1 + \frac{k_7}{k_{12} p}} m^2 \tag{2.66}$$

$$\;=\; K_{\text{D}}^{-1} \frac{k_{12} p\,(k_9 + k_7)}{k_9\,(k_{12} p + k_7)} m^2. \tag{2.67}$$

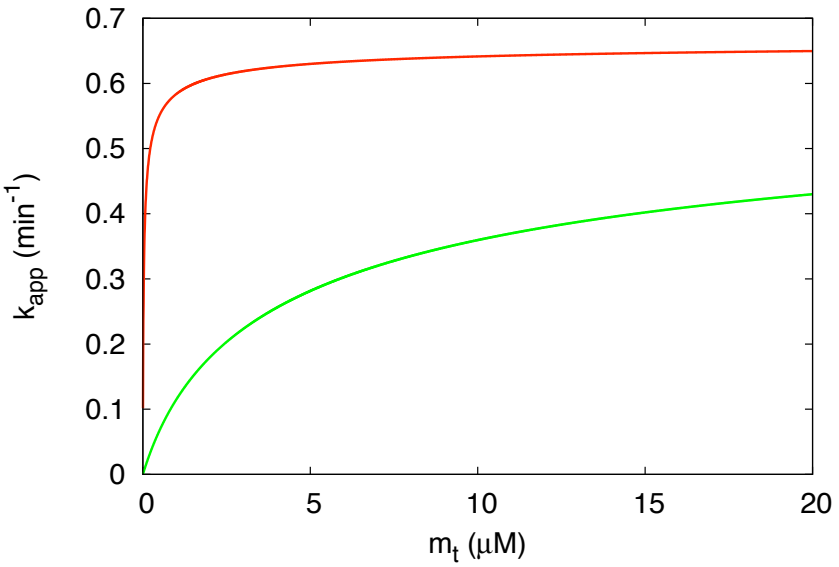


Figure 2.12: ATPase activity of MipZ as function of total MipZ concentration $m_\mathrm{t}$. The DNA concentration is $d$=1 mM. At the poles, the enzyme ParB is present at an approximate concentration of $p = 6.6\,\mu$M, these parameters yield the red curve. The green curve mimics the situation in the bulk, where ParB is absent. The physiological MipZ concentration is at $m_\mathrm{t} = 3 - 4\,\mu$M.

Where $k_7$ is the effective binding constant for MipZ to DNA assuming that DNA is present in excess, like it is the case in the cell. Here, we wish to explore the *in vitro* behavior with variable DNA concentrations. For this reason we now use $k_7 = \tilde{k}_7 d$, where $d$ is the DNA concentration.

With a modified dissociation constant $\tilde{K}_\mathrm{D}$, defined as:

$$\tilde{K}_\mathrm{D}(p,d) = K_\mathrm{D}\frac{k_9\left(k_{12}p + \tilde{k}_7 d\right)}{k_{12}p\left(k_9 + \tilde{k}_7 d\right)} \tag{2.68}$$

equation (2.67) can be written in the form:

$$\tilde{K}_\mathrm{D}(m_2 + b) = (m_\mathrm{t} - 2(m_2 + b))^2 . \tag{2.69}$$

This is the same type of equation as (2.53) for the total dimer concentration $m_2 + b$. Together with (2.59), the ATPase activity curves of MipZ in the presence of ParB and DNA are given

by:

$$k_{\mathrm{app}}\left(m_{\mathrm{t}}, p, d\right) = 2k_9 \left( \frac{1}{2} + \frac{\tilde{K}_{\mathrm{D}} - \sqrt{8m_{\mathrm{t}}\tilde{K}_{\mathrm{D}} + \left(\tilde{K}_{\mathrm{D}}\right)^2}}{8m_{\mathrm{t}}} \right). \tag{2.70}$$

From equation (2.68), we see that for $d = 0$ it is true that $\tilde{K}_{\mathrm{D}} = K_{\mathrm{D}}$. Thus, ParB concentration does not have an influence on the ATPase activity in absence of DNA. In the absence of ParB, dimers would decay to monomers with the rate constant $k_9$ instead of $k_{12}p$. Also for this situation, equation (2.68) gives us $\tilde{K}_{\mathrm{D}} = K_{\mathrm{D}}$. In conclusion, in the presence of either ParB or DNA, the ATPase activity of MipZ is not affected. Only when both are present at the same time, there is a cooperative influence.

This cooperative effect is illustrated in Figure 2.12. The green curve shows the ATPase activity curve in the absence of ParB, which could refer to the situation in the middle of the cell. The red curve simulates the situation at the poles with $k_{12} = 22\,\mu\mathrm{M}^{-1}\mathrm{min}^{-1}$ and $p = 6.6\,\mu\mathrm{M}$. Since the physiological MipZ concentration is $3 - 4\,\mu\mathrm{M}$, Figure 2.12 shows that the local dissociation constant $K_{\mathrm{pole}}$ is significantly lower for this set of parameters.

The influence of ParB concentration on the hydrolysis rate constant can be used to determine the free parameter $k_{12}$. Figure 2.13 shows this influence at a fixed MipZ concentration of $4\,\mu\mathrm{M}$ for various parameters $k_{12}$. If this curve was to be recorded, a fit could determine $k_{12}$ and ultimately decide if our model 3 is true or not. If there was no influence of ParB concentration on MipZ hydrolysis rate constant in the presence of DNA, ParB does not function as an enzyme, and the model is wrong.

## 2.7 Computational details

All simulations in this chapter were carried out as reaction-diffusion systems on a grid. The cell is assumed to be $2\,\mu\mathrm{m} \times 0.5\,\mu\mathrm{m} \times 0.5\,\mu\mathrm{m}$ of size. The lattice parameter was $\Delta x = 0.04\,\mu\mathrm{m}$, yielding a grid of $50 \times 12 \times 12$ reaction volumes. At the start of each simulation, 1000 MipZ monomers were placed on the lattice randomly. At position $(0.2, 0.25, 0.25)\,\mu\mathrm{m}$ and $(1.8, 0.25, 0.25)\,\mu\mathrm{m}$, we placed 200 ParB molecules each. These molecules were positioned according to a normal distribution with a standard deviation of $0.2\,\mu\mathrm{m}$ to reproduce the ParB concentration profiles measured by Thanbichler and Shapiro (2006b).

At every time step, the molecules diffuse by randomly choosing one of the six directions (up, down, left, right, front, back) and a diffusion length. This length was determined as follows: Within the length of one time step $\Delta t$, a molecule with diffusion constant $D$ travels an average distance $r$ of:

$$r = \sqrt{6D\Delta t}. \tag{2.71}$$

This is implemented by choosing an integer $j$ from a normal distribution with mean $r$. Then,

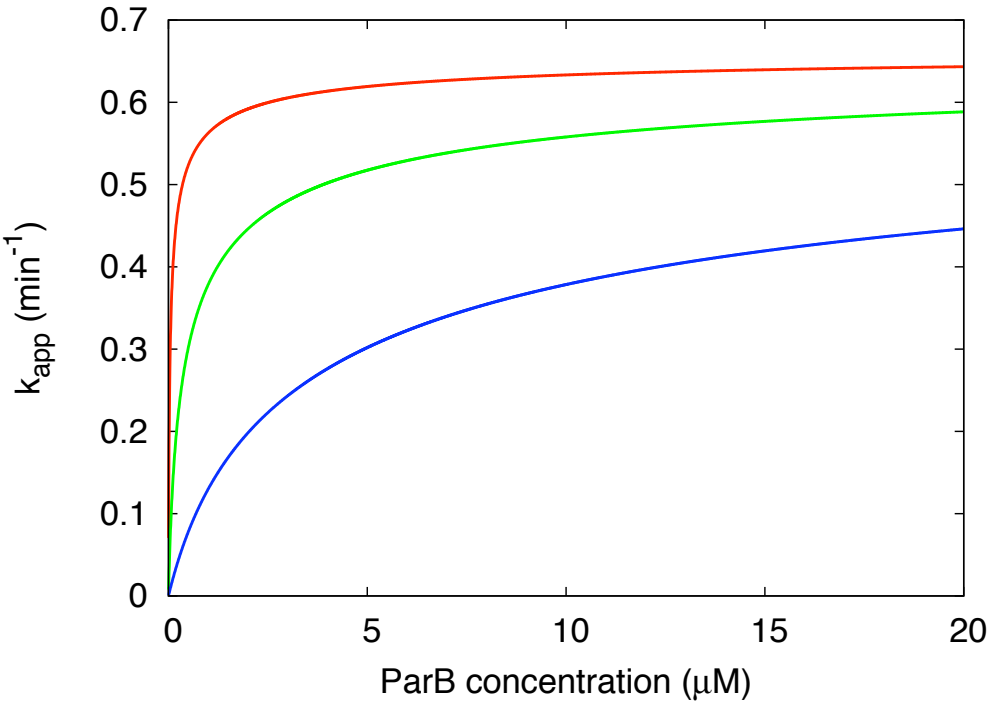


Figure 2.13: ATPase activity of MipZ as function of ParB concentration for different catalysis rate constants $k_{12}$. The DNA concentration is $d = 1\,\mathrm{mM}$, and the total MipZ concentration is $m_\mathrm{t} = 4\,\mu\mathrm{M}$. This approximately resembles physiological concentrations. The ParB catalysis rate constants are $k_{12} = 22\,\mu\mathrm{M}^{-1}\mathrm{min}^{-1}$ (red line), $k_{12} = 2\,\mu\mathrm{M}^{-1}\mathrm{min}^{-1}$ (green line), and $k_{12} = 0.2\,\mu\mathrm{M}^{-1}\mathrm{min}^{-1}$ (blue line). If the dependence of $k_\mathrm{app}$ on ParB concentration was measured, a fit could determine $k_{12}$.

$j$ is the number of reaction volumes the molecule travels.

After all molecules diffused, reactions were carried out. To implement the reactions, the respective rate constants $k_i$ had to be transformed into reaction probabilities $p_i$. For a molecule within a volume $V$, $p_i$ denotes the probability per reaction partner that the molecule performs reaction $i$ within time $\Delta t$. It is given by:

$$p_i = \frac{k_i \Delta t}{V^{\nu-1}} \tag{2.72}$$

whereas $V = (\Delta x)^3$ is the volume, the reaction takes place in, and $\nu$ is the order of reaction $i$ (Gillespie, 1976). The order of a reaction is the number of participating reactants.

The discretization time step $\Delta t$ was chosen such that the molecule with the lowest diffusion

constant on average moves one reaction volume per time step. Thus, with the law of diffusion we chose $\Delta t$ according to:

$$\Delta t = \frac{(\Delta x)^2}{6D_{\min}} \tag{2.73}$$

where $D_{\min}$ is the diffusion constant of the slowest molecule.

Since we chose our time discretization according to (2.73), the diffusion constants in the system set the length of the time steps. The reaction probabilities are then calculated by eq. (2.72). However, if diffusion of all the molecules is fast (this is the case in our system), the reaction probabilities are all very low. As a consequence, reactions take place very rarely, in most time steps molecules are only diffusing without reacting. To improve performance of the code, we lowered the diffusion constants of the molecules such that the reaction probabilities increased but still stayed lower than one. The only moving molecules in our system are MipZ monomers and dimers. We always chose the diffusion constant of the monomers 1.5 times as high as the one of the dimers. By lowering all diffusion constants, the length of the time steps increases (eq. (2.73)). As a consequence, the reaction probabilities for all reactions increase (eq. (2.72)), leaving their ratio constant. In this way, a smaller number of time steps is needed before the system reaches a stable behavior.

The MipZ concentration profiles were created by summing over all MipZ species taking into account that one dimer consists of two monomers. All profiles shown in this chapter are averages of 100 independent runs. This is similar to the experimental results, where a fluorescence profile is created by averaging over $\approx 100$ cells. For the parameter scans shown in figures 2.8 and 2.11, the center of mass was determined after averaging over 100 runs as well. In Figure 2.10, for extremely high and low $k_5$, only 20 runs were averaged.

The 2D diffusion used to implement the toy model in section 2.4 was carried out in the same way as the 3D simulations, on a 2D grid of $100 \times 50$ points. Initially there were 50000 molecules randomly positioned on the grid.

# Chapter 3

# Dynamic localization of the Min proteins in *E. coli*

## 3.1 Introduction

A second application of the theoretical method introduced in the previous chapter is outlined in the following study. We use our computational method to get some insight in the bio-physical mechanism of the Min system and the concentration distribution of the Min proteins in the rod-shaped bacterium *E. coli*. Like in *C. crescentus*, the division site of *E. coli* is defined by a ring-like structure on the membrane, called Z-ring. It is formed by the tubulin-homolog FtsZ. The proper placement of this Z-ring is accomplished by two inhibitory systems: Nucleoid occlusion (NO) (Woldringh et al., 1991; Yu and Margolin, 1999; Margolin, 2001; Errington et al., 2003) and the Min proteins (de Boer et al., 1989; Rothfield et al., 2001; Hu et al., 2003; Shih et al., 2003). The inhibitory effect of NO is caused by a DNA binding protein (Bernhardt and de Boer, 2005). In this way, NO prevents Z-ring formation at the position of the chromosome. Right before cell division, the two daughter chromosomes are well separated in the two cell halves. Due to the action of NO, the Z-ring formation can either take place at the poles of the cell or in the cell center. The Min system prevents cell division at the poles and enhances the precision of Z-ring placement at the mid-cell position (Yu and Margolin, 1999).

The Min system operates due to the interaction of three proteins, MinC, MinD and MinE. MinC is the inhibitor of the Z-ring formation. It is co-localized with MinD, in this way, MinD is responsible for the correct placement of MinC. Thus, concerning the localization of the Z-ring, only MinD has to be taken into account. MinD was shown to oscillate from one cell pole to the other with oscillation periods of approximately 20-40 seconds (Touhami et al., 2006). The concentration of MinD, averaged over several oscillation periods, is highest at the poles of the cell and lowest in the cell center. In this way, MinC can prevent Z-ring formation at the poles of the cell and cause proper Z-ring placement in the mid-cell position. The resulting spacial gradient of the time-averaged MinD concentration has been measured experimentally (Meacci

and Kruse, 2005).

Hu et al. (2002) revealed some of the properties and chemical reactions of MinD and MinE. They showed that both MinD and MinE but not MinC are needed to get the oscillatory behavior. MinD functions as an ATPase, and only the ATP bound form of MinD can associate with the membrane. MinE binds MinD and stimulates ATPase activity. In this way, MinE causes membrane-associated MinD·ATP to dissociate from the membrane. This membrane association and dissociation cycle causes MinD and MinE to oscillate from one cell pole to the other.

There are several theoretical models that describe the oscillatory behavior of the Min proteins (Howard et al., 2001; Meinhardt and de Boer, 2001; Kruse, 2002). Our investigations are based on the model introduced by Huang et al. (2003). These authors could verify the oscillations by solving the reaction-diffusion equations for a reaction cycle in which MinD·ATP first associates with the membrane, then MinE attaches to the MinD·ATP, stimulates ATP hydrolysis, and MinE and MinD·ADP reenter the cytoplasm. Huang et al. (2003) find three qualitatively different system behaviors. In small cells (smaller then $4\,\mu$m long), there are no Min oscillations observed. Large, $12\,\mu$m long cells show so-called double oscillations with one MinD oscillation pattern in each cell half. Cells with intermediate lengths show stable oscillations of MinD concentration. For these observations, the total concentration of Min proteins in the cell is kept constant for all cell lengths. The physiological concentration of MinD and MinE was determined experimentally: There are 2000 MinD molecules and 700 MinE dimer molecules in the cell (Shih et al., 2002). As pointed out by Kerr et al. (2006) the Huang model fails to produce Min oscillations at these low concentrations.

In this work we consider two aspects using the Huang model applied to the theoretical method introduced in the previous chapter using huge computational effort. These two aspects are introduced in the following paragraphs.

Most of the interactions carried out by the Min proteins are known qualitatively but the corresponding rate constants and membrane association constants are not measured yet. Five unknown parameters have to be used for numerical simulation of the Huang model. We are interested in the influence of changes in these parameters as robustness towards fluctuations is a very important issue for a biological system. For example the reaction rate constants are temperature dependent and the numbers of proteins can vary greatly from cell to cell (Elowitz et al., 2002; Ozbudak et al., 2002; Smits et al., 2006). Furthermore the model is extended to study the interplay with the polymer forming protein FtsZ that determines the position of the division site, see also chapter 2.

The second aspect which we consider is the dependence of the concentration distribution of the Min system on external parameters, that is the length of the cell and the overall number of molecules. This is interesting because the protein concentrations in *E. coli* can be regulated by the cell. Depending on the external conditions *E. coli* grows at different doubling times $T_\mathrm{D}$ ranging from 20 minutes to several hours (reviewed by Bremer et al. (1996)). Its cell length

depends on $T_D$, fast-growing cells are larger than slow growing cells (Pierucci, 1978). If the expression level of a gene is not regulated, the number of that protein per cell is constant for all growth rates. Thus, in the fast-growing large cells, the concentration of an unregulated protein is lower than in a slow growing cell. Up to now, it was not found that the expression of the Min proteins is regulated. If this is true, the number of proteins is constant as function of cell length and the shape of the concentration profiles of the Min proteins should be almost the same for a large range of total concentrations.

This chapter is organized as follows, we first describe in section 3.2 the model by Huang et al. (2003) in detail and reproduce their results with our simulation program. In section 3.3, we present our results of a systematic parameter study. We discuss robustness of the system towards alterations in the model parameters. For one particular set of parameters, we vary the cell lengths and molecule numbers independently to see how the model responds to concentration regulation. After having observed the behavior of the Min proteins in the cell, we extended the model by the additional protein FtsZ as introduced in section 3.4. Finally in sections 3.5 and 3.6, we demonstrate how the different oscillation patterns of the Min molecules influence the FtsZ localization.

## 3.2 The model

In this section we introduce the model by Huang et al. (2003). The model considers two proteins, MinD and MinE and their interactions. MinD molecules can either exist in the cytoplasm or be associated with the membrane. Therefore we identify molecules in the cytoplasm with an index (c) and membrane-associated molecules with an index (m).

The first reaction that is taken into account considers MinD in the cytoplasm. MinD can either bind ADP or ATP. The ADP bound form of MinD performs nucleotide exchange in the cytoplasm,

$$\mathrm{MinD} \cdot \mathrm{ADP}_{(\mathrm{c})} \xrightarrow{k_{\mathrm{ATP}}} \mathrm{MinD} \cdot \mathrm{ATP}_{(\mathrm{c})} \tag{3.1}$$

with rate constant $k_{\mathrm{ATP}}$. This is the only reaction in the system that takes place in the cytoplasm. All other processes are restricted to the interface between cytoplasm and membrane, because at least one of the participating molecules is membrane-associated.

Only the ATP bound form of MinD can associate with the membrane,

$$\mathrm{MinD} \cdot \mathrm{ATP}_{(\mathrm{c})} \xrightarrow{\kappa_{\mathrm{MinD}}} \mathrm{MinD} \cdot \mathrm{ATP}_{(\mathrm{m})}. \tag{3.2}$$

The membrane association of MinD is a self-enhancing effect, because MinD molecules at the membrane promote the association of other MinD molecules that are still in the cytoplasm:

$$\mathrm{MinD} \cdot \mathrm{ATP}_{(\mathrm{c})} + \mathrm{MinD} \cdot \mathrm{ATP}_{(\mathrm{m})} \xrightarrow{k_{\mathrm{mem}}} 2\ \mathrm{MinD} \cdot \mathrm{ATP}_{(\mathrm{m})}. \tag{3.3}$$

Table 3.1: Set of parameters used to implement the processes (3.1) - (3.5)

| **Parameter** | $k_{\mathrm{ATP}}$ | $\kappa_{\mathrm{MinD}}$ | $k_{\mathrm{mem}}$ | $k_{\mathrm{DE}}$ | $k_{\mathrm{off}}$ |
|---|---|---|---|---|---|
| **Value** | $0.5\,\mathrm{s}^{-1}$ | $0.125\,\mu\mathrm{m/s}$ | $0.075\,\mu\mathrm{m}^3\mathrm{s}^{-1}$ | $0.082\,\mu\mathrm{m}^3\mathrm{s}^{-1}$ | $0.75\,\mathrm{s}^{-1}$ |

This reaction leads to a crowding effect of MinD at the membrane, because once MinD is associated with the membrane, it causes other MinD molecules to associate as well.

Membrane-associated MinD·ATP is dissociated from the membrane by MinE. This dissociation process is performed in two steps: First, MinE binds to $\mathrm{MinD{\cdot}ATP_{(m)}}$,

$$\mathrm{MinE_{(c)}} + \mathrm{MinD \cdot ATP_{(m)}} \xrightarrow{k_{\mathrm{DE}}} \mathrm{MinE \cdot MinD \cdot ATP_{(m)}} \tag{3.4}$$

and subsequently stimulates ATPase activity of MinD. The ATP hydrolysis causes both MinD and MinE to dissociate from the membrane:

$$\mathrm{MinE \cdot MinD \cdot ATP_{(m)}} \xrightarrow{k_{\mathrm{off}}} \mathrm{MinE_{(c)}} + \mathrm{MinD \cdot ADP_{(c)}}. \tag{3.5}$$

In summary, the processes (3.1) - (3.5) describe a cycle of MinD behavior. First, ADP bound MinD, that can not associate with the membrane is charged with ATP in the cytoplasm. Then MinD·ATP accumulates at the membrane in a self-enhancing way (reactions (3.2) and (3.3)). Finally, MinD is dissociated from the membrane in the ADP bound form by MinE (reactions (3.4) and (3.5)).

We performed numerical reaction-diffusion simulations of the processes (3.1) - (3.5) with our self-written code. We first chose the parameters given in Table 3.1 which are similar to the ones used earlier in the literature (Huang et al., 2003; Kerr et al., 2006) and we get the same results as these earlier studies.

The processes (3.1) - (3.5) cause the MinD·ATP molecules to perform a periodic movement from one pole of the cell to the other. Thus, the concentration of MinD·ATP, $c_{\mathrm{MinD}}(x,t)$, does not only depend on the sub-cellular position $x$, but also on time $t$.

The proper localization of MinC, the division inhibitor, is performed by MinD·ATP (Hu and Lutkenhaus, 1999). Thus, in order to function properly, the residence time of MinD·ATP has to be highest at the cell poles and lowest in the cell center. In order to quantify this, we calculate the time average of MinD·ATP concentration,

$$\langle c_{\mathrm{MinD}} \rangle_t (x) = \frac{1}{t_{\max}} \int_0^{t_{\max}} c_{\mathrm{MinD}}\,(x,t)\,dt \tag{3.6}$$

to classify the behavior of the system.

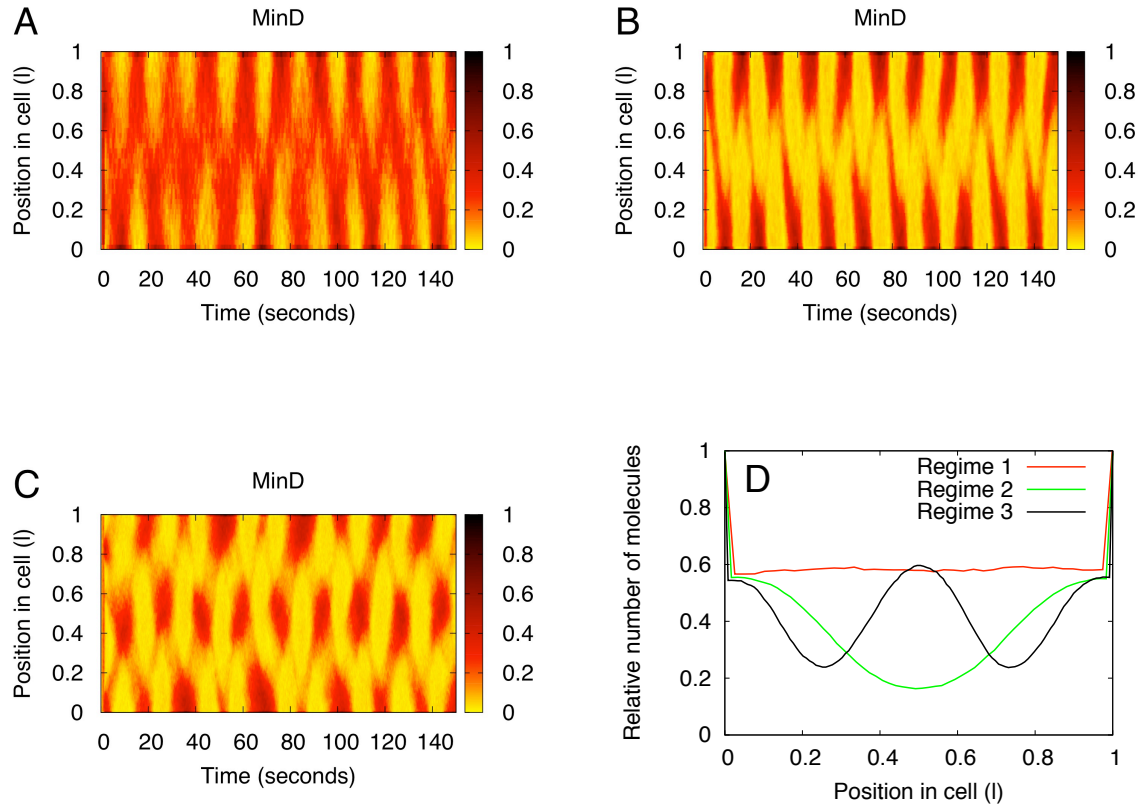


Figure 3.1: Different behavioral regimes of Min oscillations. (A) - (C): MinD concentration as function of time (horizontal axes) and position in cell (vertical axes) for different cell lengths $l$ and numbers of Min molecules $N_{\mathrm{tot}}$. (A): $l = 4\,\mu$m and $N_{\mathrm{tot}} = 5400$. (B): $l = 6\,\mu$m and $N_{\mathrm{tot}} = 8100$. (C): $l = 12\,\mu$m and $N_{\mathrm{tot}} = 16400$. (D): Time average of MinD concentration $\langle c_{\mathrm{MinD}} \rangle_t (x)$ for the Min oscillations shown in (A) (red), (B) (green), and (C) (black).

## 3.3 Systematic analysis of the parameter space

In the following simulations we used the recently measured diffusion constants of MinD and MinE (Meacci and Kruse, 2005). We performed simulations for different cell lengths $l$ with varying total number of molecules in the cell $N_{\mathrm{tot}}$. It turns out that depending on $l$ and $N_{\mathrm{tot}}$ there are three fundamentally different shapes of $\langle c_{\mathrm{MinD}} \rangle_t (x)$ as outlined in Figure 3.1. In this way, the parameter space $(l, N_{\mathrm{tot}})$ is divided into three regimes.

In the first regime, $\langle c_{\mathrm{MinD}} \rangle_t (x)$ has no minimum. This can result from an equal distribution of $c_{\mathrm{MinD}} (x, t) = \mathrm{const}$. It is also possible, that MinD·ATP does show a weak oscillation pattern (seen in Figure 3.1 (A)), but no minimum in $\langle c_{\mathrm{MinD}} \rangle_t (x)$ (Figure 3.1 (D), red line). In some cases, $\langle c_{\mathrm{MinD}} \rangle_t (x)$ even shows a weak maximum.

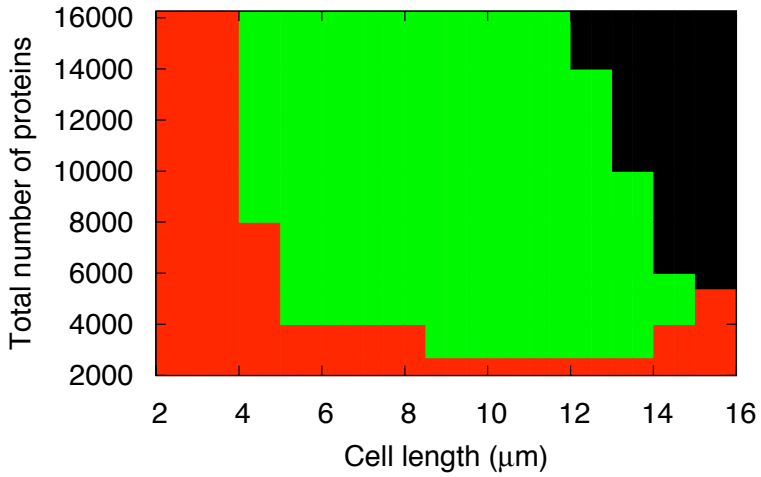


Figure 3.2: The property classes of Min behavior are shown for varying cell length and number od MinD. Red: unstable oscillations as seen in Figure 3.1 (A). Green: Stable single oscillations as seen Figure 3.1 (B), Black: Double oscillations.

The second regime of $(l, N_{\text{tot}})$-space is that of stable single oscillations as shown in Figure 3.1 (B). For this oscillation pattern, $\langle c_{\text{MinD}} \rangle_t (x)$ shows a clear minimum in the cell center (see Figure 3.1 (D) green curve). Regime 2 is the physiologically most important because this behavior can lead to normal Z-ring placement in the cell center.

In the third regime, MinD·ATP performs double oscillations as seen in Figure 3.1 (C). This oscillation pattern consists of one oscillation in one cell half each. The time average of MinD·ATP concentration (Figure 3.1 (D), black line) has a maximum in the cell center and two minima at 1/4 and 3/4 the cell length $l$.

In all of the regimes, $\langle c_{\text{MinD}} \rangle_t (x)$ has a sharp peak at positions $x = 0$ and $x = l$ (Figure 3.1 (D)). This is due to the fact that there is more membrane in these positions, namely the tips of the cell.

These results agree with the findings of Huang et al. (2003). It is important to note that the model failed to produce stable Min oscillations for small protein numbers (Kerr et al., 2006) although such small numbers are the experimentally determined physiological value for *E. coli* (Shih et al., 2002). Therefore we investigated the influence of the parameters $(l, N_{\text{tot}})$ on the behavior of the system in more detail. With high numerical effort, we performed a scan

of parameter values for cell length $l$ and number of molecules per cell $N_{\mathrm{tot}}$ and classified the behavior with respect to the three regimes presented above. Figure 3.2 shows the results of this parameter scan. It can be seen that regime 1 is shown for small number of particles and small cell lengths. regime 3 is shown for large number of particles and long cells. The most relevant regime 2 is shown for intermediate values.

This behavior is very unstable. Small variations in the system parameters have a strong influence on the position of the boundaries. The tendency however is the same for all sets of parameters: Stable single oscillations become double oscillations for high cell lengths and high molecule numbers. The behavior breaks down for small particle numbers where we find no oscillations.

We want to note that we found one specific set of interesting parameters. Using the parameters listed in table 3.1 but instead of $k_{\mathrm{DE}} = 0.082\,\mu\mathrm{m}^3\mathrm{s}^{-1}$ a value $k_{\mathrm{DE}} = 0.2\,\mu\mathrm{m}^3\mathrm{s}^{-1}$ we found single oscillations for small particle numbers $N_{\mathrm{tot}} = 2700$. This is the experimentally determined value for wild-type *E. coli* (Shih et al., 2002). We come back to this finding in section 3.6. But first we extend the simulations of the Min system to cells that contain FtsZ.

## 3.4 Investigations of the reaction of FtsZ

In this section we go one step further and extend the model in a way that FtsZ localization is included. FtsZ forms polymers consisting of several monomers each (Chen and Erickson, 2005; Chen et al., 2005). By cross-linking of these polymers on the membrane the complete Z-ring is formed (Dajkovic et al., 2010). This ring has a highly dynamical structure, the subunits are exchanged rapidly (Anderson et al., 2004; Stricker et al., 2002).

FtsZ is produced in the cytoplasm. It associates with the membrane,

$$\mathrm{FtsZ}_{(\mathrm{c})} \xrightarrow{\kappa_{\mathrm{FtsZ}}} \mathrm{FtsZ}_{(\mathrm{m})}. \tag{3.7}$$

In the cytoplasm, the polymerization is blocked by NO (Bernhardt and de Boer, 2005). In our model, FtsZ polymerization takes place only at the membrane. Once FtsZ molecules are membrane associated, the polymerization is described by the reaction

$$\mathrm{FtsZ}_{(\mathrm{c})} + \mathrm{FtsZ}_{(\mathrm{m})} \xrightarrow{k_{\mathrm{poly}}} 2\,\mathrm{FtsZ}_{(\mathrm{m})}. \tag{3.8}$$

Note that this process has the same form as the association of MinD at the membrane (3.3). However, the membrane associated molecules differ in an important respect. MinD can diffuse in the membrane, whereas polymerized FtsZ cannot.

As mentioned above, the FtsZ filaments have a highly dynamical structures, which permanently assembles and disassembles. The disassembly is taken into account by the process:

$$\mathrm{FtsZ}_{(\mathrm{m})} \xrightarrow{k_{\mathrm{break}}} \mathrm{FtsZ}_{(\mathrm{c})}. \tag{3.9}$$

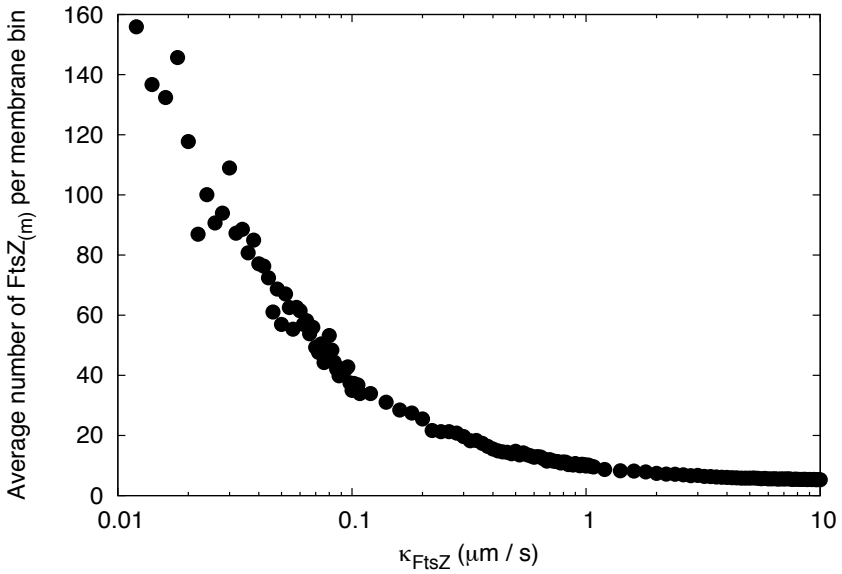


Figure 3.3: Mean number of $\mathrm{FtsZ_{(m)}}$ molecules per membrane bin. The processes (3.7), (3.8) and (3.9) were implemented, and $\mathrm{FtsZ_{(m)}}$ assembly on the membrane was followed. After equilibration the average number of $\mathrm{FtsZ_{(m)}}$ per membrane bin was measured as function of the parameter $\kappa_{\mathrm{FtsZ}}$.

The rate constants of the filament assembly and disassembly were determined by (Chen and Erickson, 2005) as $k_{\mathrm{poly}} = 6\,\mu\mathrm{M}^{-1}\mathrm{s}^{-1}$ and $k_{\mathrm{break}} = 3\,\mathrm{s}^{-1}$.

The parameter $\kappa_{\mathrm{FtsZ}}$ has to be used as a free model parameter. We want to fix it to a reasonable value. For this reason, we performed simulations of the processes (3.7), (3.8) and (3.9) in the cell. In the literature, there are discrepancies about the number of FtsZ molecules in one cell, ranging from 3500 (Pla et al., 1991; Rueda et al., 2003) to far over 10000 (Lu et al., 1998) copies per cell. We started our simulations with 7000 FtsZ monomers. These molecules were placed in the cytoplasm randomly. After letting the system equilibrate (indicated by the number of cytoplasmic FtsZ), we determined the average number of the membrane associated $\mathrm{FtsZ_{(m)}}$ molecules per membrane bin. Figure 3.3 shows this average number as function of $\kappa_{\mathrm{FtsZ}}$.

The shape of the curve seen in 3.3 can be understood as follows: At time $t = 0$, all FtsZ is cytoplasmic. Then, FtsZ molecules start to associate with the membrane. The probability for the association process is determined by $\kappa_{\mathrm{FtsZ}}$. For low values of $\kappa_{\mathrm{FtsZ}}$, molecule association takes place very rarely. Once the first $\mathrm{FtsZ_{(m)}}$ molecule is located on a membrane bin, it pulls

other $\mathrm{FtsZ}_{(c)}$ molecules to the same spot by reaction (3.8) with rate constant $k_{\mathrm{poly}}$. For very low $\kappa_{\mathrm{FtsZ}}$ only very few $\mathrm{FtsZ}_{(c)}$ molecules associate with the membrane and subsequently long $\mathrm{FtsZ}_{(m)}$ filaments forms. In this way, the average number of $\mathrm{FtsZ}_{(m)}$ molecules per membrane bin is high, because there are only a few very long filaments. If $\kappa_{\mathrm{FtsZ}}$ is increasing, there are more $\mathrm{FtsZ}_{(c)}$ molecules associating with the membrane and more filaments formed. As a consequence, the average filament length decreases. For $\kappa_{\mathrm{FtsZ}} \to \infty$, it is given by the number of $\mathrm{FtsZ}_{(m)}$ molecules divided by the number of membrane bins. For the simulations shown in Figure 3.3, we used 7000 FtsZ and 1344 membrane bins, thus, for $\kappa_{\mathrm{FtsZ}} \to \infty$, the average number of FtsZ per membrane bin is approximately 5.2.

In conclusion, in the regime where $\kappa_{\mathrm{FtsZ}}$ is high, the membrane association process is dominated by the process (3.7), for low $\kappa_{\mathrm{FtsZ}}$ by the process (3.8). We want to study the system in the intermediate regime, because on one hand we want the membrane association process to be caused by the polymerization, on the other and, we do not want one single long filament. In addition, when we additionally place MinD in the cell, it will dissociate FtsZ from the membrane. Then FtsZ has to have the ability to re-associate within reasonable time. Therefore, $\kappa_{\mathrm{FtsZ}} = 0.4\,\mu\mathrm{m/s}$ seems to be a reasonable choice.

As outlined below in section 3.7, we use a spacial discretization of $\Delta x = 0.1\,\mu\mathrm{m}$. One FtsZ molecule is 4-5 nm long (Romberg et al., 2001). For $\kappa_{\mathrm{FtsZ}} = 0.4\,\mu\mathrm{m/s}$ the average number of $\mathrm{FtsZ}_{(m)}$ per membrane bin is approximately 20. This choice makes sense, because the $\mathrm{FtsZ}_{(m)}$ molecules fit in the bin, and could connect to those in adjacent bins. The average number of FtsZ per membrane bin is depending on the discretization. Thus, it is not a good quantity to observe. However, a different discretization does not alter the choice for $\kappa_{\mathrm{FtsZ}}$.

To summarize, in order to simulate the process of FtsZ polymerization, we use the three fixed parameters $k_{\mathrm{poly}} = 6\,\mu\mathrm{M}^{-1}\mathrm{s}^{-1}$, $k_{\mathrm{break}} = 3\,\mathrm{s}^{-1}$ and $\kappa_{\mathrm{FtsZ}} = 0.4\,\mu\mathrm{m/s}$.

## 3.5 FtsZ localization influenced by MinD double oscillations

In this section, we want to combine the process of the FtsZ polymerization with the case of a double oscillation of MinD. We chose the parameters given in table 3.1 for the interactions of MinD and MinE, a cell length of $l = 12\,\mu\mathrm{m}$ and $N_{\mathrm{tot}} = 16400$ proteins in the cell. For this set of parameters, MinD·ATP showed a double oscillation pattern as presented in section 3.2. For the FtsZ related processes, we chose the parameters given in section 3.4

For this set of parameters, we consider the inhibiting effect of the Min system on FtsZ polymerization. This inhibition of Z-ring formation is performed by MinC, that we take into account indirectly. MinC binds to MinD and thus co-localizes with MinD. In our model, MinD dissociates $\mathrm{FtsZ}_{(m)}$ from the membrane,

$$\mathrm{MinD \cdot ATP}_{(m)} + \mathrm{FtsZ}_{(m)} \xrightarrow{k_{\mathrm{des}}} \mathrm{MinD \cdot ATP}_{(m)} + \mathrm{FtsZ}_{(c)}. \tag{3.10}$$

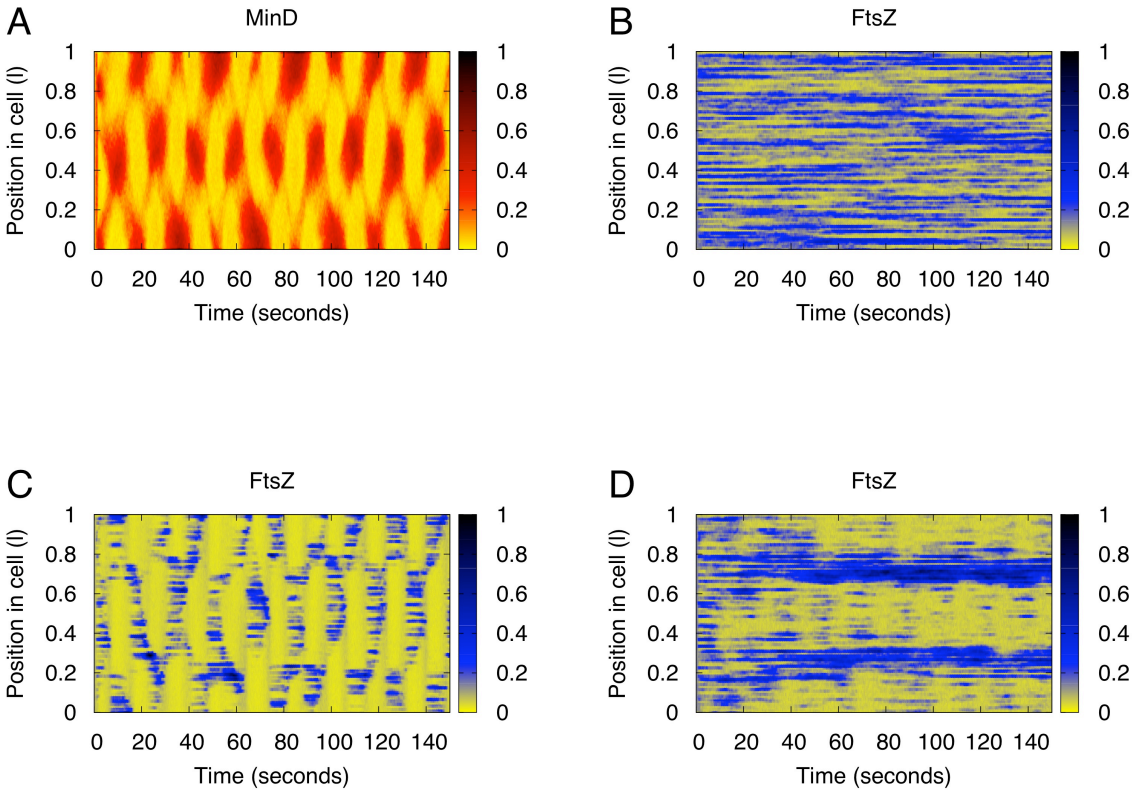


Figure 3.4: Temporal and spacial behavior of molecules in a 12 $\mu$m long cell. (A): MinD concentration as function of time (horizontal axes) and position in cell (vertical axes). (B): FtsZ concentration for $k_{\mathrm{des}} = 10^{-6}\,\mu\mathrm{m}^3\mathrm{s}^{-1}$. (C): FtsZ concentration for $k_{\mathrm{des}} = 0.005\,\mu\mathrm{m}^3\mathrm{s}^{-1}$.(D): FtsZ concentration for $k_{\mathrm{des}} = 0.0005\,\mu\mathrm{m}^3\mathrm{s}^{-1}$.

In this way, the free parameter $k_{\mathrm{des}}$ determines the strength of the MinD - $\mathrm{FtsZ}_{(\mathrm{m})}$ interaction. Figure 3.4 shows the results of the simulation for different values of $k_{\mathrm{des}}$. For a very small value of $k_{\mathrm{des}}$, $k_{\mathrm{des}} = 10^{-6}\,\mu\mathrm{m}^3\mathrm{s}^{-1}$, the concentration of FtsZ, $c_{\mathrm{FtsZ}}(x,t)$ is constant, see Figure 3.4 (B). There is no influence of MinD·ATP on the concentration of $\mathrm{FtsZ}_{(\mathrm{m})}$. On the other hand, if $k_{\mathrm{des}}$ is very high, $k_{\mathrm{des}} = 0.005\,\mu\mathrm{m}^3\mathrm{s}^{-1}$, the interaction of MinD and FtsZ is very strong. As a consequence, FtsZ avoids MinD·ATP and always localizes where there is no MinD·ATP in the cell. This can be seen by comparing $c_{\mathrm{MinD}}(x,t)$ and $c_{\mathrm{FtsZ}}(x,t)$ (Figures 3.4 (A) and (C), respectively). For an intermediate value of $k_{\mathrm{des}}$, $k_{\mathrm{des}} = 0.0005\,\mu\mathrm{m}^3\mathrm{s}^{-1}$, MinD·ATP causes FtsZ to accumulate at positions $x = 0.25\,l$ and $x = 3/4\,l$ as seen in Figure 3.4 (D).

This behavior is also aparent, when comparing the time average concentration profiles $\langle c_{\mathrm{MinD}}\rangle_t(x)$ and $\langle c_{\mathrm{FtsZ}}\rangle_t(x)$ in Figure 3.5. Here, $\langle c_{\mathrm{FtsZ}}\rangle_t(x)$ (green line) has maxima where $\langle c_{\mathrm{MinD}}\rangle_t(x)$ (red line) is minimal.

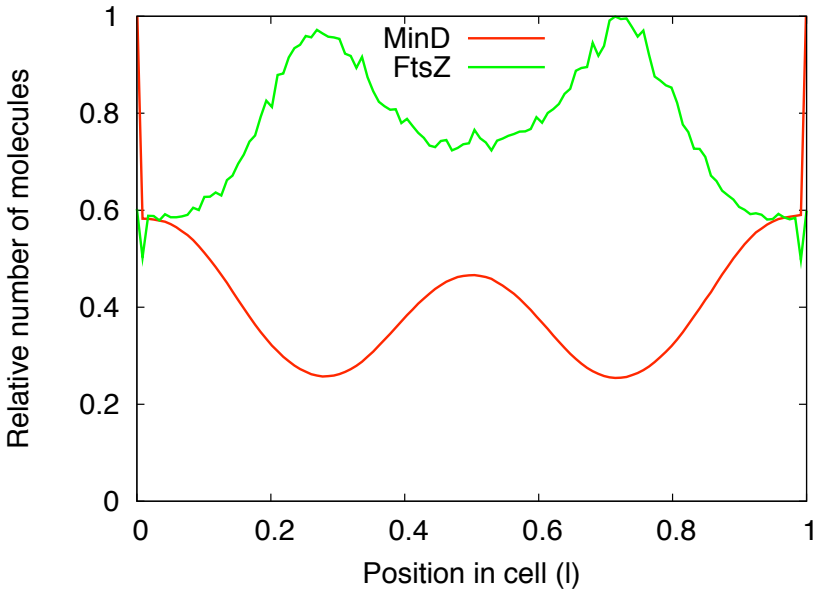


Figure 3.5: Time average of concentrations. $\langle c_{\mathrm{MinD}} \rangle_t (x)$ is shown in red and $\langle c_{\mathrm{FtsZ}} \rangle_t (x)$ is shown in green.

A cell with such a behavior of $\langle c_{\mathrm{FtsZ}} \rangle_t (x)$ will form two Z-rings at positions $x = 0.25\ l$ and $x = 3/4\ l$ and have an abnormal division behavior. Thus, *E. coli* wants to prevent this. Experimentally, MinD double oscillations have been found in *ftsZ*$^-$ mutants, cells without FtsZ. The wild-type does not show double oscillations (Raskin and de Boer, 1999). In the next section, will discuss the possibility that double oscillations are avoided in a cell with physiological MinD and MinE concentrations.

## 3.6 Simulations with the physiological amount of molecules

Finally, we performed simulations with $N_{\text{tot}} = 2700$ Min proteins in the cell, the physiological amount (Shih et al., 2002). We and discuss the range of the values for the rate constants that lead in the experimentally found single oscillation pattern of the MinD concentration. As mentioned at the end of section 3.3 one possible set of parameters are the values of table 3.1 but taking $k_{\text{DE}} = 0.2\,\mu\text{m}^3\text{s}^{-1}$. The results of the simulations are shown in Figure 3.6.

Figure 3.6 (A), shows the MinD·ATP oscillations, the oscillation period is $\approx 20\,\text{s}$. This is close to the measured value described by Touhami et al. (2006). Figures 3.6 (B)-(D) show the FtsZ concentration for different values of $k_{\text{des}}$ than in Figure 3.4. The parameter $k_{\text{des}}$ again determines the strength of the interaction between MinD and FtsZ. For very low values of $k_{\text{des}}$, $k_{\text{des}} = 10^{-5}\,\mu\text{m}^3\text{s}^{-1}$, there is no interaction at all and FtsZ distributes equally (Figure 3.6

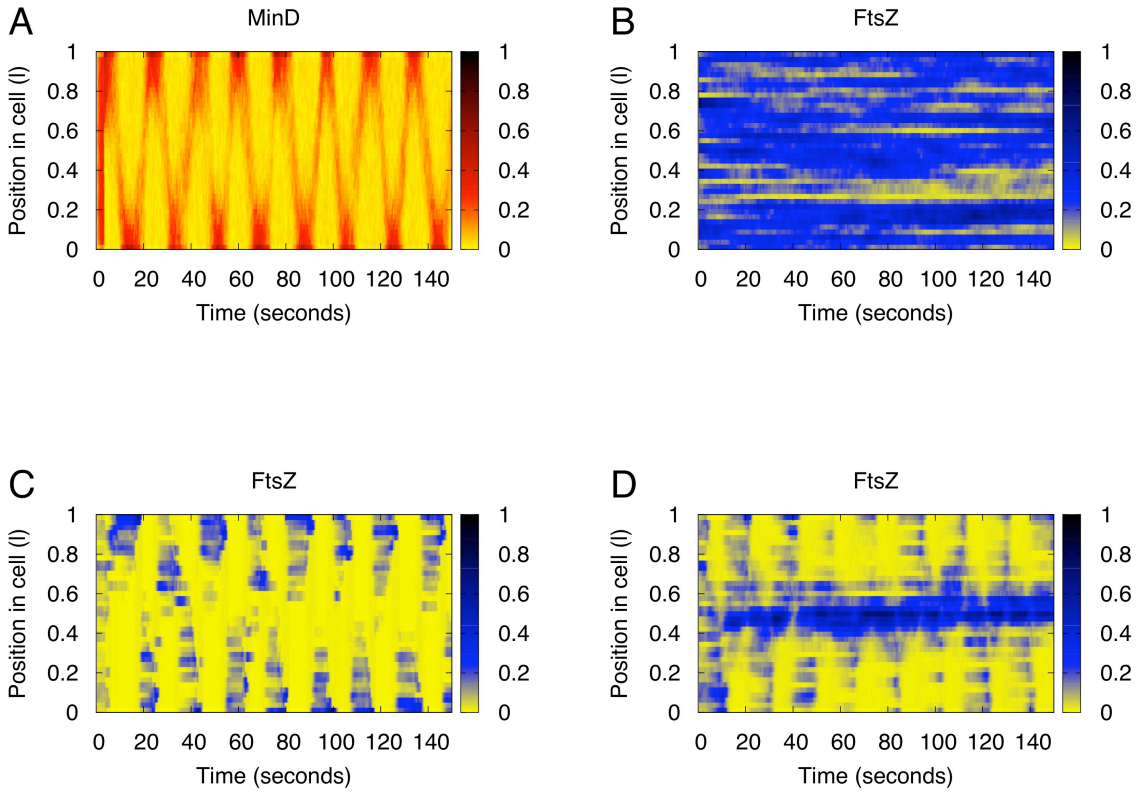


Figure 3.6: Temporal and spacial behavior of molecules in a $4\,\mu\text{m}$ long cell. (A): MinD concentration as function of time (horizontal axes) and position in cell (vertical axes). (B): FtsZ concentration for $k_{\text{des}} = 10^{-5}\,\mu\text{m}^3\text{s}^{-1}$. (C): FtsZ concentration for $k_{\text{des}} = 0.1\,\mu\text{m}^3\text{s}^{-1}$.(D): FtsZ concentration for $k_{\text{des}} = 0.005\,\mu\text{m}^3\text{s}^{-1}$.

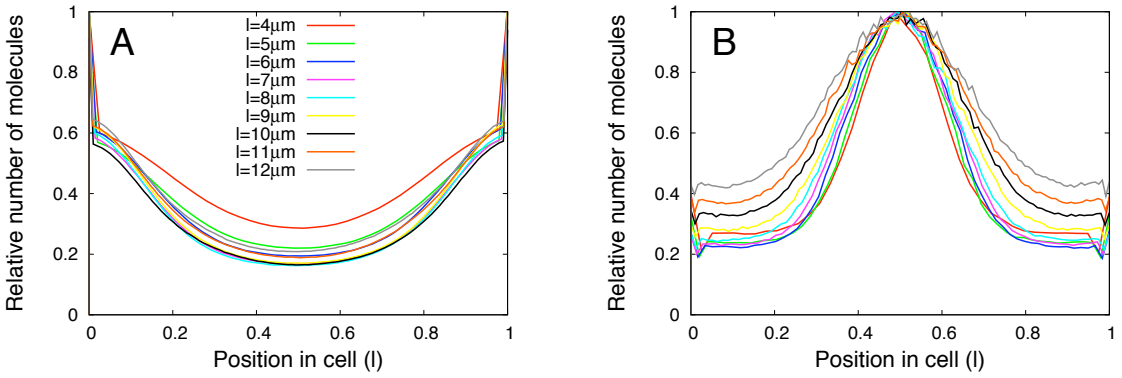


Figure 3.7: Time average of the molecule concentrations. (A): $\langle c_{\mathrm{MinD}} \rangle_t (x)$ as given in equation (3.6) for different cell lengths $l$. (B): $\langle c_{\mathrm{FtsZ}} \rangle_t (x)$ for different cell lengths, colors are the same as in (A).

(B)). For very high values of $k_{\mathrm{des}}$, $k_{\mathrm{des}} = 0.1\,\mu\mathrm{m}^3\mathrm{s}^{-1}$, FtsZ performs an oscillation in the cell by avoiding the MinD·ATP position (Figure 3.6 (B)). A mid-cellular FtsZ positioning is seen in Figure 3.6 (D) for a value of $k_{\mathrm{des}} = 0.005\,\mu\mathrm{m}^3\mathrm{s}^{-1}$. Since this is the expected WT behavior, we chose $k_{\mathrm{des}} = 0.005\,\mu\mathrm{m}^3\mathrm{s}^{-1}$ to perform simulations with different cell lengths.

We quantify the localizations of proteins with the time averaged concentrations $\langle c_{\mathrm{MinD}} \rangle_t (x)$ and $\langle c_{\mathrm{FtsZ}} \rangle_t (x)$. These quantities are shown in Figure 3.7 for different cell lengths $l$. As can be seen in Figure 3.7 (A),$\langle c_{\mathrm{MinD}} \rangle_t (x)$ displays a localized minimum in the cell center. This leads to a mid-cellular maximum of $\langle c_{\mathrm{FtsZ}} \rangle_t (x)$ as seen in Figure 3.7 (B). As a consequence, the cell could form Z-rings in the cell center for all cell lengths. However, the parameter range for which this behavior holds is not very large. Table 3.2 gives the ranges of the stable behavior.

## 3.7 Computational details

For the simulations described in this chapter, we used the same simulation principle as explained in section 2.7. In the simulations on MipZ in *C. crescentus*, the molecules were always reflected by the bounding box of the cell. For the simulations on the Min system presented in this chapter, the outer planes of the grid function as the membrane. When a molecule with membrane association constant $\kappa_{\mathrm{i}}$ hits the membrane, it has a probability

$$p = \frac{\kappa_{\mathrm{i}}}{\Delta x} \Delta t \tag{3.11}$$

to associate. $\Delta x$ and $\Delta t$ are the spacial and temporal resolutions, respectively. If a molecule is not associating to the membrane, it is reflected back into the cytoplasm. Diffusion within the membrane is restricted to the membrane planes. Reactions of membrane proteins and with

Table 3.2: Ranges of parameters for which stable oscillations are shown a cells with length $l = 4\,\mu$m and $N_{\text{tot}} = 2700$ proteins.

| **Parameter** | $k_{\text{ATP}}$ | $\kappa_{\text{MinD}}$ | $k_{\text{mem}}$ | $k_{\text{DE}}$ | $k_{\text{off}}$ |
|---|---|---|---|---|---|
| **Range** | 0.45-0.7 | $\infty$ | 0.05-0.15 | 0.12-0.8 | 0.55-0.8 |
| **Unit** | $\text{s}^{-1}$ | $\mu\text{ms}^{-1}$ | $\mu\text{m}^3\text{s}^{-1}$ | $\mu\text{m}^3\text{s}^{-1}$ | $\text{s}^{-1}$ |

cytoplasmic proteins were always carried between the membrane protein and the neighboring cytoplasmic protein. The diffusion constants for MinD and MinE were determined experimentally both in the cytoplasm and in the membrane as

$$D_{\text{MinD(c)}} = 16\,\mu\text{m}^2\text{s}^{-1} \tag{3.12}$$

$$D_{\text{MinD(m)}} = 10\,\mu\text{m}^2\text{s}^{-1} \tag{3.13}$$

$$D_{\text{MinE(c)}} = 0.16\,\mu\text{m}^2\text{s}^{-1} \tag{3.14}$$

$$D_{\text{MinE(m)}} = 0.1\,\mu\text{m}^2\text{s}^{-1} \tag{3.15}$$

(Meacci and Kruse, 2005). We chose the diffusion constants of FtsZ

$$D_{\text{FtsZ(c)}} = 14.5\,\mu\text{m}^2\text{s}^{-1}, \tag{3.16}$$

because of its mass, 40 kD compared to that of MinD, 30 kD (see ecocyc.org). We converted the mass to the diffusion constant using the Stokes-Einstein relation by assuming a constant density. As FtsZ is supposed to polymerize on the membrane, it does not diffuse within the membrane.

For all simulations presented here, the spacial discretization is $\Delta x = 0.1\,\mu$m. The cells are always $1\,\mu$m wide and deep. The time average profiles $\langle c_{\text{MinD}} \rangle_t (x)$ and $\langle c_{\text{FtsZ}} \rangle_t (x)$ shown are averages over 20 independent simulation runs.

# Chapter 4

# Noise and individuality in bacterial populations

## 4.1 Introduction

The macroscopic properties of bacterial populations are characterized by a few well-defined quantities such as growth rate, total cellular volume or mass, DNA content, or number of ribosomes (Bremer et al., 1996). At the same external conditions, these observables have sharp values and show hardly any variation between different measurements. On the single cell level however, many biological processes are intrinsically noisy. This leads to strong variations in composition and properties of individual cells belonging to the same population. The above mentioned quantities such as cell volume, mass, DNA content, etc. vary greatly within the population (Koppes et al., 1978). However, these cell-to-cell variations do not affect the strictly deterministic behavior on the population level. The characteristic values of the macroscopic variables are obtained from ensemble averages over a very large number of cells.

Cells of a genetically homogeneous population can also exhibit phenotypic diversity leading to individual behavior (Smits et al., 2006; Davidson and Surette, 2008). Important examples include the delay times in uptake of new nutrients (Megerle et al., 2008), variations in chemotactic tumbling behavior (Spudich and Koshland, 1976), entry into dormant state (Balaban et al., 2004; Levin, 2004; Shah et al., 2006), sporulation and competence (Maughan and Nicholson, 2004; Veening et al., 2006). In many cases, this diversification is caused by transcriptional noise (Elowitz et al., 2002; Ozbudak et al., 2002; Smits et al., 2006).

However, there are some cellular processes that seem to be tightly regulated in order to suppress the associated fluctuations. One important example is cell division of *E. coli*. This process is very precisely implemented and a mother cell can divide into two daughter cells that only differ at most by 10% of mass (Koppes et al., 1978; Trueba, 1982; Guberman et al., 2008). If this high precision is indeed a consequence of a tight regulation then one expects that there is an evolutionary advantage in cell division precision. In ecology and population genetics

it is well-known that noise can have an advantageous effect on a population in fluctuating environments. This effect is known as bet-hedging (Philippi and Seger, 1989). Typically, in these systems members of a population choose individual noise-induced strategies to cope with environmental fluctuations. Examples in which bet-hedging is believed to provide an advantage are seed germination of dessert annuals (Cohen, 1966), or diapause of insects (Menu et al., 2000). In this study we apply similar ideas to the growth of a bacterial population in a fluctuating environment. In this case, noise at the transcriptional level becomes important since it can lead to significant cell-to cell variations in protein levels (Elowitz et al., 2002).

In particular, fluctuations in the transcription process might lead to the production of proteins that are not needed for the given growth conditions. Generally, the production of unneeded proteins leads to an additional burden reducing the growth rate (Koch, 1983). However, there are situations where this burden is compensated. For example, for a population growing in a fluctuating environment (with varying nutrients) the production of these additional proteins could be useful for the individual cells. It is *a priori* not clear if it is better to just produce the molecular machineries required to grow on the currently present nutrients or to produce additional machineries required for other (currently not present) nutrients. The first strategy has the advantage that the protein burden is lower thus leading to a higher growth rate for the current nutrient. However, the drawback is that after a shift in the medium (or if the current nutrient is running out) new metabolic machinery has to be produced leading to a lag phase. In the second strategy there is no lag phase but the higher protein burden leads to a slower growth rate for all different nutrients. In fact, both strategies can be favorable depending on the switching time, the duration of the lag phase and the growth rates supported by nutrients in the medium. For *E. coli* both strategies have been observed (see Kovarova-Kovar and Egli (1998) and references therein). For example, an *E. coli* population grown in glucose-limited conditions with a doubling time of $0.6\,\mathrm{h}^{-1}$ keeps growing without a lag-phase when transferred to a medium with excess of fructose, mannose, maltose, and ribose. A lag phase occurs when the population is transferred to a galactose or arabinose rich medium (Lendenmann and Egli, 1995).

In this chapter, we theoretically analyze the influence of noise on the growth behavior of a bacterial population in homogeneous and fluctuating environments. To do so, we developed a model to simulate bacterial growth on the single cell level. The growth of the individual cells is affected by noise acting either on the division process or on the choice of growth strategy.

As a first step (in section 4.2), we study the influence of noise in the division process of single cells on the properties of the population. Here, the environment is kept constant, and describes a situation found in lab experiments. In section 4.2.3, we focus on population doubling time. This quantity is most important for the cells, because the population tries to grow as fast as possible. We classify the situations in which noise on the single cell level has an influence on population doubling time and if it acts positive or negative. In the following section 4.2.4 we discuss the influence of single cell division noise on other population properties

such as the average volume of the cells.

As a next step (in section 4.3), we address the question whether it is favorable for a bacterial population to diversify in a fluctuating environment, i.e. to form a heterogeneous population in which both of the above mentioned strategies are realized. Heterogeneous populations have been observed in different instances. An important example is that of entry into dormant state (Balaban et al., 2004; Levin, 2004; Shah et al., 2006). In this state cells cannot grow which reduces the growth rate of the population. However, in hostile environments, for example, if the population is exposed to antibiotics, the dormant cells do not die, and enable survival of the population after the antibiotics is removed from the medium. In a similar way, a population can survive nutritional stress conditions by having some non-growing cells sporulate (Errington, 1993).

The model we present in this work does not cover these very severe environmental conditions. It is quite obvious that diversification of the population is advantageous under these conditions since otherwise the population dies out completely. In this study we only consider environmental conditions under which populations can grow on by investigating if under these conditions diversification leads to an increase in growth rate. Thus, we implemented a bacterial population making use of a bet-hedging procedure. In section 4.3.2, we explore if the bacterial population can draw a growth advantage from a diversification under fluctuating conditions. To further clarify our results, we test the influence of our basic model assumptions in section 4.3.3. Finally, we discuss the differences between our model and those used in other studies in section 4.3.4.

## 4.2 Growth in non-fluctuating conditions

### 4.2.1 Growth behavior of a population with cell division noise

We first analyzed the influence of single cell division noise on exponentially growing bacterial populations in a homogeneous (non-changing) medium. As mentioned, there are many cellular processes that could be affected by the presence of noise. Here, we focused on its influence on cell division. We investigated if the growth rate of a bacterial population depends on the precision of cell division. In our model, an inexact cell division event produces two sister cells of unequal length and mass. The smaller of the two daughter cells has less mass and thus, less ribosomes, less transporter proteins and other molecular machinery needed to grow. Accordingly, the smaller daughter cell needs a longer time until the next cell division than its larger sister. The time between birth and division of an individual cell is denoted by inter division time $\tau$.

Details about the numerical implementation of this model are given in section 4.5. Briefly, the formation of a bacterial population is simulated by a sequence of cell division events. We start from one single newborn cell and simulate growth and division of this cell and its

daughter cells. All cells have the same individual doubling time $T_\mathrm{D}$ (the time a cell needs to double its mass). The doubling time is set by the surrounding medium. Because there are strong indications that cell division is coupled to mass (Donachie and Begg, 1989) we assumed that the mass of the mother cell at cell division has a fixed value $m_\mathrm{D}$. In the absence of noise the mother thus divides into two daughter cells of birth mass $m_\mathrm{B} = m_\mathrm{D}/2$ . Hence, all cells have the same interdivision time $\tau = T_\mathrm{D}$.

If on the other hand the division process is noisy, the mother cell divides into two daughter cells of mass $m_\mathrm{B}$ and $m_\mathrm{D} - m_\mathrm{B}$. In our simulations, $m_\mathrm{B}$ is given by a random number drawn from a normal distribution centered around $m_\mathrm{D}/2$ with standard deviation $\sigma$. To keep track of the division events in the population, we use the "time until division" (tud) that represents the time a cell has left until division. At birth, it is equal to the inter division time $\tau$. In every time step of the simulations, the tud of each cell is decreased by one. Since an individual cell is characterized by its tud (in the following denoted by $x$), the population is characterized by the tud distribution $n\,(x,t)$ of its comprising cells. At time $t$, $n\,(x,t)$ denotes the number of cells that have a tud of $x$. In particular, $n\,(0,t)$ is the number of dividing cells at time $t$.

To calculate the tud distribution from the birth mass distribution we have to make some specific assumptions on how single cells increase their mass. In the literature mainly two modes of mass increase have been discussed: Linear mass increase (Kubitschek, 1986) (where the mass of a cell increases linearly with time) and exponential mass increase (Ecker and Kokaisl, 1969; Cooper, 1988).

As function of tud $x$, the mass of a single cell is given by:

$$m\,(x) = m_\mathrm{D}\left(1 - \frac{x}{2T_\mathrm{D}}\right) \tag{4.1}$$

for linear mass increase, and by

$$m\,(x) = m_\mathrm{D}2^{-\mu x} \tag{4.2}$$

for exponential mass increase, where $\mu = (T_D)^{-1}$. Note that the cells have reached the division mass $m_\mathrm{D}$, when tud is equal to zero. The total mass of the population $M(t)$ is then given by:

$$M\,(t) = \int_0^\infty m\,(x)\,n\,(x,t)\,dx. \tag{4.3}$$

With the help of this model we can investigate how noise on the single cell level influences the growth of the population. First, we checked that in the absence of noise our model leads to exponential growth of the population. Therefore, we calculated an OD-plot. This plot shows the total mass of the population $M(t)$ as function of time $t$. As can be seen in Figure 4.1 the population clearly grows exponentially for both linear and exponential mass increase of the individual cells. The difference of total population mass for cells with linear (red) and

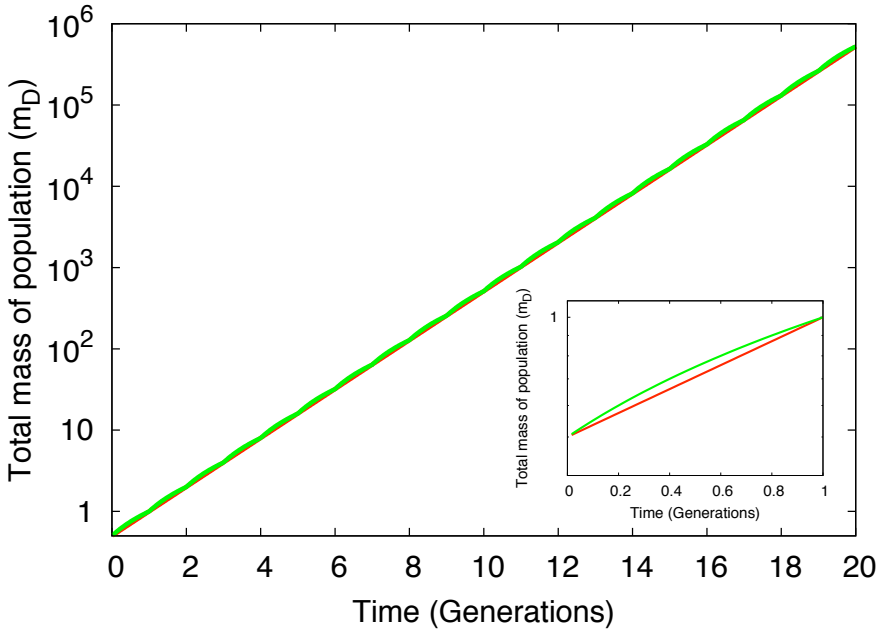


Figure 4.1: OD-Plot of a growing population in the absence of divisional noise. The OD plot was obtained by calculating the total mass of the population $M(t)$ as function of time $t$ for cells with linear (green) and exponential (red) mass increase. Mass is measured in units of $m_D$ (the division mass), time $t$ in units of generation time $T_D$. Population mass always doubles after one generation showing that the population indeed grows with prescribed doubling time $T_D$. The inset shows the mass increase within one generation.

exponential (green) mass increase is very small ( Figure 4.1, inset).

In the same way we obtained OD-plots for populations in the presence of divisional noise. The observed doubling time of the population $T_{pop}$ is then obtained from the slope of the OD-plot. Figure 4.2 shows the observed population doubling time $T_{pop}$ as function of the standard deviation $\sigma$ of birth mass that quantifies the divisional noise.

Surprisingly, noise does not have any effect on the growth rate of a population with cells that have an exponential mass increase (red dots). Even more astonishing is the behavior of a population with cells that have a linear mass increase (green dots). Here, the population doubling time decreases with increasing noise, indicating that an imprecise cell division is favorable for the growing population but this effect is not very strong. For example for $\sigma = 25\%$ of division mass $m_D$, one finds a 2.5% decrease in population doubling time. To find the origin

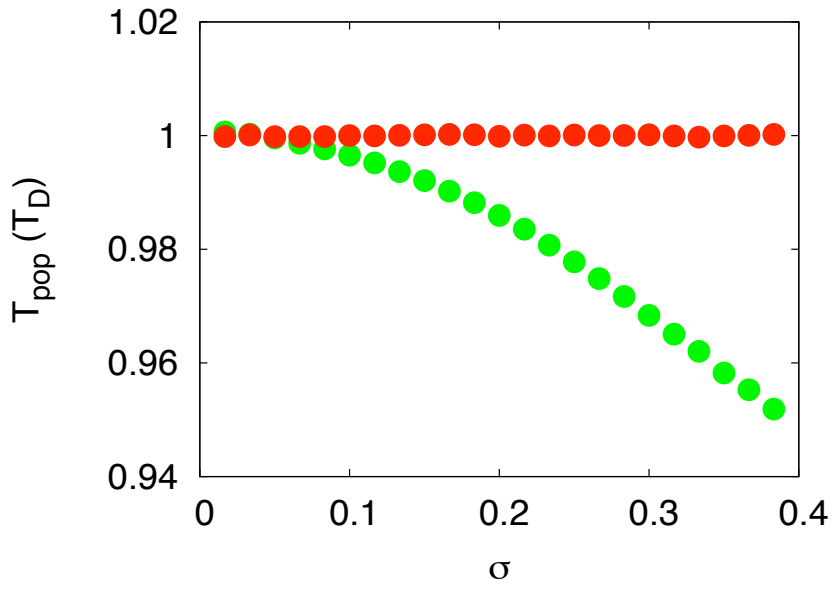


Figure 4.2: Dependence of population doubling time on strength of divisional noise. Doubling times $T_{\mathrm{pop}}$ of populations were calculated by fitting an exponential to OD-Plots. At every cell division event the mass of the newborn cells are drawn from a normal distribution with mean $m_{\mathrm{D}}/2$ and standard deviation $\sigma$. Data shown are for populations of cells with linear mass increase (green symbols) and exponential mass increase (red symbols).

of this astonishing behavior we analytically analyzed our numerical model in the next sections.

### 4.2.2 The tud distribution

In this section, we analyze the behavior of the tud distribution that characterizes the growing population. We consider the case of linear mass increase on the single cell level. In this case, the probability distribution $P(\tau)$ for the inter division times $\tau$ of the daughter cells is given by:

$$P(\tau) = \frac{2}{\sigma\sqrt{2}} \exp\left(-\frac{1}{2}\left(\frac{\tau - T_{\mathrm{D}}}{\sigma}\right)^2\right). \tag{4.4}$$

It is normalized to two, because every mother divides into two daughter cells. With the help of this, the dynamics of the tud distribution $n(x,t)$, can be understood as follows: Knowing $n(x,t)$ at time $t$, after a fixed time-span $\tilde{t}$ has passed, the amount of cells carrying a tud of $x$

changes due to aging of cells and birth of new cells:

$$n\left(x, t+\tilde{t}\right) = n\left(x+\tilde{t}, t\right) + \int_0^{\tilde{t}} n\left(t', t\right) P\left(x+\tilde{t}-t'\right) dt'. \tag{4.5}$$

The first summand in equation (4.5) represents the aging effect: Cells with tud of $x$ had a tud of $x+\tilde{t}$, $\tilde{t}$ ago. The integral in equation (4.5) takes into account the contribution of newborn cells within the time-span $\tilde{t}$: It is the sum of the number of cell division events at time $t-t'$, $n\left(t', t\right)$, multiplied by the probability for the newborn cell to obtain an inter division time of $x+\tilde{t}-t'$ at birth.

The integral equation (4.5) can be transformed into a differential equation by derivation with respect to $\tilde{t}$ and the limit $\tilde{t} \to 0$. This yields:

$$\partial_t n\left(x, t\right) - \partial_x n\left(x, t\right) = n\left(0, t\right) P\left(x\right). \tag{4.6}$$

Equation (4.6) describes the time evolution of the growing population.

An important quantity is the total number of cells $N\left(t\right)$ in the population, because it explains the overall growth behavior

$$N\left(t\right) = \int_0^{\infty} n\left(x, t\right) dx. \tag{4.7}$$

From (4.7) it follows with equation (4.6) that:

$$\begin{aligned} \partial_t N\left(t\right) &= \int_0^{\infty} \left(\partial_x n\left(x, t\right) + n\left(0, t\right) P\left(x\right)\right) dx && (4.8)\\ &= n\left(\infty, t\right) - n\left(0, t\right) + 2n\left(0, t\right) && (4.9)\\ &= n\left(0, t\right). && (4.10) \end{aligned}$$

Thus, the increase of the population size at time $t$ is the number of cell divisions.

With the help of quantity $N\left(t\right)$, the relative tud distribution $\tilde{n}\left(x, t\right)$, giving the relative numbers of cells with time until division $x$ is created:

$$\tilde{n}\left(x, t\right) := \frac{n\left(x, t\right)}{N\left(t\right)}. \tag{4.11}$$

Numerical simulations of equation (4.6) for various initial distributions $n\left(x, 0\right)$ show, that the relative tud distribution $\tilde{n}\left(x, t\right)$ becomes stationary. Hence, $\tilde{n}\left(x, t\right)$ becomes independent

on time and $\partial_t \tilde{n}(x,t) = 0$. In this case, because of equation (4.10) it is true that:

$$\partial_t \tilde{n}(x,t) = \frac{N(t)\,\partial_t n(x,t) - n(x,t)\,\partial_t N(t)}{N(t)^2} = 0 \tag{4.12}$$

$$\Rightarrow \partial_t n(x,t) = n(x,t)\,\frac{\partial_t N(t)}{N(t)} \tag{4.13}$$

$$= n(x,t)\,\frac{n(0,t)}{N(t)}. \tag{4.14}$$

Insertion of (4.14) into the differential equation for $n(x,t)$, equation (4.6), leads to:

$$\tilde{n}(x,t)\,\tilde{n}(0,t) = \partial_x \tilde{n}(x,t) + \tilde{n}(0,t)\,P(x). \tag{4.15}$$

Equation (4.15) determines the stationary behavior of the tud histogram.
An equation like (4.15) of the form

$$cf(x) = f'(x) + cP(x) \tag{4.16}$$

with

$$c = f(0) \tag{4.17}$$

and $P(x)$ as in equation (4.4) is solved by:

$$f(x) = ce^{c(x-T_\mathrm{D})}\left(e^{cT_\mathrm{D}} + e^{\frac{c^2\sigma^2}{2}}\left(\mathrm{erf}\left(\frac{c\sigma^2 - T_\mathrm{D}}{\sqrt{2}\sigma}\right) - \mathrm{erf}\left(\frac{c\sigma^2 - T_\mathrm{D} + x}{\sqrt{2}\sigma}\right)\right)\right). \tag{4.18}$$

With

$$\mathrm{erf}(x) = \frac{2}{\sqrt{\pi}}\int_0^x e^{-y^2}\,dy, \tag{4.19}$$

the Gaussian Error Function. The constant $c = \tilde{n}(0,t)$ can be determined by the requirement of integrability of $\tilde{n}(x,t)$:

$$\int_0^\infty \tilde{n}(x,t)\,dx = 1. \tag{4.20}$$

It is interesting to note that for function $f(x)$ from equation (4.18), it is sufficient to find $c$ with

$$\lim_{x\to\infty} f(x) = 0 \tag{4.21}$$

thus, solving:

$$e^{cT_\mathrm{D}} + e^{\frac{c^2\sigma^2}{2}}\left(\mathrm{erf}\left(\frac{-T_\mathrm{D} + c\sigma^2}{\sqrt{2}\sigma}\right) - 1\right) = 0 \tag{4.22}$$

because for other choices of $c$, $f(x)$ is divergent and not normalizable. The constant $c$ has an

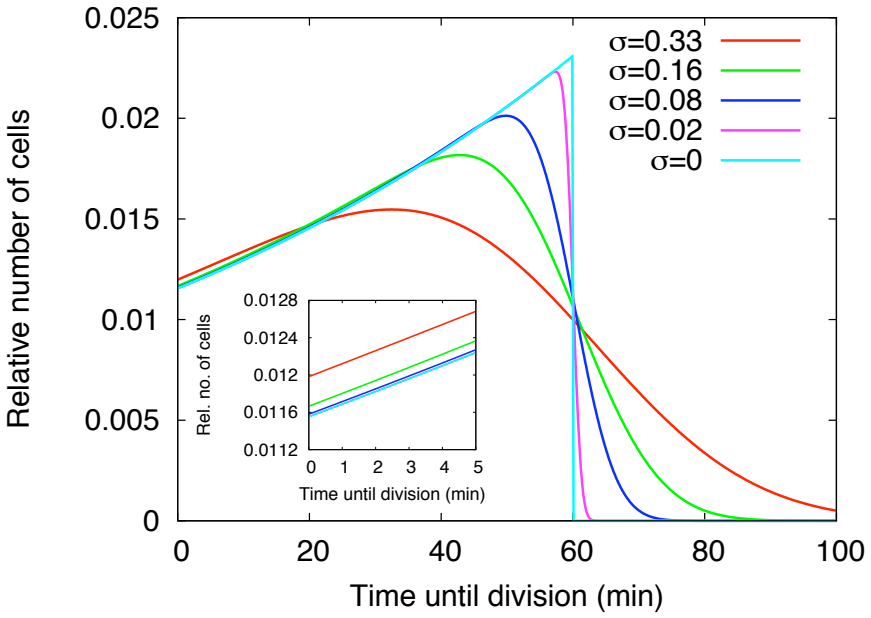


Figure 4.3: Stationary relative time until division distributions for different noise levels. The stationary relative tud distributions as given by equation (4.18) are shown for different strength of inter divisional noise (quantified by the standard deviation $\sigma$ of birth masses of the daughter cells). Data shown are for $\sigma = 0.33$ (red), $\sigma = 0.16$ (green), $\sigma = 0.08$ (blue), $\sigma = 0.02$ (magenta) and $\sigma = 0$ (cyan), where $\sigma$ is given in units of division mass. The prescribed doubling time is $T_{\mathrm{D}} = 60\,\mathrm{min}$ for all populations. The inset shows the behavior is for small tud.

important meaning for the population. From equation (4.10) it follows that:

$$\partial_t N\,(t) = \tilde{n}\,(0,t)\,N\,(t)\,. \tag{4.23}$$

Thus the total number of cells in the population $N(t)$ grows exponentially, and $c = \tilde{n}\,(0,t)$ is the growth rate of the population. Figure 4.3 shows stationary relative tud distributions for different noise levels $\sigma$. In for very small noise $\sigma \to 0$ this distribution scales as $2^x$ with the tud $x$ (cyan line in Figure 4.3). In this case, the age $y$ of a cell obeys $y = T_{\mathrm{D}} - x$ , and our results are in agreement with classical results on age distribution in growing populations (Powell, 1956).

In the presence of noise, the relative tud distributions are an overlap of a $2^x$ accounting for the fact that there are twice as many newborn cells as old cells and an error function resulting

from the Normal Distribution of the division noise. The increase in growth rate in the presence of noise can be directly seen from the inset of Figure 4.3. As mentioned, $\tilde{n}(0,t)$ is the population growth rate and this quantity can be directly read off from the distribution of relative tud. As one can see from Figure 4.3, $\tilde{n}(0,t)$ increases with increasing standard deviation $\sigma$ implying a higher growth rate at stronger noise. This implies the drop in doubling time in Figure 4.2. In the next section, we will further explain the influence of individual division noise on population doubling time.

### 4.2.3 Influence of division noise on population doubling time

In this section, we proceeded with the theoretical analysis of equation (4.6) to investigate the fundamental difference between populations of cells with exponential and with linear mass increase. As explained in section 4.2.1, the total mass of the population as function of time is given by equation (4.3). Its derivative, which is the mass increase of the population, is:

$$\partial_t M(t) = \int_0^\infty m(x)\,\partial_t n(x,t)\,dx. \tag{4.24}$$

Insertion of (4.6) yields:

$$\begin{aligned}
\partial_t M(t) &= \int_0^\infty m(x)\left(\partial_x n(x,t) + n(0,t)\,P(x)\right)dx && (4.25)\\
&= \left[m(x)\,n(x,t)\right]_0^\infty - \int_0^\infty n(x,t)\,\partial_x m(x)\,dx + \int_0^\infty n(0,t)\,m(x)\,P(x)\,dx && (4.26)\\
&= -m_{\mathrm{D}} n(0,t) - \int_0^\infty n(x,t)\,\partial_x m(x)\,dx + n(0,t)\int_0^\infty m(x)\,P(x)\,dx. && (4.27)
\end{aligned}$$

Now, we take a closer look at the last term: $P(x)$ is the distribution of inter division times. We get it from the birth mass distribution:

$$P(x) = 2\int_0^{m_{\mathrm{D}}} \delta\left(x - x(m)\right) P(m)\,dm \tag{4.28}$$

It is normalized to two, $P(m)$ is the birth mass distribution, and $\delta(x)$ is the Dirac delta function. It follows:

$$\int_0^\infty m(x)\,P(x)\,dx = 2\int_0^\infty m(x)\,dx \int_0^{m_{\mathrm{D}}} \delta\left(x - x(m)\right) P(m)\,dm \tag{4.29}$$

thus, with $m(x(m)) = m$:

$$\int_0^\infty m\,(x)\,P\,(x)\,dx = 2\int_0^{m_\mathrm{D}} mP\,(m)\,dm. \tag{4.30}$$

The last integral is the expectation value of $P(m)$. This is equal to $m_\mathrm{D}/2$, because the birth mass distribution is centered around half the division mass of the mother. It follows:

$$\int_0^\infty m\,(x)\,P\,(x)\,dx = m_\mathrm{D}. \tag{4.31}$$

In this way, equation (4.27) simplifies:

$$\partial_t M\,(t) = -\int_0^\infty n\,(x,t)\,\partial_x m\,(x)\,dx. \tag{4.32}$$

Now, we are interested in the difference between linear and exponential single cell mass growth. For linear growth, the mass as function of tud is given by:

$$m\,(x) = m_\mathrm{D}\left(1 - \frac{x}{2T_\mathrm{D}}\right) \tag{4.33}$$

$$\Rightarrow \partial_x m\,(x) = -\frac{m_D}{2T_\mathrm{D}}. \tag{4.34}$$

With equation (4.32), it follows for the mass increase of the population:

$$\partial_t M\,(t) = \frac{m_\mathrm{D}}{2T_\mathrm{D}} N\,(t) \tag{4.35}$$

where $N(t)$, is the total number of cells in the population as given be equation (4.7). For exponential growth, the mass as function of tud is given by:

$$m\,(x) = m_\mathrm{D} 2^{-\mu x} \tag{4.36}$$

$$\Rightarrow \partial_x m\,(x) = -\frac{\ln(2)}{T_\mathrm{D}} m\,(x) \tag{4.37}$$

with $\mu = (T_\mathrm{D})^{-1}$. From equation (4.32), it follows that:

$$\partial_t M\,(t) = \frac{\ln(2)}{T_\mathrm{D}} M\,(t)\,. \tag{4.38}$$

In conclusion, if the single cells are growing exponentially, the population mass increase is proportional to the population mass. Thus, such a population always grows exponentially with the medium prescribed doubling time $T_\mathrm{D}$ independent on how the total mass is partitioned

between the different cells. Note, that in this case the change in total mass does not depend on the number of cells $N(t)$ at time $t$ in the population. For this reason the divisional noise does not affect growth of the population.

On the other hand, for linear single cell mass increase, the total change in mass of a population is given by equation (4.35) and does depend on $N(t)$. Thus, in this case, the growth rate of the population increases with an increasing number of cells. An uneven mass partitioning during the noisy division process now effectively increases the number of cells in the population. This increase is a rather subtle effect.

To illustrate its origin we consider the unrealistic case where the mass is very unevenly partitioned between the daughter cells. For example we consider the specific case where the newborn daughters get 75% and 25% of the mother's division mass, respectively. Furthermore, we assume that in the absence of divisional noise the medium supports a doubling time $T_{\mathrm{D}} = 120\,\mathrm{min}$. Correspondingly, the larger newborn cell has an inter division time of 60 min, while the smaller one has an inter division time of 180 min. The growth of this population is illustrated in Figure 4.4 A.

To see how the noisy cell division leads to a doubling time of less than 2 hours we start with a single cell that divides at time $t = 0$ into cell #1 with a tud of 60 min and cell #2 with a tud of 180 min. After 1 hour cell #1 has divided into cell #3 with a tud of 60 min and cell #4 with a tud of 180 min. Cell #2 has a tud of 120 min left. After 2 hours cell #3 divides into 2 cells (cells #5 and #6). Thus, after 2 hours the population consists of 2 cells with a tud of 60 min (cells #5 and #2), one cell with a tud of 120 min (cell #4), and one cell with a tud of 180 min (cell #6). If the population were growing with a doubling time of 2 hours then the population would consist of 2 cells with a tud of 60 min and 2 cells with a tud of 180 min. Thus, cell #4 has a smaller tud leading to the observed increase in population doubling time.

This example can easily be generalized to an arbitrary number of cells. We start from a population with size $N(t)$. A population with precise cell division will double after 120 minutes, see Figure 4.4 B. Now we want to compare how many cells there are in the noisy population after 120 minutes to see if it grows faster. At time $t$, the noisy population consists of $n(60, t)$, $n(120, t)$ and $n(180, t)$ cells with a tud of 60, 120 and 180 minutes, respectively. Thus,

$$N(t) = n(60, t) + n(120, t) + n(180, t). \tag{4.39}$$

After 60 minutes, division events take place, yielding 50% cells with inter division time 60 min and 50% cells with inter division time 180 min. This gives us:

$$n(60, t + 60) = n(60, t) + n(120, t). \tag{4.40}$$

The first term is the number of newborn cells with an interdivision time of $\tau = 60\,\mathrm{min}$, the second term is due to aging of the cells that had a tud of 120 min at time $t$. In addition, it is

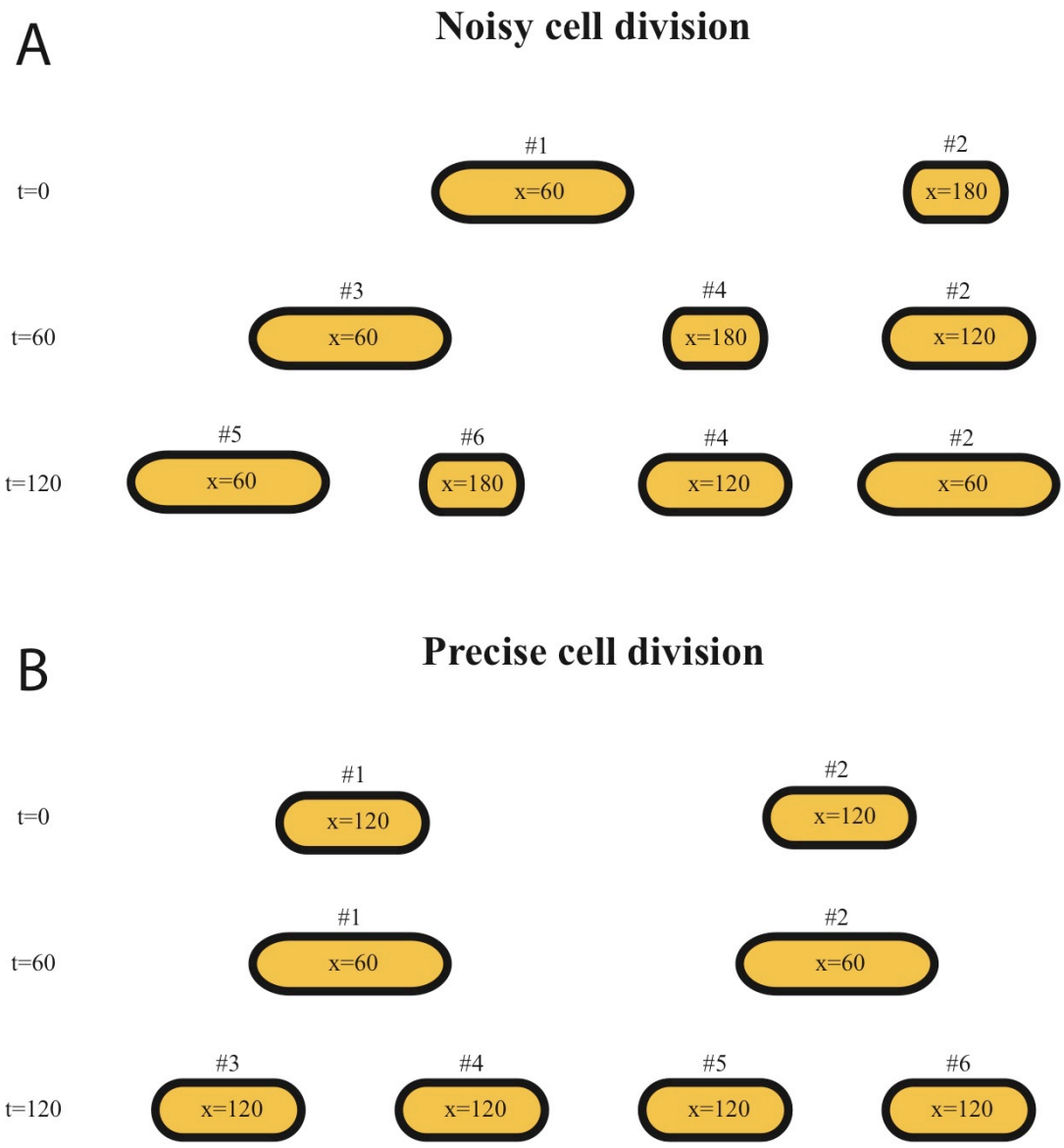


Figure 4.4: Comparison of a noisy cell division process to a precise cell division process, the medium prescribed doubling time is $T_D = 120\,\text{min}$. (A) Noisy division: At every cell division event, the mother cell produces two daughters of 25% and 75% of its division mass, respectively. Thus, the smaller and the larger daughter have an inter division time of 180 min and 60 min, respectively. At time $t = 60$, cell #1 divides, at $t = 120$, cell #3 divides. (B) Precise division: Every mother divides into two equal daughter cells, that consequently have an inter division time of 120 min each. At $t = 120$, cells #1 and #2 divide.

true that:

$$n\,(120, t+60) = n\,(180, t) \tag{4.41}$$

because of aging, and

$$n\,(180, t+60) = n\,(60, t) \tag{4.42}$$

due to division.

If we apply the iterative equations (4.40) - (4.42) once again, we see that after 120 minutes, it is true that:

$$\begin{aligned} n\,(60, t+120) &= n\,(60, t) + n\,(120, t) + n\,(180, t) && (4.43)\\ n\,(120, t+120) &= n\,(60, t) && (4.44)\\ n\,(180, t+120) &= n\,(60, t) + n\,(120, t)\,. && (4.45) \end{aligned}$$

And thus, for the total number of cells in the population:

$$N\,(t+120) = 2N\,(t) + n\,(60, t) - n\,(180, t)\,. \tag{4.46}$$

To decide if this noisy population grows faster than the precise one, we have to find out if it consists of more cells with a tud of 60 minutes or 180 minutes. From equations (4.40) and (4.42) we can see that:

$$n\,(60, t) = n\,(60, t-60) + n\,(120, t-60) \tag{4.47}$$

and:

$$n\,(180, t) = n\,(60, t-60)\,. \tag{4.48}$$

Hence,

$$n\,(60, t) - n\,(180, t) = n\,(120, t-60) > 0, \tag{4.49}$$

i.e. there are indeed more cells with a tud of 60 min than with a tud of 180 min in the population. Substituting this finding into equation (4.46) shows that

$$N\,(t+120) > 2N\,(t)\,. \tag{4.50}$$

This implies that the noisy population indeed has a doubling time lower than 120 min, which is the doubling time of the precise population. Similar arguments apply to less noisy division processes where the two daughter cells are of more similar size.

### 4.2.4 Influence of division noise on other population observables

Given the surprising result of section 4.2.3, we now analyzed whether single cell noise also affects other population observables apart from doubling time. Many quantities of single cells like volume, number of ribosomes, proteins, or RNA and DNA content change during the cell cycle, presumably in a linear or exponential manner (Ecker and Kokaisl, 1969; Kubitschek, 1986; Donachie and Begg, 1989). Note that we still assume linear mass increase on the single cell level. The population average can be calculated from the tud distribution. As an example, we consider the population average for the cell volume $V(x)$:

$$\overline{V} = \frac{1}{T_\mathrm{D}} \int_0^{T_\mathrm{D}} dt \int_0^{\infty} \tilde{n}\,(x,t)\, V\,(x)\, dx. \tag{4.51}$$

If $\tilde{n}\,(x,t)$ is stationary (independent of $t$), the integration with respect to $t$ can be carried out easily. We consider two scenarios, an exponential increase of volume during the cell cycle,

$$V_\mathrm{exp}\,(x) = V_\mathrm{D} 2^{-\mu x} \tag{4.52}$$

and a linear increase of volume during the cell cycle,

$$V_\mathrm{lin}\,(x) = V_\mathrm{D}\left(1 - \frac{x}{2T_\mathrm{D}}\right) \tag{4.53}$$

with $\mu = (T_\mathrm{D})^{-1}$, and $V_\mathrm{D} = V(0)$ volume at cell division.

First, we will consider the case of exact cell division, with no statistical effects on inter division times of the cells. In this case,

$$\tilde{n}\,(x,t) = \delta\,(x - t)\,, \tag{4.54}$$

where $\delta(x)$ is the Dirac delta function. Substituting this in equation (4.51) and integrating with respect to $x$ yields:

$$\overline{V}_\mathrm{exp} = \frac{1}{T_\mathrm{D}} \int_0^{T_\mathrm{D}} V_\mathrm{D} 2^{-\mu t} dt = \frac{1}{2\ln(2)} V_\mathrm{D} \tag{4.55}$$

in the exponential case and

$$\overline{V}_\mathrm{lin} = \frac{1}{T_\mathrm{D}} \int_0^{T_\mathrm{D}} V_\mathrm{D}\left(1 - \frac{t}{2T_\mathrm{D}}\right) dt = \frac{3}{4} V_\mathrm{D}. \tag{4.56}$$

in the linear case.

Now, we want to compare this finding with observables of noisy populations. Thus, we have to consider the relative tud distribution $\tilde{n}(x,t)$ as given by equation (4.18). As a first step, we will discuss the behavior for small (but non-zero) noise.
In the limit $\sigma \to 0$, the stationary tud distribution as given by equation (4.18) becomes:

$$\lim_{\sigma\to 0} \tilde{n}(x,t) = \begin{cases} ce^{c(x-T_\mathrm{D})}\left(e^{cT_\mathrm{D}} - (\mathrm{erf}(-\infty) - \mathrm{erf}(-\infty))\right) & \text{for } x < T_\mathrm{D} \\ ce^{c(x-T_\mathrm{D})}\left(e^{cT_\mathrm{D}} - (\mathrm{erf}(-\infty) - \mathrm{erf}(\infty))\right) & \text{for } x > T_\mathrm{D} \end{cases} \tag{4.57}$$

this can be written as:

$$\lim_{\sigma\to 0} \tilde{n}(x,t) = ce^{c(x-T_\mathrm{D})}\left(e^{cT_\mathrm{D}} - 2\theta(x-T_\mathrm{D})\right), \tag{4.58}$$

with $\theta(x)$, the Heaviside step function. The constant $c$ is determined from the normalization:

$$1 = \int_0^\infty \tilde{n}(x,t) = \int_0^{T_\mathrm{D}} ce^{c(x-T_\mathrm{D})}e^{cT_\mathrm{D}} = \int_0^{T_\mathrm{D}} ce^{cx}, \tag{4.59}$$

thus, $c$ has to obey:

$$1 = e^{cT_\mathrm{D}} - 1 \Rightarrow c = \frac{\ln 2}{T_\mathrm{D}}. \tag{4.60}$$

We get the stationary tud distribution by inserting $c$ into (4.58):

$$\tilde{n}(x,t) = \frac{\ln(2)}{T_\mathrm{D}} 2^{\mu x}\left(1 - \theta(x - T_\mathrm{D})\right), \tag{4.61}$$

again with $\mu = (T_\mathrm{D})^{-1}$. In this case, the population observables are:

$$\overline{V}_\mathrm{exp} = \frac{\ln(2)}{T_\mathrm{D}} V_\mathrm{D} \int_0^{V_\mathrm{D}} dx = \ln(2)\, V_\mathrm{D} \tag{4.62}$$

and

$$\overline{V}_\mathrm{lin} = \frac{\ln(2)}{T_\mathrm{D}} V_\mathrm{D} \int_0^{T_\mathrm{D}} 2^{\mu x}\left(1 - \frac{x}{2T_\mathrm{D}}\right) dx = \frac{1}{2\ln(2)} V_\mathrm{D}. \tag{4.63}$$

Up to now, we discussed population observables of linear and exponential properties $V(x)$ in the case of small division noise or no division noise at all, equations (4.55), (4.56), (4.62) and

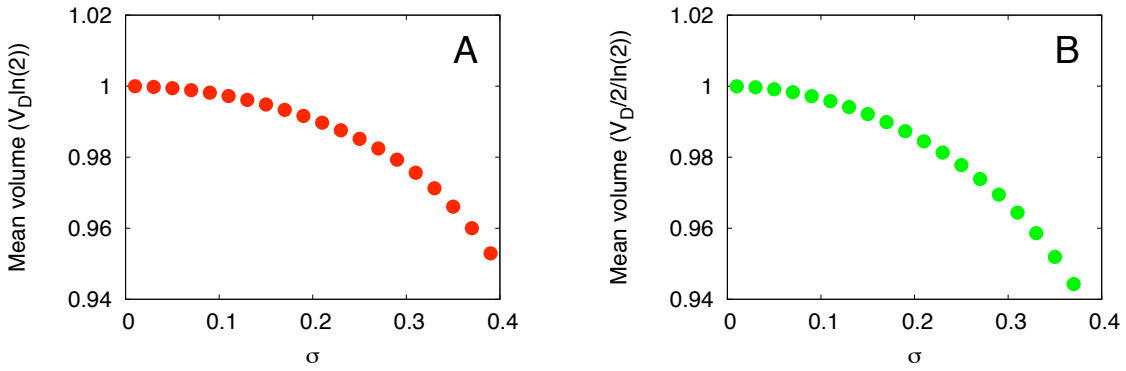


Figure 4.5: Influence of noise on the mean volume of the population $\overline{V}$ as given by equation (4.51). The mean volume is measured in units of its value for $\sigma \to 0$. (A) The single cell volume grows exponentially, as given by equation (4.52). (B) The single cell volume grows linearly, as given by equation (4.53).

(4.63). The differences are not very large:

$$\frac{1}{2\ln(2)} \approx 0.72 \tag{4.64}$$

$$\frac{3}{4} = 0.75 \tag{4.65}$$

$$\ln(2) \approx 0.69. \tag{4.66}$$

To compare the analytical results of these special cases above with the full system with noise, we numerically integrated equation (4.51) with a relative tud distribution given by (4.18). The results are shown in Figure 4.5. For small $\sigma$, the population average saturates to the value of the analytical case above with small but non-zero noise (equations (4.56), (4.62)). With growing $\sigma$, the noise dependence of the average volume is approximately the same as for the populations doubling time $T_{\text{pop}}$ (see Figure 4.2). This is a consequence of the rather small differences in the tud distributions as seen in Figure 4.3.

It is interesting to note that there is a difference between populations with exact cell division and populations with very small noise. This difference originates from the fact that the tud distribution of a population with exact cell division $\tilde{n}(x,t) = \delta(x-t)$ is not stationary. In fact, noise is needed for the population to reach a stationary tud distribution. If cell division of all cells is exact, all cells divide at the same time $t = \nu \cdot T_{\text{D}}$, with $\nu$ an integer. Thus, the tud distribution depends on the time that passed since the last cell division events.

In this section, we derived analytical expressions of the mean volume of populations with exact cells division and with small division noise. Then we compared these values with those

for noisy populations (Figure 4.5). The differences are small. Thus, from an experiment on the population level, we can not distinguish between the magnitude of noise on the single cell level. The same is true for the difference between linear and exponential single cell volume increase.

## 4.3 Growth in fluctuating environments

### 4.3.1 Optimal growth strategy for homogeneous populations

In the previous section 4.2, we have considered growth in homogeneous environments. In a next step we ask whether the presence of noise could provide an advantage for growth in fluctuating environments. To analyze this general question in a specific context we have developed a theoretical model that describes the growth of a bacterial population in an environment with fluctuating supply of nutrients. More specifically, we consider a situation where the nutrients in the growth medium switch periodically (with period $T_S$). For simplicity we consider periodic switching between two limiting nutrients A and B.

There are mainly two strategies how an individual cell can cope with these changing conditions. One strategy (in the following denoted as strategy 1) is to produce only the molecular machinery required to grow on the nutrient that is currently present in the medium: if nutrient A is available only the machinery for A is produced. If nutrient B is present the machinery required to grow on B is only produced. Thus, if in the environment the availability of one nutrient switches to the other, new molecular machinery has to be produced. This requires an adaption time $T_A$ during which the cells can not grow. After adaptation, the cells grow with doubling time $T_1$. For simplicity we assume that the growth rate is identical for growth on both nutrients. Our results do not depend on this assumption.

A different strategy (in the following denoted as strategy 2) is to produce all molecular machinery to grow on A and B independent on which nutrient is currently present in the medium. In this way no adaption is required after a switch in nutrients and the cells simply keep growing. Strategy 2 cells grow with doubling time $T_2$ (again for both nutrients), and because of the extra-burden of producing not-needed proteins one expects $T_2 > T_1$.

Both strategies have been observed experimentally in different situations (Lendenmann and Egli, 1995; Kovarova-Kovar and Egli, 1998). Therefore, we first analyzed if our model would also yield that different strategies are advantageous depending on the values of the relevant parameters (adaption, doubling and switching time). The growth of a population with strategy 1 and one with strategy 2 in fluctuating environments is shown in Figure 4.6. For the set of parameters used, the strategy 1 population (shown in red) grows faster than the strategy 2 population (shown in blue).

To quantify the growth advantage, we determined the effective doubling time of homogeneous populations (consisting either of cells with strategy 1 or with strategy 2) in fluctuating environments. As can be seen in Figure 4.6, it can be determined by the slope within one

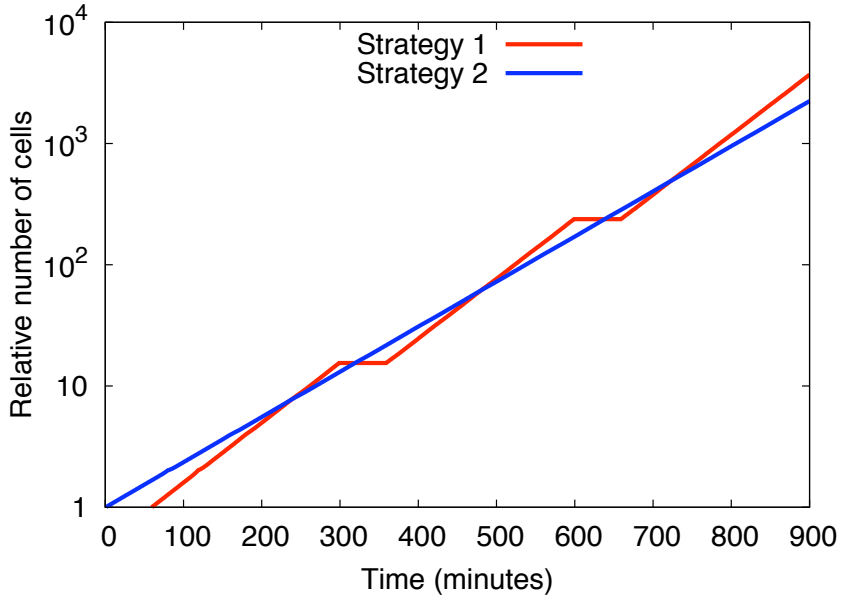


Figure 4.6: Growth curves of homogeneous populations in a fluctuating environment. The number of cells in homogeneous populations is recorded as function of time. All cells in the population grow with strategy 1 (red) or strategy 2 (blue). Data shown are for a switching period of $T_S = 300\,\text{min}$ and an adaptation time of $T_A = 50\,\text{min}$. The doubling times are $T_1 = 60\,\text{min}$ and $T_2 = 80\,\text{min}$. For these parameters, strategy 1 is advantageous. The effective doubling times of the populations are $T_1^{\text{eff}} = 72\,\text{min}$ and $T_2^{\text{eff}} = 80\,\text{min}$.

growth period $T_S$. For a strategy 1 population the effective doubling time is then given by:

$$T_1^{\text{eff}} = \frac{T_1 T_S}{T_S - T_A}, \tag{4.67}$$

while for a strategy 2 population one has

$$T_2^{\text{eff}} = T_2. \tag{4.68}$$

Figure 4.7 shows the ratio $T_1^{\text{eff}}/T_2^{\text{eff}}$ calculated from equations (4.67) and (4.68) as function of adaptation time $T_A$ and switching time $T_S$. The blue region in Figure 4.7 corresponds to the region in parameter space where this ratio is larger than 1 and the strategy 2 population grows faster. For these parameter values strategy 2 is advantageous over strategy 1. In contrast, strategy 1 is advantageous in the red regions of Figure 4.7. Thus, the strategy 2 population grows faster for large adaptation times and small switching times. The phase boundary between

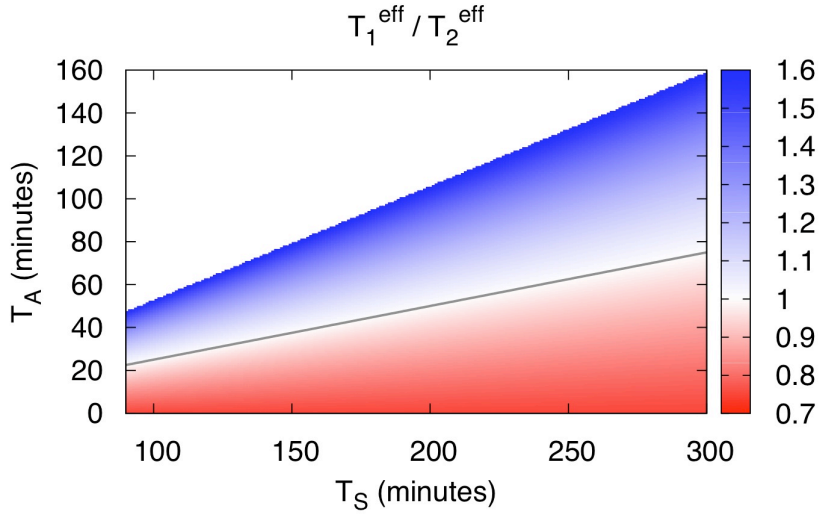


Figure 4.7: Optimal growth strategy for homogeneous populations. The ratio $T_1^{\text{eff}}/T_2^{\text{eff}}$ of the effective doubling times of homogeneous populations growing with either strategy 1 or strategy 2 is shown for varying adaptation times $T_{\text{A}}$ and switching times $T_{\text{S}}$. The effective doubling times of populations growing with strategy 1 and strategy 2 are given by equations (4.67) and (4.68), respectively. In the parameter range where $T_1^{\text{eff}}/T_2^{\text{eff}}$ is larger than 1 (region shown in blue) strategy 2 is advantageous (i.e. the population with strategy 2 cells grows faster). In the region where $T_1^{\text{eff}}/T_2^{\text{eff}}$ is smaller then 1 (shown in red), strategy 1 is advantageous. The grey line represents the phase boundary parameterized by equation (4.69). Data shown are for $T_1 = 60\,\text{min}$ and $T_2 = 80\,\text{min}$.

these two regions (shown as grey line in Figure 4.7) is given by

$$T_{\text{A}} = T_{\text{S}} \left(1 - \frac{T_1}{T_2}\right). \tag{4.69}$$

Figure 4.7 clearly shows that both strategies can be advantageous depending on how long it takes to adapt to the new nutrient and how often the switching takes place. Thus, both growth strategies are only advantageous in a limited range of parameters ($T_{\text{A}}$,$T_{\text{S}}$).

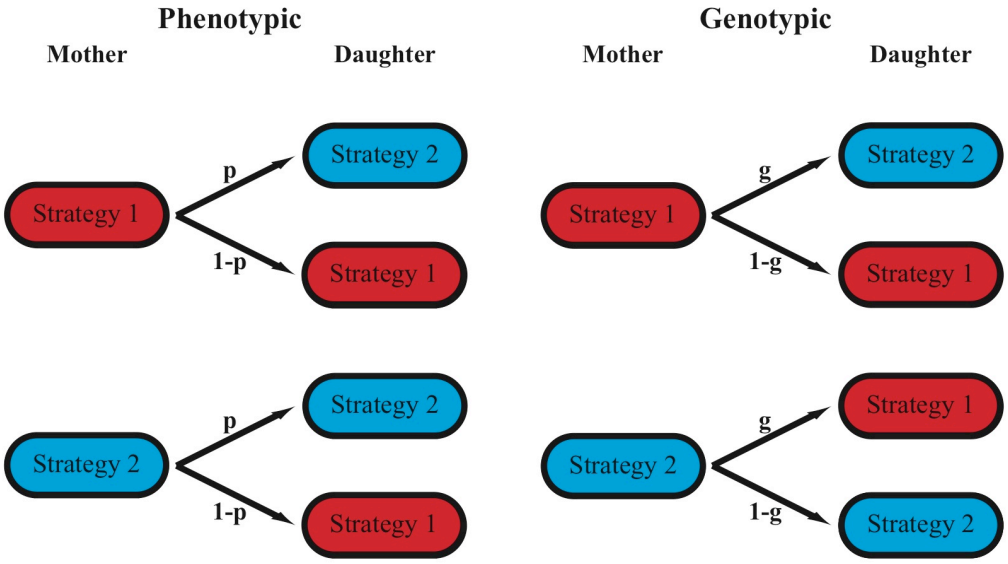


Figure 4.8: Division scheme for the two diversification models. A newborn cell randomly chooses a growth strategy. In case of phenotypic diversification, strategy 2 is chosen with probability $p$ and strategy 1 is chosen with probability $1-p$ independent of the strategy of the mother cell. For genotypic diversification this scheme is different, since here the probability of choosing strategy 1 or 2 depends on the strategy of the mother cell. Here, $g$ denotes the probability that a newborn cell chooses a different strategy than its mother.

### 4.3.2 Heterogeneous populations with noise in growth strategy

In the previous section, we compared homogeneous populations growing either with strategy 1 or with strategy 2. Depending on the system parameters, one or the other strategy can by advantageous. In a next step, we ask if it might be favorable for a homogeneous population to diversify, i.e. to consist of a noise induced mixture of strategy 1 and strategy 2 cells. With such a diversification a homogeneous population consisting of cells with, say, strategy 1 might extend the advantageous parameter range by allowing some of its cells to convert to strategy 2. To test this possibility we analyzed if there are parameter values $T_{\mathrm{A}}$ and $T_{\mathrm{S}}$ for which such a diversified population grows faster than both of the homogeneous populations (where all cells grow with the same strategy).

For this analysis we implemented two different diversification models as illustrated in Figure 4.8. In both models, individual newborn cells are either growing with strategy 1 or with strategy 2. The choice of strategy is noise-induced. In our first model (phenotypic diversification) the cells choose a growth strategy (1 or 2) because of environmental influences. In particular, the choice of strategy is independent of the strategy of their mother. In the following, we denote

by $p$ the probability that a newborn cell chooses strategy 2. Whenever a daughter cell chooses a different growth strategy than the mother cell, it has to adapt to the external conditions. This also requires an adapting time, denoted by $T_{\mathrm{A}}^{\mathrm{B}}$, adaptation time at birth. This adaptation process is either caused by the production of additional metabolic machinery (for cells that switch from strategy 1 to strategy 2) or the adjustment to higher growth rate (for cells that switch from strategy 2 to strategy 1). In the following we focus on the special case where these two adaption times are equal: $T_{\mathrm{A}}^{\mathrm{B}} = T_{\mathrm{A}}$. The influence of this assumption on our results is discussed in more detail in section 4.3.3.

To formulate this model mathematically it is again useful to use a continuum description. At time $t$, there are $n_i(x,t)$ cells using growth strategy $i$ with time until division $x$. At birth the interdivision time of a newborn cell with strategy $i$ is drawn from the distributions $P_i(x)$ with mean $T_i$ for $i \in \{1,2\}$. The time evolution of the population then implies:

$$\partial_t n_1(x,t) = \partial_x n_1(x,t) + (1-p)\cdot n_1(0,t)\,P_1(x) + (1-p)\cdot n_2(0,t)\,P_1(x) \quad (4.70)$$

$$\partial_t n_2(x,t) = \partial_x n_2(x,t) + p\cdot n_1(0,t)\,P_2(x) + p\cdot n_2(0,t)\,P_2(x)\,. \quad (4.71)$$

The second model describes diversification on the genotypic level. In this case, the growth behavior is assumed to depend only on the genetic code. Thus, at birth a newborn cell enters a different growth strategy than the mother cell by a mutation. This transition occurs at a diversification probability $g$. In this genotypic diversification model, one has:

$$\partial_t n_1(x,t) = \partial_x n_1(x,t) + (1-g)\cdot n_1(0,t)\,P_1(x) + g\cdot n_2(0,t)\,P_1(x) \quad (4.72)$$

$$\partial_t n_2(x,t) = \partial_x n_2(x,t) + g\cdot n_1(0,t)\,P_2(x) + (1-g)\cdot n_2(0,t)\,P_2(x)\,. \quad (4.73)$$

For both models the total number of cells $N(t)$ at time $t$ is given by:

$$N(t) = \int_0^\infty (n_1(x,t) + n_2(x,t))\,dx. \quad (4.74)$$

With the help of this quantity, the growth curve of a diversified population can be created. This allows the calculation of the doubling time $T_{\mathrm{div}}$ of the diversified population by fitting the growth curve with an exponential function. To determine whether a diversification can provide an advantage in fluctuating environments we calculated $T_1^{\mathrm{eff}}/T_{\mathrm{div}}$ and $T_2^{\mathrm{eff}}/T_{\mathrm{div}}$. If these ratios are larger than one, the diversified population grows faster than the homogeneous one. These quantities are shown as function of adaptation and switching time for different diversification rates $p$ and $g$ in figures 4.9 and 4.10. From direct inspection of these plots it becomes clear that a diversified population can at most grow faster than one homogeneous population (regions shown in blue), but never faster than both homogeneous populations.

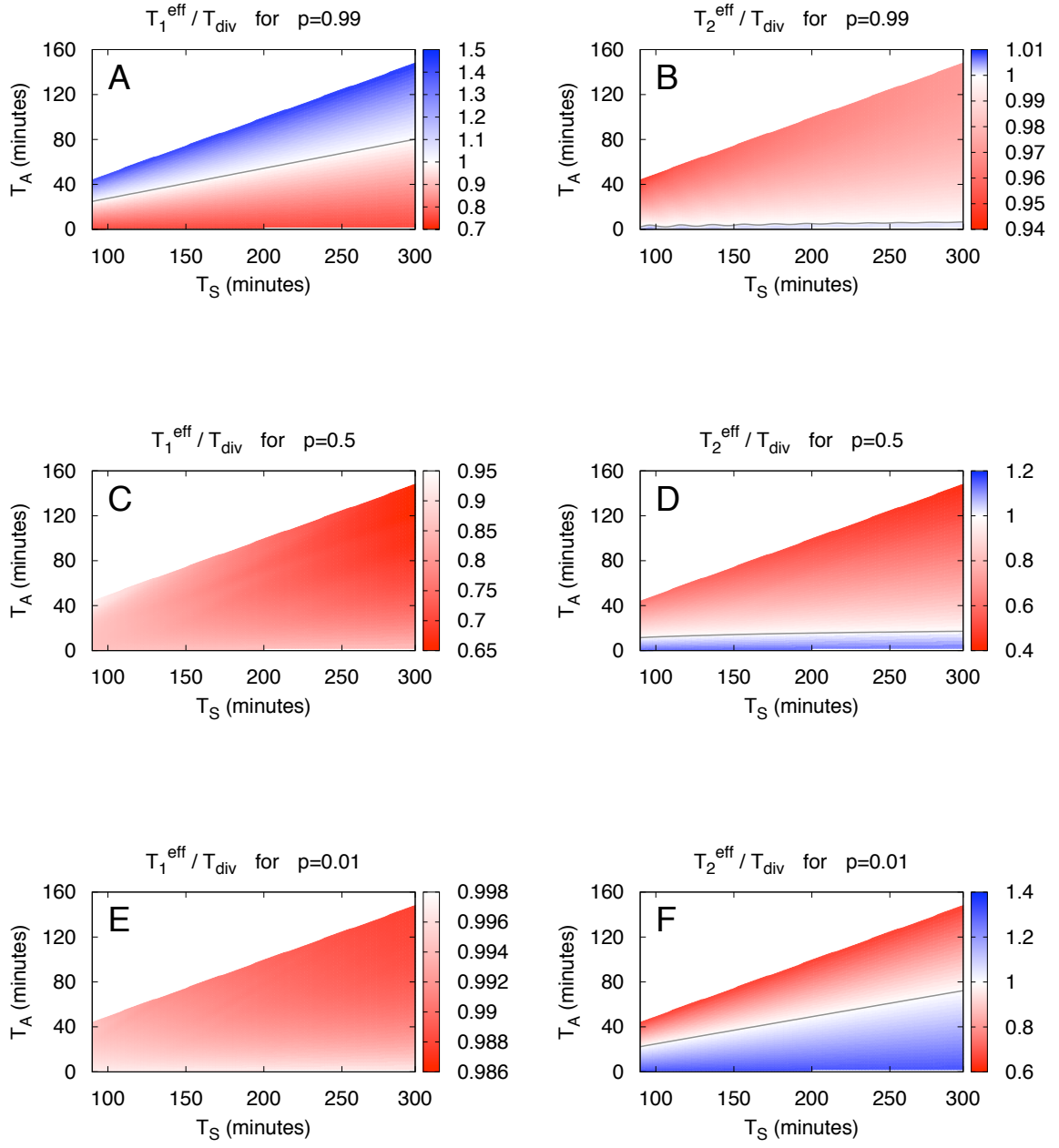


Figure 4.9: Growth comparison of a diversified population to homogeneous populations as function of $T_\mathrm{S}$ and $T_\mathrm{A}$ for varying diversification rates $p$. Single cell diversification is implemented according to the phenotypic model, see Figure 4.8. The diversified population grows with doubling time $T_\mathrm{div}$, a homogeneous population grows with $T_i^\mathrm{eff}$ when using strategy $i \in \{1, 2\}$. The ratios $T_i^\mathrm{eff}/T_\mathrm{div}$ are shown for different diversification rates $p$: $p = 0.99$ in figures (A) and (B), $p = 0.5$ in figures (C) and (D), and $p = 0.01$ in figures (E) and (F).

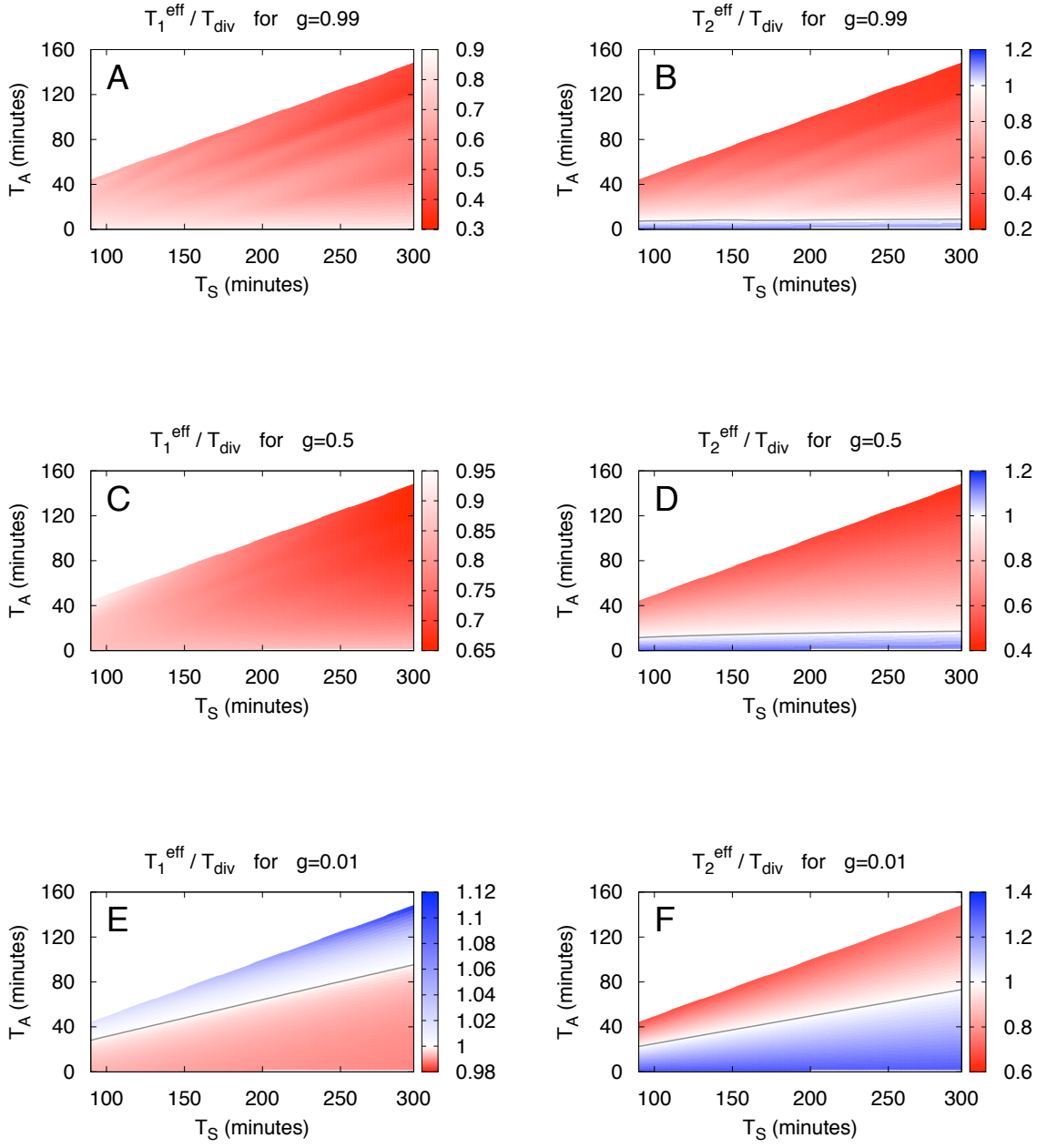


Figure 4.10: Growth comparison of a diversified population to homogeneous populations as function of $T_{\mathrm{S}}$ and $T_{\mathrm{A}}$ for varying diversification rates $p$. Single cell diversification is implemented according to the genotypic model, see Figure 4.8. The diversified population grows with doubling time $T_{\mathrm{div}}$, a homogeneous population grows with $T_i^{\mathrm{eff}}$ when using strategy $i \in \{1, 2\}$. The ratios $T_i^{\mathrm{eff}}/T_{\mathrm{div}}$ are shown for different diversification rates $g$: $g = 0.99$ in figures (A) and (B), $g = 0.5$ in figures (C) and (D), and $g = 0.01$ in figures (E) and (F).

For example consider phenotypic diversification with a diversification rate $p = 0.99$ (Figure 4.9, (A) and (B)). For $T_A = 60\,\text{min}$ and $T_S = 200\,\text{min}$, the diversified population grows faster than a homogeneous with strategy 1 (see Figure 4.9, (A)). However, for the same parameter values a homogeneous population with strategy 2 grows faster than the diversified one, as seen in fig. 4.9, (B). Such a behavior can be found for all parameter values both for the phenotypic and in the genotypic diversification model.

In this section we found that the fastest growing population in the fluctuating environment is always homogeneous, and never the diversified population. Which of the homogeneous populations is growing fastest we discussed in section 4.3.1. In other words, Figure 4.7 tells u s the optimal growth strategy (1 or 2) in the environment. In the following section, we will further clarify the influence of our basic assumptions on the general outcome of our model.

### 4.3.3 Testing the impact of our model assumptions

The conclusion that one of our homogeneous populations is always advantageous towards a heterogeneous population is surprising in light of earlier results on similar models (Thattai and van Oudenaarden, 2004; Kussell and Leibler, 2005). These studies claim that diversification can be advantageous in fluctuating environments. To clarify which of our model assumptions is responsible for our main outcome, we looked for advantages of diversification in a variety of additional conditions.

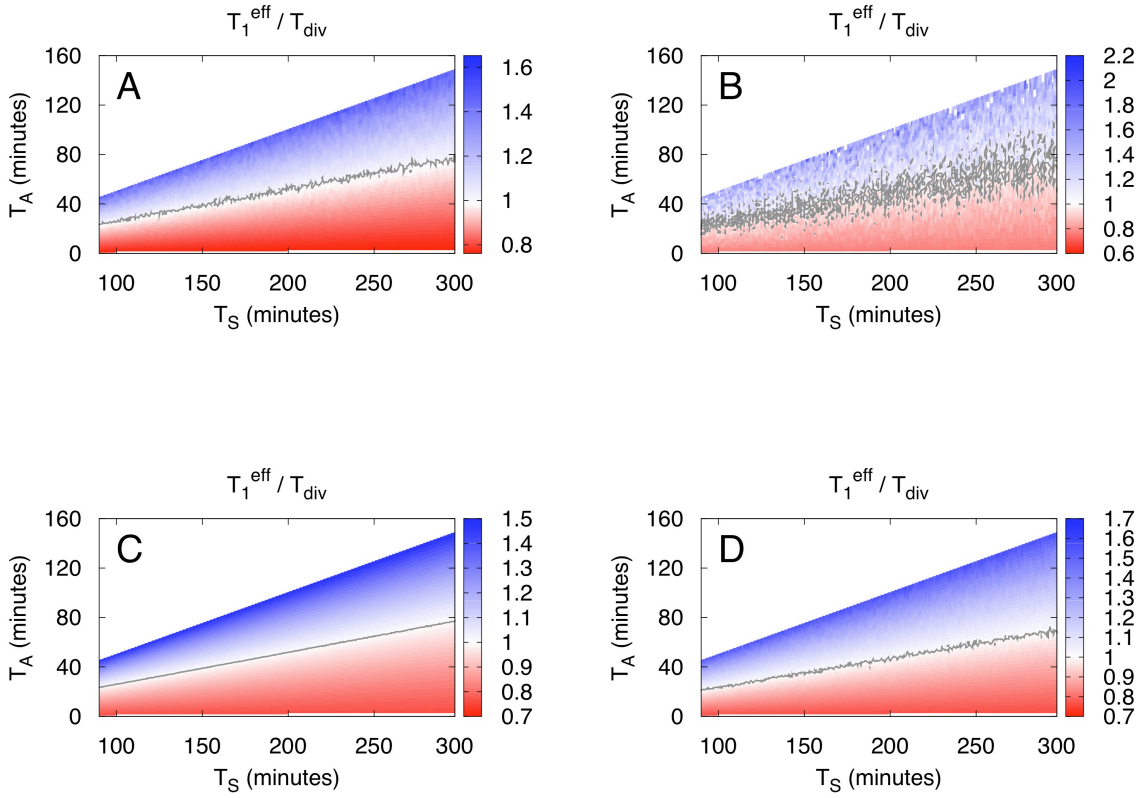


Figure 4.11: Effect of noisy switching: $T_1^{\text{eff}}/T_{\text{div}}$ is shown for a phenotypically diversified population as function of average switching time $T_{\text{S}}$ and adaptation time $T_{\text{A}}$. The diversification rate is $p = 0.99$. In figures (A) and (B), the population growth was followed over 8 switching periods. In (A) Switching times are drawn from a normal distribution, in (B) from an exponential distribution. Figures (C) and (D) show averages over 100 runs with Gaussian and exponential switching, respectively.

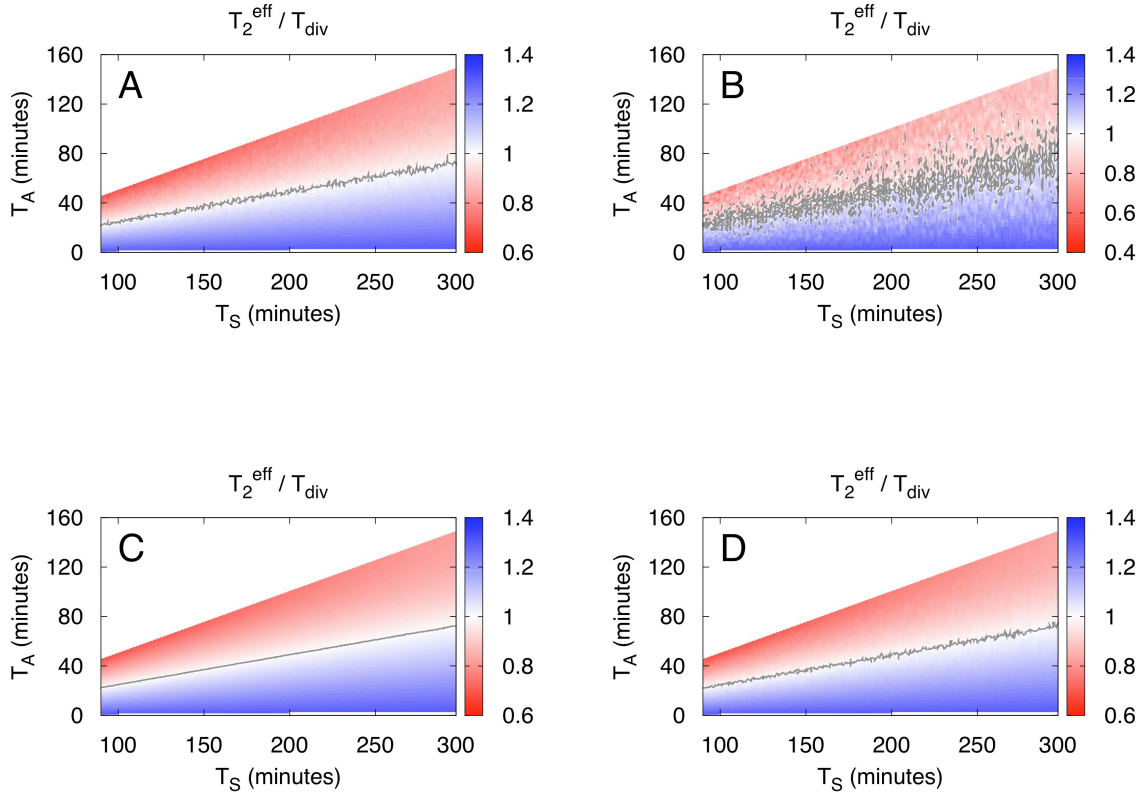


Figure 4.12: Effect of noisy switching: $T_2^{\text{eff}}/T_{\text{div}}$ is shown for a genotypically diversified population as function of average switching time $T_{\text{S}}$ and adaptation time $T_{\text{A}}$. The diversification rate is $g = 0.01$. In figures (A) and (B), the population growth was followed over 8 switching periods. In (A) switching times are drawn from a normal distribution, in (B) from an exponential distribution. Figures (C) and (D) show averages over 100 runs with Gaussian and exponential switching, respectively.

### Stochastically switching environments

Our model as presented above assumes periodic switching in external conditions. Now we analyze our model in a more realistic scenario where $T_{\text{S}}$ is not constant. We implemented two different randomly switching environments. In the first environment, switching times are chosen from a normal distribution with mean $T_{\text{S}}$. In the second environment, switching occurs as a Poisson process. Thus, the switching times are chosen from an exponential distribution, again with mean $T_{\text{S}}$.

Results for a phenotypically diverse population in a stochastically switching environment are shown in Figure 4.11. We determined $T_1^{\text{eff}}/T_{\text{div}}$ by following population growth over eight switching periods (figures 4.11 (A) and (B)). When comparing these results to the behavior in

a periodic environment (Figure 4.9 (A)), we can see fluctuations in $T_1^{\text{eff}}/T_{\text{div}}$. However, when we average over 100 of these runs (figures 4.11, (C) and (D)), the behavior more and more resembles that of periodic switching.

A similar behavior is found for the genotypic diversification model. As an example, we choose the quantity $T_2^{\text{eff}}/T_{\text{div}}$ for a diversification rate $g = 0.01$. The behavior in the corresponding periodically switching environment can be seen in Figure 4.10, (F). When following growth over eight switching periods, fluctuations in populations behavior can be seen (Figure 4.12). However, averaging over 100 runs shows that on the long run, the system will behave like in a periodic environment.

Performing the same analysis for other parameter values $p$ and $g$ always yields the behavior like in the above examples. Thus, a randomly switching environment (with mean switching time $T_{\text{S}}$) allows the same population doubling time $T_{\text{div}}$ as a periodic environment. In fact, the doubling times of all three populations, $T_1^{\text{eff}}$, $T_2^{\text{eff}}$, $T_{\text{div}}$ only depend on the average switching rate.

### Adaptation time at a strategy switch

In our model cells have to adapt when choosing a different growth strategy than their mother cell. Above, we assumed that this adaptation process takes the same time as adaptation after an environmental switch: $T_{\text{A}}^{\text{B}} = T_{\text{A}}$. To test the influence of this assumption, we systematically varied the adaptation time $T_{\text{A}}^{\text{B}}$. In case $T_{\text{A}}^{\text{B}} = T_{\text{A}}$, a diversified population is never growing the fastest as discussed in section 4.3.2. If $T_{\text{A}}^{\text{B}} > T_{\text{A}}$, this is still true, because it simply slows the growth of the diversified population. But for $T_{\text{A}}^{\text{B}} < T_{\text{A}}$, the doubling time of the diversified population $T_{\text{div}}$ continuously decreases. As we are looking for situations where diversification is advantageous, we thus focus on the case $T_{\text{A}}^{\text{B}} = 0$. Systematic analysis of this scenario showed that phenotypic diversification still never provides a growth advantage (data not shown).

Genotypic diversification however can be advantageous, as shown in Figure 4.13 (C) for a diversification rate of $g = 1$. In this figure, we show the ratio of the minimum of $T_1^{\text{eff}}$ and $T_2^{\text{eff}}$ over $T_{\text{div}}$. Thus, this Figure compares the doubling time of the faster growing homogeneous population with that of the diversified population. For parameters ($T_{\text{S}}$,$T_{\text{A}}$) in the blue region of Figure 4.13 (C), is true that both $T_1^{\text{eff}}/T_{\text{div}} > 1$ and $T_2^{\text{eff}}/T_{\text{div}} > 1$, and the diversified population grows fastest. One example is $T_A = 50\,\text{min}$ and $T_S = 140\,\text{min}$. The growth of the diversified population at these parameter values is shown in Figure 4.13 (D).

Since $g = 1$, every newborn cell chooses a different strategy than its mother cell. After a switch in growth medium, strategy 1 cells do not grow and divide. However, every cell division of a strategy 2 cell produces two strategy 1 cells. Thus, the number of strategy 1 cells increases, while that of strategy 2 cells decreases. When the adaptation is over, strategy 1 cells start to grow. Since strategy 1 cells produce two strategy 2 cells, now the number of strategy 2 cells increases. As a result of this division behavior, the population grows in a strange fashion, as

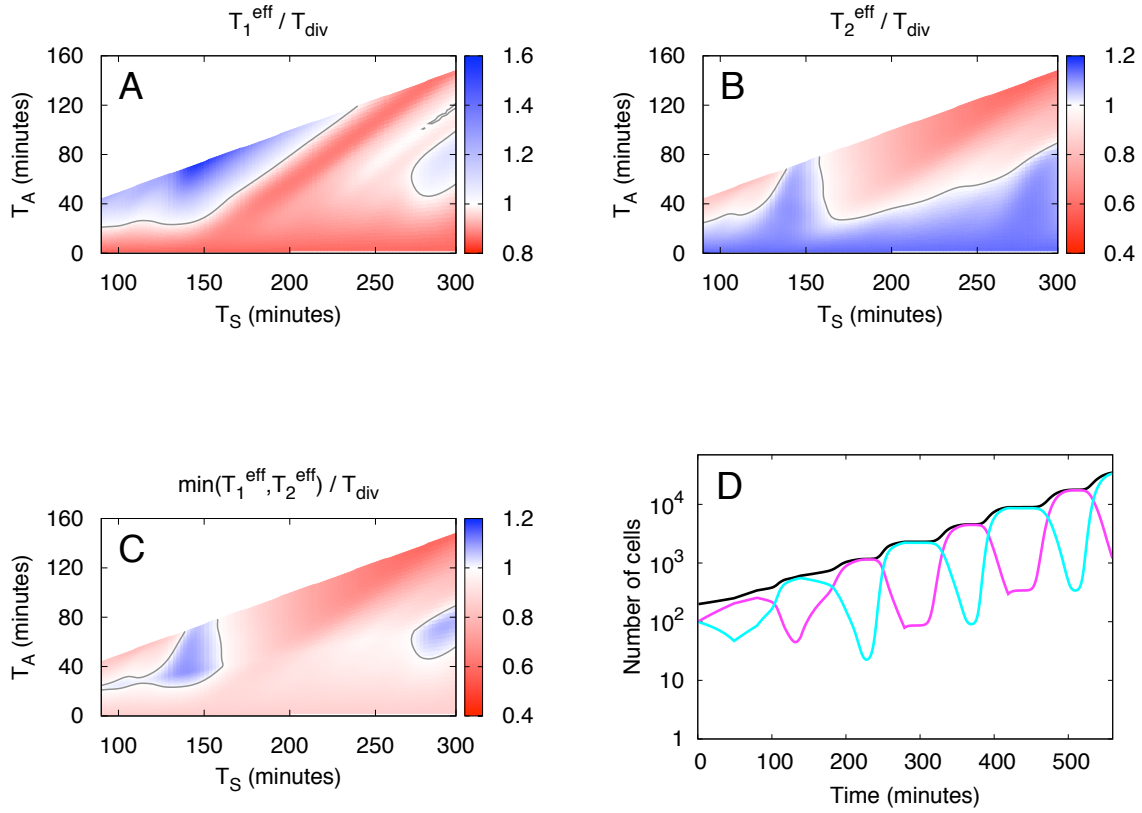


Figure 4.13: Genotypically diverse population (with $g = 1$) growing without adaptation at a strategy switch: $T_{\mathrm{A}}^{\mathrm{B}} = 0$. $T_1^{\mathrm{eff}}/T_{\mathrm{div}}$ and $T_2^{\mathrm{eff}}/T_{\mathrm{div}}$ is shown as function of switching time $T_{\mathrm{S}}$ and adaptation time $T_{\mathrm{A}}$ in (A) and (B), respectively. Figure (C) shows $\min\left(T_1^{\mathrm{eff}}, T_2^{\mathrm{eff}}\right)/T_{\mathrm{div}}$, thus compares the diversified population with the faster growing homogeneous population. Figure (D) shows the growth of the diversified population for $T_{\mathrm{A}} = 50\,\mathrm{min}$ and $T_{\mathrm{S}} = 140\,\mathrm{min}$. Total number of cells $N(t)$ at time $t$ is shown in black. The number of cells growing with strategy 1 and 2 are shown in magenta and cyan, respectively.

seen in Figure 4.13 (D): The black line shows the total number of cells in the population, the magenta and cyan lines show the number of cells growing with strategy 1 and 2, respectively. In the beginning, the two sub-populations have 100 cells each, and the strategy 1 cells have to adapt. When the adaptation time is over, almost all cells in the population are strategy 1 cells. Subsequently, the number of strategy 1 cells decreases and the number of strategy 2 cells increases, because the strategy 1 cells grow faster then the strategy 2 cells. This carries on until the population exclusively consists of strategy 2 cells. Then, switching occurs, and the number of strategy 2 cells decreases, the number of strategy 1 cells increases, yielding a population that exclusively consists of strategy 1 cells and so on.

As can be seen from Figure 4.13 (C), the diversified population is only advantageous in a small region of phase space indicating that some fine-tuning of growth parameters ($T_1$,$T_2$) with environmental parameters ($T_S$,$T_A$) is required. For decreasing $g$ the parameter range for which the diversified population is growing the fastest is getting smaller until it vanishes at $g = 0.5$.

### 4.3.4 Comparison of our model to other studies

In several different studies, it was shown that diversification can be advantageous under fluctuating conditions (Philippi and Seger, 1989; Thattai and van Oudenaarden, 2004; Kussell and Leibler, 2005). Our system on the other hand does not yield a growth advantage due to diversification, and shows that a homogeneous population grows fastest. Many systems, for which a diversification was found to be advantageous under fluctuating conditions, fundamentally differ from our model. For example, in the systems discussed by Philippi and Seger (1989) the diversification rates depend on time and growth condition, whereas in our model they are constant.

There are two particular studies on models that at first glance resemble our system, but draw a contradicting conclusion (Thattai and van Oudenaarden, 2004; Kussell and Leibler, 2005). Now, we discuss the differences of these models to our model in more detail.

Our model differs from that of Thattai and van Oudenaarden (2004) in several ways. The cells in their model do not have to adapt after an environmental switch. A switch is implemented by exchanging the doubling times of the cells. For example, at condition A, strategy 1 and strategy 2 cells grow at doubling times $T_1$ and $T_2$, respectively. When the environment switches to condition B, strategy 1 cells grow at $T_2$ and vice versa. Thus, under each condition one part of the population can grow fast (at $T_1$). In what they call a homogeneous population, slow growing cells become fast growing cells at rate $k_1$. Their heterogeneous population differs from the homogeneous population such that fast growing cells can also become slow growing cells, at rate $k_0$. Diversification is considered advantageous, if the fastest growth is shown by a population with $k_0 > 0$. Thus, according to our definition, non of the populations that are compared are homogeneous.

The model of Kussell and Leibler (2005) compares a population that adapts to the current conditions (which they call responsive switching) to a population that randomly chooses a phenotype (this is called stochastic switching). They find that under some conditions stochastic switching is favored over responsive switching. In other words, a diversified population grows faster than a population that adapts to the current conditions. Thus, in our terminology, they find that a heterogeneous population is advantages towards a homogeneous strategy 1 population. Our model reproduces this finding. The diversified population can grow faster than a homogeneous population growing with strategy 1, see figures 4.9 and 4.10. However, in our model the diversified population is then slower than the homogeneous population growing with strategy 2, a population that they do not consider.

## 4.4 Discussion

It has been demonstrated with many different approaches that on the single cell level fundamental cellular processes are significantly affected by the presence of noise. Molecular noise might originate from a variety of sources such as inhomogeneities in growth medium, uneven partitioning of regulator proteins at cell division, mutations etc. In this study, we analyzed if such noise affects the macroscopic properties of growing bacterial populations. In particular, we analyzed the effects of uneven cell division and of noise in transcriptional regulation of metabolic machineries that are required for growth on specific nutrients.

If two bacterial populations were competing in a given environment, the faster growing population could outnumber the slower growing population. For this reason, we are particularly interested in the population doubling time as it displays a growth advantage. We investigated two situations in which single cell noise could affect the population doubling time, and provide an advantage or a disadvantage for the population. Under constant conditions, single cell division noise does not significantly affect the population doubling time if cells are growing with exponential mass increase. If the cells increase their mass linearly, division noise even increases population growth rate. In fluctuating conditions, noise in growth strategy always provides a disadvantage to the population. As a consequence, it is beneficial for the population to be homogeneous under fluctuating conditions.

First, we analyzed the influence of noise in the division process on the growth behavior of a population growing in non-changing environmental conditions. Experimentally, such a scenario would be realized by growth in a chemostat or in batch culture under non-limiting conditions. To study this scenario we have developed a simple mathematical model in which the growth of the population is the result of the growth and division of the individual cells belonging to the population. Because of the presence of noise every cell division leads to two daughter cells of different mass. As an important consequence the two daughter cells have different individual inter division times, i.e. the larger born daughter cell divides earlier than the smaller one. For our analysis it is not important from which detailed molecular processes this difference arises. For example, uneven partitioning of ribosomes, or regulator proteins could be responsible for it or even simpler, the larger daughter has to produce less mass to reach its division mass.

From the mathematical analysis of our model, we found, to our own surprise, that divisional noise has no effect on the growth rate of a population of cells with exponential mass increase. The effect of noise in cell division on growth rate is more dramatic for cells with linear mass increase. Here, the results of our analysis suggest that noise leads to a growth advantage. It is advantageous for a growing bacterial population to implement cell division such that it produces two daughters of uneven mass. The increase in growth rate is the larger the more the two daughter cells differ in birth mass. In the light of our findings it is therefore very surprising that the division machinery shows such high precision in determining the mid-cell position. In *E. coli*, typically cell division occurs 3%-10% (of total length) from midcell (Koppes et al.,

1978; Trueba, 1982; Guberman et al., 2008). The correct placement of the bacterial division site is achieved by a combination of two inhibitory effects, the min system (de Boer et al., 1989; Rothfield et al., 2001; Hu et al., 2003; Shih et al., 2003) and nucleoid occlusion (NO) (Woldringh et al., 1991; Yu and Margolin, 1999; Bernhardt and de Boer, 2005; Margolin, 2001; Errington et al., 2003). The min system prevents cell division at the poles of the cells, while NO inhibits Z-ring formation in direct vicinity of the chromosome. In this way DNA triggers the placement of the division site and the precision of cell division may be a consequence of the physical properties of DNA.

Our results also seem to indicate that for populations the presence of transcriptional and translation noise does not necessarily lead to a growth advantage at least not in the specific scenario considered here, where such noise affects the metabolic program of individual cells in a fluctuating environment. We considered the growth of bacterial populations that have two different strategies of coping with changing nutritional conditions: strategy 1 (where they only produce the metabolic machinery required to grow on the present nutrients) and strategy 2 (where additionally metabolic machinery for nutrients not available in the growth medium are produced). In our model noise influences the strategy chosen by a newborn cell, yielding a diversified population.

We implemented two different diversification models: A diversification on the genotypic level originates from a mutation. On the other hand, a phenotypic diversification is due to random environmental influences on the cell. It could be caused by inhomogeneities in the growth medium, uneven partitioning of regulator proteins, or transcriptional noise. As a consequence, in the phenotypic model the strategy chosen by the newborn cell is independent of the strategy of the mother cell, whereas for the genotypic model it does depend on the strategy of the mother cell.

Interestingly, in both cases (i.e. for both phenotypic and genotypic diversification), the noise-induced mixture of cells never grows faster than a homogeneous population. For all parameter values at least one of the homogeneous populations is growing faster implying that a noise-induced diversification is evolutionary unstable. These findings can be understood as follows: For given growth conditions either strategy 1 or strategy 2 is advantageous.

Let's assume that for the given conditions strategy 1 is advantageous. Then, the fastest growing population consists only of strategy 1 cells. For such a strategy 1 population diversification leads to formation of a subpopulation of cells with strategy 2. However, because strategy 2 cells grow (under the given conditions) slower than strategy 1 cells, this diversification just implements the wrong strategy in some of cells leading to a decrease in growth rate of the population. For a strategy 2 population, however, diversification leads to an increase in growth rate since now some of the cells grow faster with strategy 1. In particular, the strategy 2 population grows the faster the larger the fraction of (diversified) strategy 1 cells is. Thus, in both cases the noise-induced fluctuations drive the system towards a homogeneous population with strategy 1. Similarly, for growth conditions that favor strategy 2 the noise-induced fluctuations

drive the system towards a homogeneous strategy 2 population.

Other studies (Thattai and van Oudenaarden, 2004; Kussell and Leibler, 2005) have found that diversification can be favorable in fluctuating environments. However, we believe that their findings are the consequence of an incomplete comparison of all possible realizations of populations. For example, in the model by Thattai and van Oudenaarden (2004) cells do not have to adapt to environmental changes. In addition, the ground state is already diversified (according to our definition). The model by Kussell and Leibler (2005) compares the heterogeneous population only to one possible homogeneous population.

Nevertheless, we wanted to further elaborate the origin of our findings. For this reason, we looked for conditions providing advantages for diversified populations in our model. As a first step, we questioned our assumption that the medium switches periodically. However, it turned out that a random switching mechanism does not change our results. The population doubling time of the homogeneous as well as of the diversified populations only depend on the average switching time. In other words, the growth rate is robust against statistical fluctuations of the switching times.

The independence of population growth on randomized switching is interesting when regarding fluctuating environments as a natural habitat for bacteria (in contrast to constant conditions in the laboratory). The average switching rate reflects the long-term properties of the habitat. As the choice of optimal growth strategy depends on the average switching time and not on the current one, it is independent on short-term behavior.

We found diversification to be favorable only for non-realistic conditions. Namely, for a genotypically diversified population that does not have to adapt to the change in growth strategy at birth ($T_{\mathrm{A}}^{\mathrm{B}} = 0$) and that diversifies at high rates $g > 0.5$. That this corresponds to a rather artificial growth strategy that also requires quite some fine-tuning of parameters can be made clear by considering the case $g = 1$. In this case all newborn cells have a different strategy than their mother. Let's consider the case where a switching event occurs at $t = 0$. Then, all strategy 1 cells stop growing (due to adaptation) while strategy 2 cells keep growing and dividing. Because only strategy 2 cells divide and $g = 1$, the fraction of strategy 1 cells increases while that of strategy 2 cells decreases. Thus, for appropriately chosen $T_{\mathrm{A}}$, the population mainly consists of strategy 1 cells at time $t = T_{\mathrm{A}}$. In this way large parts of the population grow with the higher growth rate $(T_1)^{-1}$ right after adaption time is over. In this way the diversification strategy optimizes growth in the lag phase (by having a large fraction of strategy 2 cells for $t < T_{\mathrm{A}}$) and the growth after adaption (by having a large fraction of strategy 1 cells for $t > T_{\mathrm{A}}$). As growth proceeds the strategy 1 cells all divide giving rise to a population that mainly consists of strategy 2 cells. This leads to an oscillation of the composition of the population that alternates between the two homogeneous populations. Thus, the degree of diversification is not constant and in contrast to the other scenarios there are no stable subpopulations. It also clear that this strategy only works if $T_1$, $T_2$, $T_{\mathrm{S}}$ and $T_{\mathrm{A}}$ are chosen properly. We don't believe that this scenario has any relevance for biological systems since it

involves parameter fine-tuning and unrealistic high mutation rates.

Our main results that homogeneous populations always grow faster than a heterogeneous one, implies that individuality in bacterial populations does not reflect a growth advantage under the conditions that we take into account. However, the observed variation in bacterial populations can be due to advantages under conditions that are not covered by our model. We can only speculate here about its origin. For example, it is possible that the costs for a more precise regulatory system exceed the benefit of being homogeneous. Or the individuality might provide a mechanism to keep phenotypic or genotypic variations alive that guarantee survival of the population under more severe or irreversible changes in the environment.

## 4.5 Computational details

The simulation of the growth of bacterial population in a homogeneous environment started from a single newborn cell that divides after $t = T_{\mathrm{D}}$. To determine when cells divide, we keep track of the time until division $x$ of every cell. A simulation step represents one time step and in every time step x is reduced by one for all present cells. At every time step, all cells with $x = 0$ divide into two new cells. For each of these two cells, an inter division time $\tau$ is determined and given to the cell by setting its time until division to $x = \tau$. In the absence of noise, every cell is given an inter division time of $\tau = T_{\mathrm{D}}$. Thus, every cell divides after a time $t = T_{\mathrm{D}}$ has passed. In the presence of noise, one newborn cell is given a birth mass $m_{\mathrm{B}}$ from a normal distribution with mean $m_{\mathrm{D}}/2$ and standard deviation $\sigma$. $m_{\mathrm{D}}$ is the division mass of the mother cell. Its sister cell is given the birth mass $m_{\mathrm{D}}/2 - m_{\mathrm{B}}$. Then the birth mass of every cell is transformed into the inter division time $\tau$ according to:

$$\tau = -T_{\mathrm{D}} \log_2 \left( \frac{m}{m_{\mathrm{D}}} \right) \tag{4.75}$$

or

$$\tau = 2T_{\mathrm{D}} \left( 1 - \frac{m}{m_{\mathrm{D}}} \right) \tag{4.76}$$

for exponential and linear single cell mass increase, respectively. We created a time until division distribution $n\,(x,t)$ at time $t$ by simply counting the number of cells with a tud of $x$. With the help of the tud distribution we calculated the total mass of the population for an OD-Plot by summation:

$$M\,(t) = \int_0^\infty n\,(x,t)\, m\,(x)\, dx, \tag{4.77}$$

whereas the mass increase of a single cell is given by equations (4.33) and (4.36).

The growth of populations in fluctuating environments is simulated by keeping track of the tud distributions $n(x,t)$. For a growing homogeneous population, the time evolution of the tud distribution is given by equation 4.6. Strategy 1 and strategy 2 populations behave like

homogeneous populations except for the lag phase of strategy 1 populations during which the tud distribution is kept constant. The population doubling times are obtained by fitting the total number of cells in the population

$$N(t) = \int_0^\infty n(x,t)\,dx \tag{4.78}$$

at time $t$ with an exponential function.

The diversified populations grow according to equations (4.70) - (4.73). Again, during the lag phase, the tud distribution of the strategy 1 sub population $n_1(x,t)$ is kept constant. The population doubling time $T_{\text{div}}$ is obtained by fitting the total number of cells (equation (4.74)) to en exponential function.

All simulations were implemented in self-written C Programs.

# Chapter 5

# Concluding Remarks

In this work, we studied biological systems that are related to bacterial cell division. In these systems the macroscopic behavior is determined by the properties on the microscopic level.

First, we focused on mechanisms that control the position of the division site in a bacterial cell. We numerically simulated reaction-diffusion processes in the cell taking into account the properties of the molecules known to participate in the localization of cell division. The collective action of these proteins is responsible for the correct placement of the division site.

Second, we simulated the growth of a the bacterial population as a whole. The growth behavior of the population is influenced by the growth behavior of the single cells in the population. We discuss how noise in the division process of the single cells affects the properties on the population level. In particular we investigated the effects of noise on the growth rate of the population.

In chapter 2 we try to find the mechanism how the position of cell division is determined in *C. crescentus*. It was found that the localization of the division site is controlled by the inhibiting action of the protein MipZ. The MipZ molecules are not equally distributed over the cell but show a concentration minimum in the cell center where cell division takes place. We simulated the diffusion and the chemical reactions of MipZ and those molecules that interact with MipZ. MipZ acts as an ATPase and exists as a monomer as well as a dimer. The dimer is able to bind to DNA, therefore the diffusion of the dimers is hindered compared to that of the monomers. In the region of the cell pole, the DNA binding protein ParB is located. MipZ can bind to ParB: Because of the positioning of ParB at the cell poles, this reaction does not take place in the bulk of the cell, but exclusively at the cell poles. We have implemented in the simulations all reactions for which the rate constants are measured experimentally and found that these known reactions alone do not result in a gradient of the concentration of MipZ. The reason is, that the reaction of MipZ with ParB at the cell poles does not influence the reactions and concentration of MipZ in the bulk phase. In order to form a concentration gradient it is necessary that one or more reactions at the cell poles result in a concentration shift compared to the bulk. One possibility for such a reaction seems to be that the binding process

of MipZ to ParB influences the reaction rate constant of MipZ dimer formation. However, experiments show, that ParB has no influence on the ratio of MipZ dimers to monomers *in vitro*. Thus, the action of ParB can not change the dimer-monomer equilibrium. However, this experimental finding does not exclude the possibility that ParB acts catalytically on the MipZ dimer formation. Such a catalytic activity does not alter the equilibrium of the dimerization reaction but accelerates both the forward and back reactions. We simulated the system with the newly postulated catalytic activity of ParB and indeed found a MipZ concentration gradient. This gradient resembles those gradients found experimentally by fluorescent labeling of MipZ molecules in the cell. In the cell center, the minimum of MipZ concentration is shown. We could show that those MipZ molecules that are in the cell center are monomers, that do not prevent cell division. An analytical study showed the reasons of the formation of the MipZ concentration gradient. The catalytic action of ParB on MipZ dimerization and the fact that only the dimers can bind to DNA changes the concentration profile of MipZ. This collective effect of ParB and DNA results in different dissociation constants of MipZ dimers for the pole regions and the bulk phase. Together with the hindered diffusion of $(\mathrm{MipZ})_2$ this shift in the dissociation constant results in a concentration profile with a minimum in the cell center. The resulting MipZ concentration gradient reproduces experimental findings if the unknown rate constant for the catalytic effect of ParB on MipZ dimerization is in the order of $1\,\mu\mathrm{M}^{-1}\mathrm{s}^{-1}$. This rate constant can be determined experimentally. With the help of this experiment, the model can be confirmed and the exact shape of the MipZ concentration gradient can be found by simulation. Additional parameter scans of the reaction rate constants showed that the system behavior is stable towards alterations in the parameters. These parameter scans can also predict the behavior of the system when using mutant proteins. A point mutation in one of the proteins could change the reaction rate constant. If the rate constant of the mutant protein is measured experimentally, we can simulate the properties of the MipZ concentration gradients.

One important property of the reactions that cause the MipZ concentration to show a gradient is the fact the one reaction partner of MipZ, ParB, is located at the cell poles. For the Min system in *E. coli* which we considered in chapter 3 this is not the case. Here the Min proteins are responsible for the positioning of the cell division site also by an inhibitory effect. They diffuse and react in the cytoplasm as well as the membrane and there is no player in the system that is exclusively located at the poles. It was shown, that the Min proteins perform a periodic movement from one cell pole to another. Cell division inhibition is in this case caused by the fact that the time-averaged concentration of the Min proteins is maximal at the cell poles and shows a minimum in the cell center. This profile is shown if the Min proteins perform stable single oscillations. The reaction rate constants of the interactions between the Min proteins are not known from experiments. For this reason, we treated them as free parameters. Using huge computational effort, we performed a systematic parameter study by varying to the unknown rate constants. For every set of these parameters, we then changed the cell length $l$ and the

total number of molecules in the cell $N_{\mathrm{tot}}$. We found stable single oscillations, that show a minimum of the time-averaged concentration in the cell center for intermediate values of $l$ and $N_{\mathrm{tot}}$. When $l$ and $N_{\mathrm{tot}}$ increase, the Min proteins perform double oscillations. For very small values of $l$ and $N_{\mathrm{tot}}$, no oscillations are shown.

Apart from this general tendency, the exact position of the boundaries where one behavior turns to another critically depends on the choice of parameters. We found one set of parameters where stable single oscillations at physiological concentrations (2700 molecules per cell) are shown. However, there are no double oscillations at these parameters for high cell lengths of 12 $\mu$m. Nevertheless, this demonstrates that the model can show Min oscillations at physiological conditions. Since this behavior is shown for all realistic cell lengths, the number of proteins in the cell does not have to be regulated in respect to cell length. Up to now, there was no such regulation found for *E. coli*.

We also extended the model to simulate the localization of FtsZ molecules. Here, the interaction between the Min system and FtsZ plays an important role. For high values of the free parameter $k_{\mathrm{des}}$, FtsZ performs counter-oscillations and does not localize properly. For appropriately chosen $k_{\mathrm{des}}$ we showed that for single oscillations, FtsZ accumulates in the cell center. However the precision of FtsZ localization is not as high as determined experimentally. A Min double oscillation causes FtsZ to accumulate at positions at $3/4\ l$ and $1/4\ l$.

Future studies could reveal if the precision of FtsZ positioning could become more precise by adjusting $k_{\mathrm{des}}$. The analysis of the system is numerically so costly because the parameter space is huge. Experimental measurements of the reaction rate constants would remarkably decrease the parameter space and the system could be observed more efficiently.

Another interesting aspect concerning Min oscillations is cell shape. Experimentally, the Min oscillations were observed in a spherical mutant cell (Corbin et al., 2002). The oscillation pattern in these round cells is different than in rod-shaped cells. The MinD molecules move between multiple sites at the cell membrane. Further simulations could reproduce this movement and test the implications of such a behavior on the FtsZ localization.

In chapter 4, we considered the bacterial population as a whole. In particular, we investigated how fluctuations related to the division process of single cells influence the growth on the populational level. First we developed a theoretical model to simulate growth of a bacterial population in non-changing conditions. During their cell cycle, the cells increase their mass either exponentially or linearly. When the single cells grow exponentially, we found that an imprecise cell division does not affect the growth rate of the population. If the cells in the population increase their mass linearly, the division noise even increases the population growth rate. In the light of these findings, the remarkable precision of cell division in *E. coli* is surprising, because it does not help the population to grow faster. The high precision of cell division could be the cause of physical properties of the DNA.

As a next step we simulated populations that grow in a fluctuating environment. The cells choose between two different growth strategies of how to cope with the environmental

changes. First, we modeled homogeneous populations, i.e. populations in which all cells grow with the same growth strategy. Depending on the nature of the environmental fluctuations we quantified, which of the growth strategies promoted the higher population growth rate. Then, we allowed the individual cells in the population to choose their individual growth strategy. We found that this resulting heterogeneous population is never growing fastest. In all realistic scenarios, at least one of the homogeneous populations grows faster than the heterogeneous one. Thus, under the conditions considered in this work, a population can not draw a growth advantage from a diversification.

# Bibliography


Anderson, D. E., Gueiros-Filho, F. J., and Erickson, H. P. (2004). Assembly dynamics of FtsZ rings in *Bacillus subtilis* and *Escherichia coli* and effects of FtsZ-regulating proteins. *J. Bacteriol.*, 186:5775–5781.

Atlas, R. M. (1997). *Principles of Microbiology*. Wm. C. Brown Publishers.

Balaban, N., Merrin, J., Chait, R., Kowalik, L., and Leibler, S. (2004). Bacterial persistence as a phenotypic switch. *Science*, 305(5690):1622–5.

Bartosik, A. A., Lasocki, K., Mierzejewska, J., Thomas, C. M., and Jagura-Burdzy, G. (2004). ParB of *Pseudomonas aeruginosa*: interactions with its partner ParA and its target parS and specific effects on bacterial growth. *J. Bacteriol.*, 186:6983–6998.

Bernhardt, T. and de Boer, P. (2005). SlmA, a nucleoid-associated, FtsZ binding protein required for blocking septal ring assembly over chromosomes in *E. coli*. *Mol Cell*, 18(5):555–64.

Bi, E. F. and Lutkenhaus, J. (1991). FtsZ ring structure associated with division in *Escherichia coli*. *Nature*, 354(6349):161–4.

Bremer, H., Dennis, P., and Neidhart, F. (1996). *Escherichia coli and Salmonella: Cellular and Molecular Biology*, chapter Modulation of Chemical Composition and Other Parameters of the Cell by Growth Rate, pages 1553–1569. ASM Press, Washington DC.

Cano, R. J. and Borucki, M. K. (1995). Revival and identification of bacterial spores in 25- to 40-million-year-old Dominican amber. *Science*, 268:1060–1064.

Chen, Y., Bjornson, K., Redick, S. D., and Erickson, H. P. (2005). A rapid fluorescence assay for FtsZ assembly indicates cooperative assembly with a dimer nucleus. *Biophys. J.*, 88:505–514.

Chen, Y. and Erickson, H. P. (2005). Rapid in vitro assembly dynamics and subunit turnover of FtsZ demonstrated by fluorescence resonance energy transfer. *J. Biol. Chem.*, 280:22549–22554.

Cohen, D. (1966). Optimizing reproduction in a randomly varying environment. *J. Theor. Biol.*, 12:119–129.

Cooper, S. (1988). What is the bacterial growth law during the division cycle? *J Bacteriol*, 170(11):5001–5.

Cooper, S. and Helmstetter, C. E. (1968). Chromosome replication and the division cycle of *Escherichia coli* B/r. *J. Mol. Biol.*, 31:519–540.

Corbin, B. D., Yu, X. C., and Margolin, W. (2002). Exploring intracellular space: function of the Min system in round-shaped *Escherichia coli*. *EMBO J.*, 21:1998–2008.

Dajkovic, A., Pichoff, S., Lutkenhaus, J., and Wirtz, D. (2010). Cross-linking FtsZ polymers into coherent Z rings. *Mol. Microbiol.*, 78:651–668.

Davidson, C. J. and Surette, M. G. (2008). Individuality in bacteria. *Annu. Rev. Genet.*, 42:253–268.

de Boer, P., Crossley, R., and Rothfield, L. (1989). A division inhibitor and a topological specificity factor coded for by the minicell locus determine proper placement of the division septum in *E. coli*. *Cell*, 56(4):641–9.

De Robertis, E. M. (2006). Spemann's organizer and self-regulation in amphibian embryos. *Nat Rev Mol Cell Biol*, 7(4):296–302.

Deich, J., Judd, E. M., McAdams, H. H., and Moerner, W. E. (2004). Visualization of the movement of single histidine kinase molecules in live *Caulobacter* cells. *Proc Nat Acad Sci USA*, 101:15921–15926.

Donachie, W. and Begg, K. (1989). Cell length, nucleoid separation, and cell division of rod-shaped and spherical cells of *Escherichia coli*. *J Bacteriol*, 171(9):4633–9.

Driever, W. and Nuesslein-Volhard, C. (1988). A gradient of bicoid protein in *Drosophila* embryos. *Cell*, 54:83–93.

Easter, J. and Gober, J. W. (2002). ParB-stimulated nucleotide exchange regulates a switch in functionally distinct ParA activities. *Mol. Cell*, 10(2):427–34.

Ecker, R. and Kokaisl, G. (1969). Synthesis of protein, ribonucleic acid, and ribosomes by individual bacterial cells in balanced growth. *J Bacteriol*, 98(3):1219–26.

Elowitz, M., Levine, A., Siggia, E., and Swain, P. (2002). Stochastic gene expression in a single cell. *Science*, 297(5584):1183–6.

Ephrussi, A. and Johnston, D. S. (2004). Seeing is believing: the bicoid morphogen gradient matures. *Cell*, 116(2):143–52.

Errington, J. (1993). *Bacillus subtilis* sporulation: regulation of gene expression and control of morphogenesis. *Microbiol Rev*, 57(1):1–33.

Errington, J., Daniel, R., and Scheffers, D. (2003). Cytokinesis in bacteria. *Microbiol Mol Biol Rev*, 67(1):52–65.

Figge, R. M., Easter, J., and Gober, J. W. (2003). Productive interaction between the chromosome partitioning proteins, ParA and ParB, is required for the progression of the cell cycle in *Caulobacter crescentus*. *Mol Microbiol*, 47(5):1225–37.

Fuller, B. G., Lampson, M. A., Foley, E. A., Rosasco-Nitcher, S., Le, K. V., Tobelmann, P., Brautigan, D. L., Stukenberg, P. T., and Kapoor, T. M. (2008). Midzone activation of aurora B in anaphase produces an intracellular phosphorylation gradient. *Nature*, 453(7198):1132–6.

Funnell, B. E. (1991). The P1 plasmid partition complex at *parS*. The influence of *Escherichia coli* integration host factor and of substrate topology. *J. Biol. Chem.*, 266:14328–14337.

Gillespie, D. (1976). General method for numerically simulating stochastic time evolution of coupled chemical-reactions. *J Comput Phys*, 22:403–434.

Guberman, J., Fay, A., Dworkin, J., Wingreen, N., and Gitai, Z. (2008). PSICIC: noise and asymmetry in bacterial division revealed by computational image analysis at sub-pixel resolution. *PLoS Comput Biol*, 4(11):e1000233.

Harry, E. J. (2001). Bacterial cell division: regulating Z-ring formation. *Mol. Microbiol.*, 40:795–803.

Howard, M., Rutenberg, A. D., and de Vet, S. (2001). Dynamic compartmentalization of bacteria: accurate division in *E. coli*. *Phys Rev Lett*, 87(27 Pt 1):278102.

Hu, Z., Gogol, E. P., and Lutkenhaus, J. (2002). Dynamic assembly of MinD on phospholipid vesicles regulated by ATP and MinE. *Proc Natl Acad Sci USA*, 99(10):6761–6.

Hu, Z. and Lutkenhaus, J. (1999). Topological regulation of cell division in Escherichia coli involves rapid pole to pole oscillation of the division inhibitor MinC under the control of MinD and MinE. *Mol. Microbiol.*, 34:82–90.

Hu, Z., Saez, C., and Lutkenhaus, J. (2003). Recruitment of MinC, an inhibitor of Z-ring formation, to the membrane in *Escherichia coli*: role of MinD and MinE. *J Bacteriol*, 185(1):196–203.

Huang, K. C., Meir, Y., and Wingreen, N. S. (2003). Dynamic structures in *Escherichia coli*: spontaneous formation of MinE rings and MinD polar zones. *Proc Natl Acad Sci USA*, 100(22):12724–8.

Jenal, U. and Stephens, C. (2002). The *Caulobacter* cell cycle: timing, spatial organization and checkpoints. *Curr. Opin. Microbiol.*, 5:558–563.

Jensen, R. B. and Shapiro, L. (1999). The *Caulobacter crescentus smc* gene is required for cell cycle progression and chromosome segregation. *Proc Natl Acad Sci USA*, 96(19):10661–6.

Jensen, R. B., Wang, S. C., and Shapiro, L. (2002). Dynamic localization of proteins and DNA during a bacterial cell cycle. *Nat. Rev. Mol. Cell Biol.*, 3:167–176.

Kerr, R. A., Levine, H., Sejnowski, T. J., and Rappel, W.-J. (2006). Division accuracy in a stochastic model of Min oscillations in *Escherichia coli*. *Proc Natl Acad Sci USA*, 103(2):347–52.

Koch, A. (1983). The protein burden of lac operon products. *J Mol Evol*, 19(6):455–62.

Koppes, L., Woldringh, C., and Nanninga, N. (1978). Size variations and correlation of different cell cycle events in slow-growing *Escherichia coli*. *J Bacteriol*, 134(2):423–33.

Kovarova-Kovar, K. and Egli, T. (1998). Growth kinetics of suspended microbial cells: from single-substrate-controlled growth to mixed-substrate kinetics. *Microbiol Mol Biol Rev*, 62(3):646–66.

Kruse, K. (2002). A dynamic model for determining the middle of *Escherichia coli*. *Biophys J*, 82(2):618–27.

Kubitschek, H. (1986). Increase in cell mass during the division cycle of *Escherichia coli* B/rA. *J Bacteriol*, 168(2):613–8.

Kussell, E. and Leibler, S. (2005). Phenotypic diversity, population growth, and information in fluctuating environments. *Science*, 309(5743):2075–8.

Lendenmann, U. and Egli, T. (1995). Is *Escherichia coli* growing in glucose-limited chemostat culture able to utilize other sugars without lag? *Microbiology*, 141:71–78.

Leonard, T. A., Butler, P. J., and Lowe, J. (2004). Structural analysis of the chromosome segregation protein Spo0J from *Thermus thermophilus*. *Mol. Microbiol.*, 53:419–432.

Levin, B. (2004). Noninherited resistance to antibiotics. *Science*, 305(5690):1578–9.

Lin, D. C. and Grossman, A. D. (1998). Identification and characterization of a bacterial chromosome partitioning site. *Cell*, 92(5):675–85.

Lu, C., Stricker, J., and Erickson, H. P. (1998). FtsZ from *Escherichia coli*, *Azotobacter vinelandii*, and *Thermotoga maritima*–quantitation, GTP hydrolysis, and assembly. *Cell Motil. Cytoskeleton*, 40:71–86.

Margolin, W. (2001). Spatial regulation of cytokinesis in bacteria. *Curr Opin Microbiol*, 4(6):647–52.

Martin, S. G. and Berthelot-Grosjean, M. (2009). Polar gradients of the DYRK-family kinase Pom1 couple cell length with the cell cycle. *Nature*, 459(7248):852–6.

Maughan, H. and Nicholson, W. (2004). Stochastic processes influence stationary-phase decisions in *Bacillus subtilis*. *J Bacteriol*, 186(7):2212–4.

McGrath, P. T., Viollier, P., and McAdams, H. H. (2004). Setting the pace: mechanisms tying *Caulobacter* cell-cycle progression to macroscopic cellular events. *Curr. Opin. Microbiol.*, 7:192–197.

Meacci, G. and Kruse, K. (2005). Min-oscillations in *Escherichia coli* induced by interactions of membrane-bound proteins. *Phys Biol*, 2(2):89–97.

Megerle, J., Fritz, G., Gerland, U., Jung, K., and Radler, J. (2008). Timing and dynamics of single cell gene expression in the arabinose utilization system. *Biophys J*, 95(4):2103–15.

Meinhardt, H. and de Boer, P. A. (2001). Pattern formation in *Escherichia coli*: a model for the pole-to-pole oscillations of Min proteins and the localization of the division site. *Proc Natl Acad Sci USA*, 98(25):14202–7.

Menu, F., Roebuck, J. P., and Viala, M. (2000). Bet-Hedging diapause strategies in stochastic environments. *Am. Nat.*, 155:724–734.

Mohl, D. A. and Gober, J. W. (1997). Cell cycle-dependent polar localization of chromosome partitioning proteins in *Caulobacter crescentus*. *Cell*, 88(5):675–84.

Moseley, J. B., Mayeux, A., Paoletti, A., and Nurse, P. (2009). A spatial gradient coordinates cell size and mitotic entry in fission yeast. *Nature*, 459(7248):857–60.

Neidhardt, F. C., Ingraham, J. L., and Schaechter, M. (1990). *Physiology of the bacterial cell*. Sinauer Associates.

Ozbudak, E., Thattai, M., Kurtser, I., Grossman, A., and van Oudenaarden, A. (2002). Regulation of noise in the expression of a single gene. *Nat Genet*, 31(1):69–73.

Philippi, T. and Seger, J. (1989). Hedging ones evolutionary bets, revisited. *Trends in Ecology & Evolution*, 4(2):41–44.

Pierucci, O. (1978). Dimensions of *Escherichia coli* at various growth rates: model for envelope growth. *J Bacteriol*, 135(2):559–74.

Pla, J., Sanchez, M., Palacios, P., Vicente, M., and Aldea, M. (1991). Preferential cytoplasmic location of FtsZ, a protein essential for *Escherichia coli* septation. *Mol. Microbiol.*, 5:1681–1686.

Powell, E. (1956). Growth rate and generation time of bacteria, with special reference to continuous culture. *J Gen Microbiol*, 15(3):492–511.

Quardokus, E. M. and Brun, Y. V. (2003). Cell cycle timing and developmental checkpoints in Caulobacter crescentus. *Curr. Opin. Microbiol.*, 6:541–549.

Raskin, D. M. and de Boer, P. A. (1999). Rapid pole-to-pole oscillation of a protein required for directing division to the middle of *Escherichia coli*. *Proc Natl Acad Sci USA*, 96(9):4971–6.

Romberg, L., Simon, M., and Erickson, H. P. (2001). Polymerization of Ftsz, a bacterial homolog of tubulin. Is assembly cooperative? *J. Biol. Chem.*, 276:11743–11753.

Rothfield, L., Shih, Y., and King, G. (2001). Polar explorers: membrane proteins that determine division site placement. *Cell*, 106(1):13–6.

Rueda, S., Vicente, M., and Mingorance, J. (2003). Concentration and assembly of the division ring proteins FtsZ, FtsA, and ZipA during the *Escherichia coli* cell cycle. *J. Bacteriol.*, 185:3344–3351.

Shah, D., Zhang, Z., Khodursky, A., Kaldalu, N., Kurg, K., and Lewis, K. (2006). Persisters: a distinct physiological state of *E. coli*. *BMC Microbiol*, 6:53.

Shih, Y., Le, T., and Rothfield, L. (2003). Division site selection in *Escherichia coli* involves dynamic redistribution of min proteins within coiled structures that extend between the two cell poles. *Proc Natl Acad Sci U S A*, 100(13):7865–70.

Shih, Y. L., Fu, X., King, G. F., Le, T., and Rothfield, L. (2002). Division site placement in *E.coli*: mutations that prevent formation of the MinE ring lead to loss of the normal midcell arrest of growth of polar MinD membrane domains. *EMBO J.*, 21:3347–3357.

Smits, W., Kuipers, O., and Veening, J. (2006). Phenotypic variation in bacteria: the role of feedback regulation. *Nat Rev Microbiol*, 4(4):259–71.

Spudich, J. and Koshland, D. (1976). Non-genetic individuality: chance in the single cell. *Nature*, 262(5568):467–71.

Stricker, J., Maddox, P., Salmon, E. D., and Erickson, H. P. (2002). Rapid assembly dynamics of the *Escherichia coli* FtsZ-ring demonstrated by fluorescence recovery after photobleaching. *Proc. Natl. Acad. Sci. U.S.A.*, 99:3171–3175.

Thanbichler, M. and Shapiro, L. (2006a). Chromosome organization and segregation in bacteria. *J. Struct. Biol.*, 156:292–303.

Thanbichler, M. and Shapiro, L. (2006b). MipZ, a spatial regulator coordinating chromosome segregation with cell division in *Caulobacter*. *Cell*, 126(1):147–62.

Thattai, M. and van Oudenaarden, A. (2004). Stochastic gene expression in fluctuating environments. *Genetics*, 167(1):523–30.

Toro, E., Hong, S.-H., McAdams, H. H., and Shapiro, L. (2008). *Caulobacter* requires a dedicated mechanism to initiate chromosome segregation. *Proc Natl Acad Sci USA*, 105(40):15435–40.

Touhami, A., Jericho, M., and Rutenberg, A. D. (2006). Temperature dependence of MinD oscillation in *Escherichia coli*: running hot and fast. *J Bacteriol*, 188(21):7661–7.

Trueba, F. (1982). On the precision and accuracy achieved by *Escherichia coli* cells at fission about their middle. *Arch Microbiol*, 131(1):55–9.

Veening, J., Smits, W., Hamoen, L., and Kuipers, O. (2006). Single cell analysis of gene expression patterns of competence development and initiation of sporulation in *Bacillus subtilis* grown on chemically defined media. *J Appl Microbiol*, 101(3):531–41.

Viollier, P. H., Thanbichler, M., McGrath, P. T., West, L., Meewan, M., McAdams, H. H., and Shapiro, L. (2004). Rapid and sequential movement of individual chromosomal loci to specific subcellular locations during bacterial DNA replication. *Proc Natl Acad Sci USA*, 101(25):9257–62.

Wartlick, O., Kicheva, A., and González-Gaitán, M. (2009). Morphogen gradient formation. *Cold Spring Harb Perspect Biol*, 1(3):a001255.

Weiss, D. S. (2004). Bacterial cell division and the septal ring. *Mol. Microbiol.*, 54:588–597.

Woldringh, C., Mulder, E., Huls, P., and Vischer, N. (1991). Toporegulation of bacterial division according to the nucleoid occlusion model. *Res Microbiol*, 142(2-3):309–20.

Xie, X. S., Choi, P. J., Li, G. W., Lee, N. K., and Lia, G. (2008). Single-molecule approach to molecular biology in living bacterial cells. *Annu Rev Biophys*, 37:417–444.

Yu, X. and Margolin, W. (1999). FtsZ ring clusters in *min* and partition mutants: role of both the Min system and the nucleoid in regulating FtsZ ring localization. *Mol Microbiol*, 32(2):315–26.